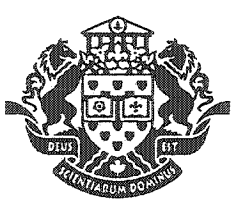

Université d'Ottawa · University of Ottawa

Université d'Ottawa · University of Ottawa

FACULTÉ DES ÉTUDES SUPÉRIEURES ET POSTDOCTORALES

FACULTY OF GRADUATE AND POSTDOCTORAL STUDIES

EDDE, Carla

AUTEUR DE LA THÈSE - AUTHOR OF THESIS

M.A.Sc. (Civil Engineering)

GRADE - DEGREE

Department of Civil Engineering

FACULTÉ, ÉCOLE, DÉPARTEMENT - FACULTY, SCHOOL, DEPARTMENT

TITRE DE LA THÈSE - TITLE OF THE THESIS

An Experimental Study and Numerical Analysis of Interface Behaviour

E. Evgin

DIRECTEUR DE LA THÈSE - THESIS SUPERVISOR

EXAMINATEURS DE LA THÈSE - THESIS EXAMINERS

M. Mohareb

S. Sivathayalan

J.-M. De Koninck, Ph.D.

LE DOYEN DE LA FACULTÉ DES ÉTUDES SUPÉRIEURES ET POSTDOCTORALES

SIGNATURE

DEAN OF THE FACULTY OF GRADUATE AND POSTDOCTORAL STUDIES

Université d'Ottawa ▪ University of Ottawa

FACULTÉ DES ÉTUDES SUPÉRIEURES ET POSTDOCTORALES

FACULTY OF GRADUATE AND POSTDOCTORAL STUDIES

Carla Edde

AUTEUR DE LA THÈSE - AUTHOR OF THESIS

M. A. Sc.

GRADE – DEGREE

Civil Engineering

FACULTÉ, ÉCOLE, DÉPARTEMENT - FACULTY, SCHOOL, DEPARTMENT

TITRE DE LA THÈSE - TITLE OF THE THESIS

An Experimental Study and Numerical Analysis of Interface Behaviour

Dr. E. Evgin

DIRECTEUR DE LA THÈSE - THESIS SUPERVISOR

EXAMINATEURS DE LA THÈSE - THESIS EXAMINERS

Names	Signatures
Dr. M. Mohareb	
Dr. S. Sivathayalan	

.....

LE DOYEN DE LA FACULTÉ DES ÉTUDES SUPÉRIEURES ET — SIGNATURE — DEAN OF THE FACULTY OF GRADUATE AND POSTDOCTRAL STUDIES

DATE DE LA SOUTENANCE
DATE OF THE THESIS DEFENCE June 16, 2003

AN EXPERIMENTAL STUDY AND NUMERICAL ANALYSIS OF INTERFACE BEHAVIOUR

Carla Edde, B.A.Sc.

A Thesis
Submitted to the School of Graduate Studies and Research
under the supervision of

Dr. Erman Evgin

In partial fulfillment of the requirement for the degree of
Master in Applied Science in Civil Engineering

Department of Civil Engineering
University of Ottawa
Ottawa, Ontario
Canada K1N 6N5

June 2003

The Master in Applied Sciences in Civil Engineering is a joint program between Carleton University and the University of Ottawa, which is administered by the Ottawa-Carleton Institute for Civil Engineering

Your file Votre référence
ISBN: 0-612-90065-7
Our file Notre référence
ISBN: 0-612-90065-7

ACKNOWLEDGMENTS

I like to express my most sincere thanks to my research supervisor, Dr. Erman Evgin, for his constant encouragement, advice and support during the research program.

I wish to acknowledge the technical assistance provided by Mr. R. J. Moore.

I also wish to express my appreciation to my brother Robert and my friend Sam for constantly giving me motivation and ambition.

Foremost, I wish to dedicate this thesis to my father and mother since they were the main reason behind the success of this Master study. Their unconditional encouragement and support is most appreciated.

ABSTRACT

For the solution of soil-structure interaction problems in geotechnical engineering, the magnitude of the load transferred at the interface and the corresponding displacements have to be known. Based on observations made in laboratory tests, the interface is defined as a thin layer of soil next to the surface of the structural member. The soil behaviour in the interface layer can be significantly different from the behaviour of soil in the soil mass due to the influence of the surface roughness of the structural member.

The development of a mathematical model for the mechanical behaviour of soil-structure interfaces requires a full knowledge of both the stress and strain states within the laboratory soil samples. It is difficult, however, to measure all components of stresses and strains experimentally everywhere in a sample. Considering the stresses, only the average values of the normal stress and shear stress acting on the contact surface are determined from the measured normal and tangential forces. In the direct shear interface tests, the tangential displacement of the interface plate and the displacement in the direction perpendicular to the top of the soil sample are measured. It is also possible to measure the amount of slip between the interface plate and soil sample if a simple shear type of apparatus is used in the experiments.

The main objective of the present investigation is to determine stresses and strains numerically in both the direct shear type and simple shear type of interface tests. The finite element method of analysis is used for this purpose. A commercial finite element program, Plaxis, is employed in the calculations.

An experimental program is carried out for two reasons: (1) to provide input data for the soil model used in the finite element analysis and (2) to assess the reliability of the numerical results given by Plaxis.

Triaxial tests were performed to determine the input parameters for the Hardening-Soil model used in the numerical analyses. The experiments on sand-concrete interface were carried out using the Cyclic Three-dimensional Interface (C3DI) apparatus. The results showed that the ratio of the interface friction angle to the soil friction angle is approximately 0.84.

The numerical analyses of interface tests, using the Hardening-Soil model in Plaxis, showed that for a specified normal stress and shear stress acting on the interface the calculated and measured tangential displacements do not agree. When the compression or dilation of the soil sample is considered, in the direction perpendicular to the interface, the calculated and measured values also become significantly different from each other. Furthermore, it was found that the state of stress and strain in the soil samples are not uniform. The stress paths followed in the simple shear interface tests are different than the stress paths in simple shear tests used for characterizing the stress strain behaviour of soils. Finally, it was observed that the principal stress axes rotate substantially during the application of the tangential displacement in both the direct shear and simple shear interface tests.

TABLE OF CONTENTS

LIST OF FIGURES

LIST OF TABLES

CHAPTER 1
INTRODUCTION

1.1 General

In many geotechnical engineering problems soils interact with structural materials. These types of problems are known as soil-structure interaction problems. A few examples are pile foundations, sheet pile walls, anchors, soil nails, retaining walls, tunnels, and pipelines. The contact zone between the soil and the structure is named the interface. It is a thin layer of soil ranging between 4 to 10 times the average particle size of the soil in which a shear band forms.

The soil behaviour in the interface layer is different than that of the soil mass. The soil behaviour in the interface layer is influenced by the surface roughness of the structural member as well as the difference in mechanical properties of the soil and the structural material. Previous studies show that, in general, the factors influencing the behaviour of the interface include the soil type and grain size distribution, relative density of soil, moisture content of soil, drainage conditions, magnitude of normal stress, and boundary conditions in the direction normal to the interface. Furthermore, sliding and debonding may occur at the interface, which in turn influences the stress-deformation behaviour of the interface.

The interface is characterized by its shear strength parameters and stress-displacement relations. Shear strength parameters, as illustrated in Figure 1.1, include adhesion, c_a, and friction angle between the soil and the structural material, δ. These parameters are normally required for stability analysis of practical engineering problems. However, for an elaborate analysis of soil-structure systems, the stress-displacement relations of interfaces are to be known. In order to achieve this objective, many interface testing devices have been used to obtain the strength parameters (Potyondy, 1961; Brummund and Leonards,

1973; etc) and stress-displacement relations (Desai et al., 1985; Boulon and Plytas, 1986; Yoshimi and Kishida, 1981; Fakharian and Evgin, 1996). However, the research on interface behaviour (Uesugi and Kishida, 1986; Evgin et al., 2003) shows that additional experimental and numerical investigations are required. Li (2001) used a simple shear type soil container in his interface tests to study the development of the interface layer. The components of the horizontal displacement were idealized schematically as shown in Figure 1.2. The total tangential displacement consisted of the displacement due to the deformation of the sand mass, δ_1, the displacement due to the deformation of the sand in the interface layer, δ_2, and the sliding displacement, δ_3 (the relative displacement between the steel plate and the bottom aluminium plate).

In order to solve soil-structure interaction problems, it is important to accurately model the interface behaviour. Several interface models have been developed (Desai et al., 1985; Ghaboussi et al., 1973; Desai and Rigby, 1995; Boulon et al., 1995), however, there are still uncertainties about the interface behaviour and reliability of existing constitutive models needs to be improved.

1.2 Statement of the problem

Four parameters are normally measured during an interface test, the normal stress, σ_n, the shear stress, τ, the volume change or normal displacement, v, and the shear or tangential displacement, u. For the common case of constant normal stress, shear stress and normal displacement variations are usually plotted against tangential displacements. These values measured in conventional interface tests are not sufficient for progress in interface studies.

To develop a realistic mathematical model for interfaces, which predicts the strain increments for the given stress increments or vice versa, the knowledge of the stress and strain states in a soil sample at all stages of an experiment is required. However, the existing experimental interface testing methods only provide information on the average normal stress and the average shear stress acting on the contact surface. There are no means to-date to determine the magnitude of the normal stress, σ_x, acting on the plane

perpendicular to the interface surface. Neither the distribution of normal stresses nor the components of strains are measured. Therefore, numerical analysis is necessary to obtain this information.

1.3 Objectives of the research

The objectives of this research are:

- To characterize the interface behaviour by determining the states of stress and strain in the laboratory experiments using the finite element method of analysis.
- To validate the finite element results by comparing the experimental data with finite element predictions.

1.4 Scope of the work

First, a literature survey was done to review commonly used constitutive models for soils. The reason for this review is that the constitutive models for interfaces are developed by modifying the models for soils. Second, a series of consolidated drained triaxial tests were performed on medium size quartz sand under three different confining pressures. The experimental results were used to obtain the soil properties and the parameters of the Hardening-Soil model. Third, a series of direct shear interface tests were conducted on a sand-concrete interface using the interface apparatus, C3DI (Fakharian and Evgin, 1996). The relationships between the average values of shear stress, normal stress, vertical displacement, and tangential displacement were determined. Fourth, various finite element analyses were performed with the finite element code, Plaxis, using the soil properties and model parameters determined experimentally. The finite element predictions of the states of stress and strain, Mohr circles and stress paths were determined in order to characterize the interface behaviour. The reliability of the finite element results was evaluated by comparing the average values of stress and displacements determined experimentally and numerically.

1.5 Outline of the thesis

Chapter 2 presents a literature review of existing constitutive soil models most commonly used in geotechnical practise and the basis on which they are formulated. The Hardening-Soil model is described in detail, which is the soil model used in this study.

Chapter 3 outlines the capabilities of the finite element code Plaxis for the analysis of geomechanics problems. The features are reviewed with emphasis on the interface element.

Chapter 4 presents the experimental triaxial test results. The input parameters for the Hardening-Soil model are then determined from the stress-strain curves. A comparison between the experimental results and the model predictions is made for further analysis.

Chapter 5 explains the C3DI interface testing device used in this study, the materials used for the tests such as sand and concrete, and the testing procedure. The test results are then presented and discussed.

Chapter 6 presents the results of two-dimensional finite element analyses of three direct shear interface tests and a simple shear interface test. The model predictions of shear stress versus tangential displacement and normal displacement versus tangential displacement are compared to experimental observations. The mean stress, relative shear stress, total volumetric strain, and normal and shear stresses along the interface are presented and discussed.

Chapter 7 presents the numerical analyses results for the states of stress and strain in a direct shear interface test and a simple shear interface test. The Mohr circles and stress paths, for various stages during the test simulations, are illustrated and discussed. Furthermore, the changes taking place in the orientation of principal stresses are presented.

Chapter 8 summarizes and concludes this study. Recommendations for future research are also presented.

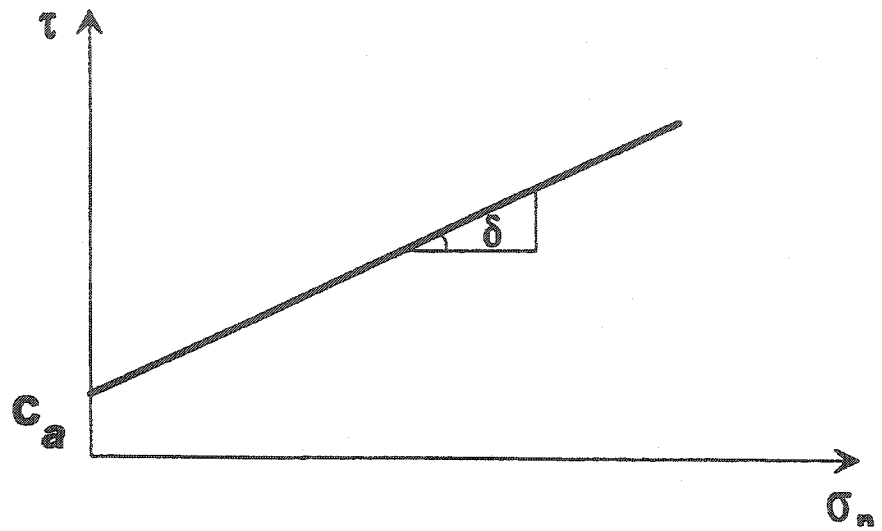

Figure 1.1 Graphical Mohr-Coulomb's failure criterion

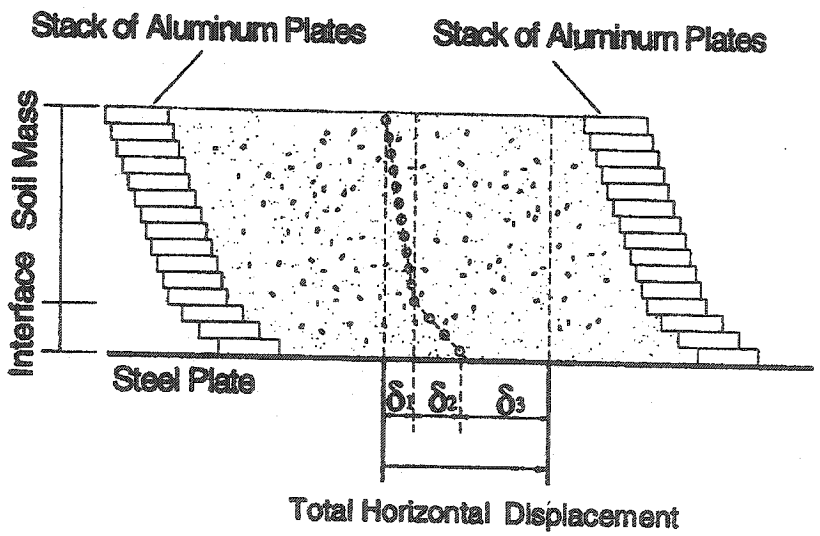

Figure 1.2 Idealized displacements in sand-steel interface tests

CHAPTER 2
CONSTITUTIVE MODELS FOR SOILS: LITERATURE REVIEW

2.1 Introduction

Constitutive models describe the soil behaviour. Mathematical equations are used to relate the stress, σ, strain, ε, and time. The most frequently used soil models can be categorized into elastic models and plastic models. Furthermore, the soil behaviour is idealized by these models using linear and/or non-linear curves.

The elastic soil model allows for the soil body to return to its original state of deformation when all the stress increments are reduced to zero as illustrated in Figure 2.1. The model is represented by either a linear, multi-linear or hyperbolic curve.

The plastic soil models assume that there exists a loading value which if exceeded, the soil will not return to its original undeformed shape when unloaded as shown in Figure 2.2. This stress point is called the yield point. The recovered and non-recovered strain components of the total strain are called elastic strain and plastic strain, respectively. The general types of plastic models are rigid or elastic, perfectly plastic and elasto-plastic.

In this chapter, various existing soil models will be summarized. The Hardening-Soil model will be described in detail since it will be further used in this study.

2.2 Linear elastic model

The stress-strain relation of this model is linear as shown in Figure 2.1. The only two soil parameters required to model the σ-ε relation are Young's modulus, E, and Poisson's ratio, ν. Hooke's Law is a well-known linear elastic model with the following simple relations for plane strain problems:

$$\begin{bmatrix}\sigma_x\\ \sigma_y\\ \tau_{xy}\end{bmatrix} = \frac{E}{(1-2\nu)(1+\nu)}\begin{bmatrix}1-\nu & \nu & 0\\ \nu & 1-\nu & 0\\ 0 & 0 & \frac{1}{2}-\nu\end{bmatrix}\begin{bmatrix}\varepsilon_x\\ \varepsilon_y\\ \gamma_{xy}\end{bmatrix} \tag{2.1}$$

In the analysis of geotechnical problems, the linear elastic model is used for structural members made of steel and concrete.

2.3 Multi-linear elastic model

The multi-linear elastic model uses the same relation as the linear elastic model, however, once certain stress levels, σ_i, are reached, Young's modulus and Poisson's ratios change to different values as seen in Figure 2.3.

2.4 Hyperbolic model

The non-linearity of stress-strain response of soils is modelled by using a tangent modulus, E_i that reduces with increasing deviator stress. The most widely used hyperbolic model is by Duncan and Chang (1970) based on the hyperbolic function by Kondner (1963).

$$(\sigma_1 - \sigma_3) = \frac{\varepsilon}{a + b\varepsilon} \tag{2.2}$$

where: $(\sigma_1-\sigma_3)$ is the deviator stress

σ_1 is the major principal stress

σ_3 is the minor principal stress

a and *b* are constants

Constants *a* and *b* define the shape of the stress-strain curve as shown in Figure 2.4 and are obtained as illustrated in Figure 2.5 where:

$$a = \frac{1}{E_i} \tag{2.3}$$

and

$$b = \frac{1}{(\sigma_1 - \sigma_3)_{ult}} = \frac{R_f}{(\sigma_1 - \sigma_3)_f} \tag{2.4}$$

where: E_i is the initial tangent modulus

$(\sigma_1-\sigma_3)_{ult}$ is the ultimate deviator stress

$(\sigma_1-\sigma_3)_f$ is the maximum deviator stress determined from experiment

R_f is the failure ratio determined from Eq. 2.4

The value of R_f is always smaller than or equal to one. Values between 0.7 and 1.0 are conventionally applied to soils. However, values as low as 0.5 have also been determined from experimental data.

If constants a and b in Eqs. 2.3 and 2.4, respectively, are substituted in Eq. 2.2, we obtain:

$$(\sigma_1 - \sigma_3) = \frac{\varepsilon}{\left[\frac{1}{E_i} + \frac{\varepsilon R_f}{(\sigma_1 - \sigma_3)_f}\right]} \tag{2.5}$$

Experiments show that the initial tangent modulus is a function of the confining stress, σ_3 in the case of triaxial testing. Eq. 2.6 is one of the forms relating the initial tangent modulus to the confining stress (Duncan and Chang, 1970).

$$E_i = Kp^{ref}\left(\frac{\sigma_3}{p^{ref}}\right)^n \tag{2.6}$$

where: p^{ref} is the reference stress

K is the modulus number

n is the modulus exponent

In most cases, the atmospheric pressure is used for the reference stress, p^{ref}.

Using the Mohr-Coulomb failure criterion, the deviator stress at failure can be determined using the following equation.

$$(\sigma_1 - \sigma_3)_f = \frac{2c\cos\phi + 2\sigma_3 \sin\phi}{1 - \sin\phi} \tag{2.7}$$

where: c is the cohesion intercept

ϕ is the angle of friction

For triaxial tests, Duncan and Chang (1970) assumed that the minor principal stress, σ_3, is constant , and therefore, the tangent modulus, E_t, can be expressed as:

$$E_t = \frac{\partial \sigma_1}{\partial \varepsilon_1} \tag{2.8}$$

By performing the differentiation of Eq. 2.8 for Eq. 2.5, the tangent modulus, E_t, becomes:

$$E_t = \frac{\dfrac{1}{E_i}}{\left[\dfrac{1}{E_i} + \dfrac{\varepsilon R_f}{(\sigma_1 - \sigma_3)_f}\right]^2} \tag{2.9}$$

If the expression of strain given in Eq. 2.5 is substituted in the above equation, the following expression is obtained.

$$E_t = \left(1 - \frac{(\sigma_1 - \sigma_3)}{(\sigma_1 - \sigma_3)_f} R_f\right)^2 E_i \tag{2.10}$$

Substituting Eqs. 2.6 and 2.7 into 2.10 gives the following key relation of the hyperbolic model, where the tangent modulus corresponds to the stress state of the soil at that instant.

$$E_t = \left[1 - \frac{(\sigma_1 - \sigma_3)R_f(1-\sin\phi)}{2c\cos\phi + 2\sigma_3\sin\phi}\right] Kp^{ref}\left(\frac{\sigma_3}{p^{ref}}\right)^n \tag{2.11}$$

Once the tangent elastic modulus is determined from Eq. 2.11, the stress-strain relation is written in the following incremental form, for a constant Poisson's ratio:

$$\begin{bmatrix}\Delta\sigma_x \\ \Delta\sigma_y \\ \Delta\tau_{xy}\end{bmatrix} = \frac{E_t}{(1-2\nu)(1+\nu)}\begin{bmatrix}1-\nu & \nu & 0 \\ \nu & 1-\nu & 0 \\ 0 & 0 & \frac{1}{2}-\nu\end{bmatrix}\begin{bmatrix}\Delta\varepsilon_x \\ \Delta\varepsilon_y \\ \Delta\gamma_{xy}\end{bmatrix} \tag{2.12}$$

This model has proven incapable of adequately predicting soil response at high stress levels. Furthermore, it does not model the effects of intermediate principal stresses, the volume increase due to shear stress, nor the strain softening.

2.5 Rigid or elastic, perfectly plastic model

The simplest form of plastic modelling is the rigid, perfectly plastic model, where there are no elastic strains and no change to a fixed yield surface. Before the soil reaches the yield point, there is no deformation as illustrated in Figure 2.6. Beyond the yield point, only plastic deformations occur. This model oversimplifies the real behaviour of soil, however, it has been used to estimate the bearing capacity of the soil.

The elastic, perfectly plastic model is similar to a rigid, perfectly plastic model, however, it allows for elastic strains to develop until the yield point is reached. The model is not adequate for granular soils in which non-recoverable strains, work hardening, and after-peak softening are common.

2.5.1 Mohr-Coulomb model

The Mohr-Coulomb model is an elastic, perfectly plastic model useful to model simple problems or problems with very limited information about the characteristics of a soil. However, it does not represent the behaviour of the soil at different states of stress very well. Only five parameters are required for this model including cohesion, friction angle, Young's modulus, Poisson's ratio, and dilatancy angle. Figure 2.7 shows typical test results modelled by the Mohr-Coulomb model.

2.6 Elasto-plastic models

Elasto-plastic models presume that elastic strains develop before the yield stress and past the yield stress, plastic strains occur. There are three types of elasto-plastic models: (1) perfectly plastic, (2) strain hardening, and (3) strain softening as illustrated in Figure 2.8. The relation between stress and strain is based on their incremental components. Furthermore, the relations are established on the basis of the following concepts: yield and failure criteria, flow rule and hardening law or hardening-softening law.

Yield and failure criteria

The yield criterion, f, is usually a function of stresses. In stress space, f represents a surface. When the state of stress remains inside the yield surface during a stress change, only elastic strains develop. If the yield surface expands during the stress change, both elastic and plastic strains occur.

The failure criterion, F, is also a function of stresses. Failure occurs when $F=k_o$ and the plastic deformation becomes unlimited. k_o is based on soil properties. The failure function, representing the failure surface in stress space, limits the yield surface.

Flow rule

The direction of the elastic strain increments is in the same direction as the stress increments. The direction of the plastic strain increments, however, does not necessarily

coincide with the direction of the stress increments. As a result, a flow rule is proposed to determine the direction of plastic strain increments. In other words, the relative magnitude of the components of plastic strain increments is determined by the flow rule.

A plastic potential function, g, defines a plastic potential surface in stress space. The direction of the plastic strain increment is normal to this surface. The relative magnitude of the components of a plastic strain increment is calculated from the following equation (i.e. the flow rule):

$$d\varepsilon_{ij}^{\ p} = \beta \frac{\partial g}{\partial \sigma_{ij}} \tag{2.13}$$

where: β is a plastic multiplier based on a hardening law

For pure elastic behaviour β is zero, whereas for plastic behaviour, β is a positive number.

A model has either an associated or non-associated flow rule. The associated flow rule implies that the plastic potential function, g, is equal to the yield function, *f*. However, the yield function of some models leads to an over-prediction of dilatancy. In order to improve predictions, various models have been developed with non-associated flow rules, where the plastic potential function is different from the yield function.

Work-hardening law

In most soil models, the yield surface expands from its initial posotion until it meets the failure surface. The expansion of the yield surface is assumed to be related to the amount of plastic work done during loading. The value of β in Eq. 2.13 is determined from the mathematical relation between the yield function and the plastic work (Lade, 1977). The work-hardening law determines the magnitude of plastic strain increments. Hardening signifies that after unloading and reloading, the soil would yield at a higher stress level than the previous yield stress level.

Prager (1959) proposed two ways to describe the yield surface evolution: isotropic and kinematic hardening. The isotropic hardening rule allows for a uniform expansion of the yield surface from the hydrostatic axis as shown in Figure 2.9. The kinematic hardening rule implies a translation of the yield surface with a stress point when this point increases beyond the current yield surface as illustrated in Figure 2.10. The isotropic models apply mainly to monotonic loading while for cyclic loading, the kinematic hardening rule is more appropriate.

2.6.1 Hardening-Soil model

The Hardening-Soil model is an advanced soil model using an non-associated flow rule, taking into account isotropic hardening behaviour of soils, including soil dilatancy, and introducing a yield cap. It is developed by Schanz and described by Plaxis (1998). It accounts for shear hardening and compression hardening. Shear hardening is used to model non-recoverable strains due to primary deviatoric loading. Compression hardening is used to model non-recoverable plastic strains due to primary compression in oedometer loading and isotropic loading.

The Hardening-Soil model can simulate the behaviour of both soft soils and stiff soils. The basic characteristics of the model are:

- Stress dependent stiffness according to a power law
- Plastic straining due to primary deviatoric loading
- Plastic straining due to primary compression
- Elastic unloading/reloading condition
- Mohr-Coulomb failure criterion

The main disadvantages of this model is that it does not account for softening due to soil dilatancy, as is the case for dense sands after the peak stress level is reached. Furthermore, since it is an isotropic hardening model, it does not model cyclic loading

Hyperbolic relationship for standard drained triaxial test results

The Hardening-Soil model uses a hyperbolic relationship between the vertical strain, ε_1, and the deviatoric stress, $(\sigma_1-\sigma_3)$, in primary triaxial loading as shown in Figure 2.11. Compression is negative. The stress-strain curves are described by:

$$-\varepsilon_1 = \frac{1}{2E_{50}} \frac{(\sigma_1-\sigma_3)}{1-(\sigma_1-\sigma_3)/(\sigma_1-\sigma_3)_a} \qquad \text{for } (\sigma_1-\sigma_3)<(\sigma_1-\sigma_3)_f \tag{2.14}$$

where: $(\sigma_1-\sigma_3)_a$ is the asymptotic value of the shear strength = $(\sigma_1-\sigma_3)_f/R_f$

R_f is the failure ratio

$(\sigma_1-\sigma_3)_f$ is the ultimate deviatoric stress, derived from the Mohr-Coulomb failure criterion, and is given by the following equation:

$$(\sigma_1-\sigma_3)_f = (c\cot\phi-\sigma_3)\frac{2\sin\phi}{1-\sin\phi} \tag{2.15}$$

E_{50} is the confining stress dependent modulus for primary loading and is given by the equation:

$$E_{50} = E_{50}^{ref}\left(\frac{c\cot\phi-\sigma_3}{c\cot\phi+p^{ref}}\right)^m \tag{2.16}$$

E_{50}^{ref} is a reference modulus corresponding to a reference confining pressure p^{ref}

m is the exponent for stress level dependent moduli

For unloading and reloading conditions, the stress-dependent modulus is:

$$E_{ur} = E_{ur}^{ref}\left(\frac{c\cot\phi-\sigma_3}{c\cot\phi+p^{ref}}\right)^m \tag{2.17}$$

where: E_{ur}^{ref} is the reference Young's modulus for unloading and reloading, given by:

$$E_{ur}^{ref} = 3p^{ref}(1-2\nu_{ur})/\kappa^* \tag{2.18}$$

$\kappa^*=\kappa/(1+e_o)$

κ is the swelling index

e_o is the initial void ratio

ν_{ur} is the Poisson's ratio for unloading and reloading

Approximations for triaxial test conditions

The yield function considering plastic strains, for drained triaxial loading conditions with $\sigma_2'=\sigma_3'$ and σ_1' being the major compressive stress, is:

$$f = \overline{f} - \gamma^p \tag{2.19}$$

where: $\overline{f}$ is a function of stress as follows:

$$\overline{f} = \frac{1}{E_{50}} \frac{(\sigma_1-\sigma_3)}{1-(\sigma_1-\sigma_3)/(\sigma_1-\sigma_3)_a} - \frac{2(\sigma_1-\sigma_3)}{E_{ur}} \tag{2.20}$$

γ^p is a function of plastic strains as follows:

$$\gamma^p = -(2\varepsilon_1^p - \varepsilon_v^p) \tag{2.21}$$

ε_1^p is the plastic vertical strain

ε_v^p is the plastic volumetric strain

For stiff soils, plastic volume changes tend to be relatively small (Plaxis, 1998). Thus, Eq. 2.21 can be approximated by:

$$\gamma^p \approx -2\varepsilon_1^p \tag{2.22}$$

When considering the primary loading of a standard drained triaxial test, the yield condition f =0 applies, thus, resulting $\gamma^p = \overline{f}$. Substituting Eqs. 2.20 and 2.21 into this relation gives:

$$-\varepsilon_1^p \approx \frac{1}{2}\overline{f} = \frac{1}{2E_{50}} \frac{(\sigma_1 - \sigma_3)}{1-(\sigma_1 - \sigma_3)/(\sigma_1 - \sigma_3)_a} - \frac{(\sigma_1 - \sigma_3)}{E_{ur}} \tag{2.23}$$

In addition to the plastic strains, the model accounts for elastic strains, which are given by the following equations:

$$-\varepsilon_1^e = \frac{(\sigma_1 - \sigma_3)}{E_{ur}} \qquad \varepsilon_2^e = \varepsilon_3^e = -\nu_{ur} \frac{(\sigma_1 - \sigma_4)}{E_{ur}} \tag{2.24}$$

For the deviatoric loading stage of the triaxial test, the axial strain is the sum of an elastic component given by Eq. 2.24 and a plastic component according to Eq. 2.23. Therefore, it follows that:

$$-\varepsilon_1 = -\varepsilon_1^e - \varepsilon_1^p \approx \frac{1}{2E_{50}} \frac{(\sigma_1 - \sigma_3)}{1-(\sigma_1 - \sigma_3)/(\sigma_1 - \sigma_3)_a} \tag{2.25}$$

Equation 2.25 matches the hyperbolic Eq. 2.14. It is thus made clear that the Hardening-Soil model yields a hyperbolic stress-strain curve under triaxial testing conditions.

Plastic volumetric strain for triaxial states of stress

The plastic volumetric strain, $\dot{\varepsilon}_v^p$, is related to the plastic shear strain, $\dot{\gamma}^p$, as expressed by the following equation. The relationship is based on the dilatancy angle of the soil.

$$\dot{\varepsilon}_v^p = \sin\psi_m \dot{\gamma}^p \tag{2.26}$$

where: ψ_m is the mobilized dilatancy angle given by:

$$\sin\psi_m = \frac{\sin\phi_m - \sin\phi_{cv}}{1 - \sin\phi_m \sin\phi_{cv}} \tag{2.27}$$

ϕ_{cv} is the critical state friction angle

ϕ_m is the mobilized friction angle given by:

$$\sin\phi_m = \frac{\sigma_1 - \sigma_3}{\sigma_1 + \sigma_3 - 2c\cot\phi} \tag{2.28}$$

The above equations are based on the stress-dilatancy theory by Rowe (1962). The theory states that a material contracts for small stress ratios ($\phi_m < \phi_{cv}$) and dilates for high stress ratios ($\phi_m > \phi_{cv}$). At failure, the mobilized friction angle equals the friction angle, ϕ, and Eq. 2.27 can be expressed by:

$$\sin\phi_{cv} = \frac{\sin\phi - \sin\psi}{1 - \sin\phi\sin\psi} \tag{2.27a}$$

Therefore, the critical state friction angle is found by the soil's friction angle, ϕ, and dilatancy angle, ψ.

Dilatancy cut-off

Following extensive shearing, materials reach a state of critical density where they can no longer dilate. This phenomenon of soil behaviour is taken into consideration by the Hardening-Soil model using a dilatancy cut-off option. The dilatancy cut-off occurs when the volume change corresponds to a state of maximum void and hence, the mobilized dilatancy angle, ψ_m, is automatically set to zero as shown in Figure 2.12. The relation between the volumetric strain, ε_v, and the void ratio, e, is:

$$-\left(\varepsilon_v - \varepsilon_v^{init}\right) = \ln\left(\frac{1+e}{1+e_{init}}\right) \tag{2.29}$$

where: ε_v is positive for dilatancy

e_{init} is the in-situ void ratio of the soil body

The initial void ratio and the maximum void ratio of the soil are required parameters to model the dilatancy cut-off behaviour.

Cap yield surface

The yield condition $f = 0$ of Eq. 2.19, generates a shear yield surface for a given a constant plastic shear strain, γ_p,. Figure 2.13 illustrates yield loci for different constant values of the plastic shear strain. However, these shear yield surfaces do not describe the plastic volume strain that is measured in isotropic compression. Therefore, a second type of yield surface is introduced to close the elastic region in the direction of the p-axis. As a result of this second cap yield surface, it becomes possible to formulate a model with independent input of both the secant modulus in drained triaxial test, E_{50}^{ref}, and the tangent modulus for oedometer loading, E_{oed}^{ref}. The triaxial modulus controls the shear yield surface and the oedometer modulus controls the cap yield surface. Actually, E_{50}^{ref} controls the magnitude of the plastic strains that are associated with the shear yield surface, and E_{oed}^{ref} controls the magnitude of the plastic strains that originate from the cap yield surface. The cap yield surface is defined by an equation similar to that of an ellipse as follows:

$$f^c = \frac{\tilde{q}^2}{\alpha^2} + p^2 - p_p^2 \qquad (a=c\cot\phi) \tag{2.30}$$

where: α is a cap parameter that relates to K_o^{nc}

K_o^{nc} is the coefficient of earth pressure at rest for normally consolidated soils

p_p is the isotropic pre-consolidation stress

$p = -(\sigma_1+\sigma_2+\sigma_3)/3$

$\tilde{q} = \sigma_1+(\delta-1)\sigma_2-\delta\sigma_3$

$\delta = (3+\sin\phi)/(3-\sin\phi)$

The position of the cap yield surface is determined by the isotropic pre-consolidation stress, p_p. The hardening law relating the pre-consolidation stress to the volumetric cap strain ε_v^{pc} is as follows:

$$\varepsilon_v^{pc} = \frac{\beta}{m+1}\left(\frac{p_p}{p^{ref}}\right)^{m+1} \tag{2.31}$$

where: β is a cap parameter that relates to E_{oed}^{ref} which is defined as:

$$E_{oed}^{ref} = p^{ref}/\lambda^* \tag{2.32}$$

$\lambda^*=\lambda/(1+e_o)$

λ is the compression index

The shape of the cap yield surface is an ellipse in the p-$\tilde{q}$ plane as indicated in Figure 2.14. The symbol p_p denotes the length of the ellipse on the p-axis and αp_p on the $\tilde{q}$-axis. In other words, p_p defines the magnitude and α the aspect ratio of the ellipse. The ellipse is used as both a yield surface and as a plastic potential. Therefore:

$$\dot{\varepsilon}^{pc} = \lambda \frac{\partial f^{c}}{\partial \underline{\sigma}} \qquad with: \lambda = \frac{\beta}{2p}\left(\frac{p_p}{p^{ref}}\right)^{m} \frac{\dot{p}_p}{p^{ref}} \tag{2.33}$$

Figure 2.14 shows the simple yield lines and Figure 2.15 shows the yield surfaces in the principal stress space.

Parameters of the Hardening-Soil model

The failure parameters of the Hardening-Soil model are:

c: Cohesion

ϕ: Friction angle

ψ: Dilatancy angle

The soil modulus parameters are:

E_{50}^{ref}: Secant modulus in standard drained triaxial test

E_{oed}^{ref}: Tangent modulus for primary oedometer loading

m: Power for stress-level dependency of moduli

Other parameters are:

E_{ur}^{ref}: Unloading/reloading modulus

ν_{ur}: Poisson's ratio for unloading/reloading

p^{ref}: Reference stress for moduli

K_o^{nc}: K_o-value for normal consolidation given by 1-sinϕ

R_f: Failure ratio $(\sigma_1-\sigma_3)_f/(\sigma_1-\sigma_3)_a$

c_{inc}: increase in cohesion with depth

Cohesion and friction angle, c and ϕ

Cohesion and the angle of friction are the parameters of the Mohr-Coulomb failure criterion. Mohr circles representing the failure conditions are plotted for all triaxial tests performed. The cohesion is the intercept of the Mohr-Coulomb failure envelope, and $\tan\phi$ is the slope of the failure envelope as shown in Figure 2.16.

Alternatively, the test data can be plotted in the p-q coordinate system. In this case, the Mohr circles are represented by their summits. At failure, $(\sigma_1-\sigma_3)_f$ /2 and $(\sigma_1+\sigma_3)_f/2$ are the values of q and p, respectively. The intercept of the line corresponding to failure in the p-q plot (alternative line) is related to the cohesion, c, and the friction angle, ϕ, is equal to $\sin^{-1}\tan\psi_{p\text{-}q}$, where $\psi_{p\text{-}q}$ is the angle between the alternative line with the horizontal axis.

Dilatancy angle, ψ

Clay soils tend to show little dilatancy ($\psi\approx0$), with the exception of heavily over-consolidated layers. On the other hand, the dilatancy of sand depends on both the density and on the friction angle. For quartz sands, the order of magnitude is $\psi\approx\phi-30^\circ$ (Plaxis, 1998). For ϕ-values less than 30°, however, the angle of dilatancy is mostly zero. A small negative value for ψ is only realistic for extremely loose sands.

Poisson's ratio, ν

By definition, for triaxial compression tests, Poisson's ratio is the ratio between the change in radial strain, $\Delta\varepsilon_r$, to the change in axial strain, $\Delta\varepsilon_a$, resulting from a change in axial stress as:

$$\nu = -\frac{\Delta\varepsilon_r}{\Delta\varepsilon_a} \tag{2.34}$$

During conventional drained triaxial testing, axial and volumetric strains, ε_a and ε_v respectively, are usually measured. Poisson's ratio is expressed in terms of these measured quantities. The change in volumetric strain is the sum of change in strain in all three directions (x, y, and z). For triaxial condition, this is equivalent to:

$$\Delta\varepsilon_v = \Delta\varepsilon_a + 2\Delta\varepsilon_r \tag{2.35}$$

or

$$\Delta\varepsilon_r = \frac{\Delta\varepsilon_v - \Delta\varepsilon_a}{2} \tag{2.36}$$

Therefore,

$$\nu = -\frac{\Delta\varepsilon_a - \Delta\varepsilon_v}{2\Delta\varepsilon_a} \tag{2.37}$$

Noting that during a triaxial test, Poisson's ratio varies considerably. Furthermore, as Poisson's ratio also varies with confining stress, different values are expected for Poisson's ratio calculated from different tests. This makes selecting a single representative value for the Poisson's ratio difficult. A value between 0.2 and 0.4, however, is usually used for drained conditions.

Moduli E_{50}^{ref}, E_{oed}^{ref} and m

The secant modulus in drained triaxial test, E_{50}^{ref}, is defined for a reference minor principal stress of $\sigma_3=p^{ref}$.

There is no relation between the secant modulus in drained triaxial test, E_{50}, and tangent modulus for primary oedometer loading, E_{oed}. The tangent modulus for one-dimensional compression is given by the following equation:

$$E_{oed} = E_{oed}^{ref}\left(\frac{c\cot\phi - \sigma_1}{c\cot\phi + p^{ref}}\right)^m \tag{2.38}$$

Where: E_{oed}^{ref} is a tangent modulus at a vertical stress of $-\sigma_1' = p^{ref}$ as in Figure 2.17

In order to simulate a logarithmic stress dependency, as observed for soft clays, *m* should be taken equal to 1.0. According to Plaxis (1998), Janbu (1963) reports values of *m* around 0.5 for Norwegian sands and silts, whilst Von Soos (1980) reports various different values in the range of $0.5<m<1.0$.

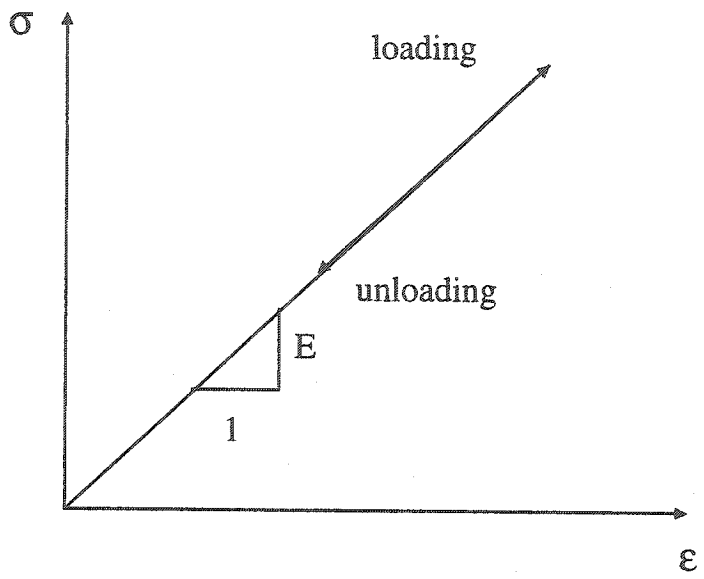

Figure 2.1 Typical stress-strain relation of a linear elastic soil behaviour

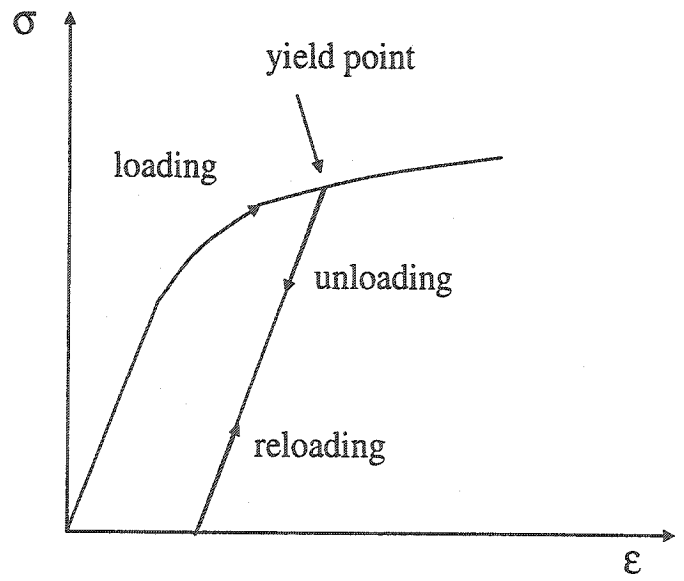

Figure 2.2 Typical stress-strain curve of a plastic soil behaviour

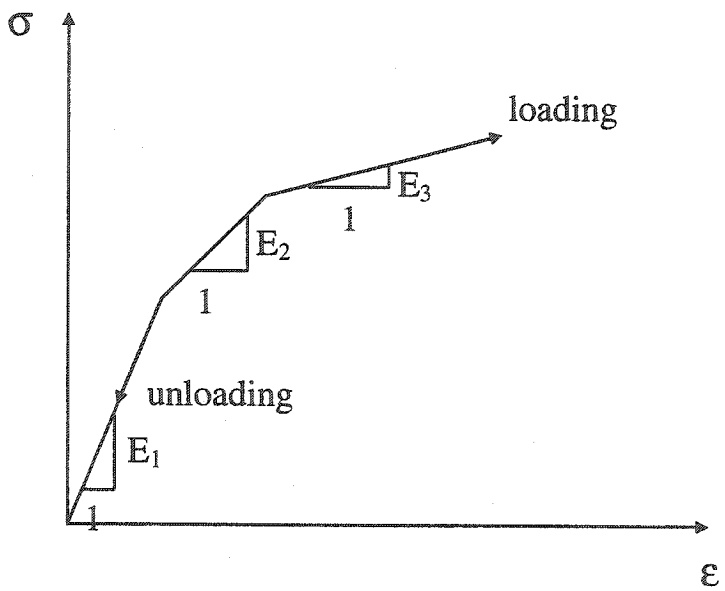

Figure 2.3 Multi-linear elastic model

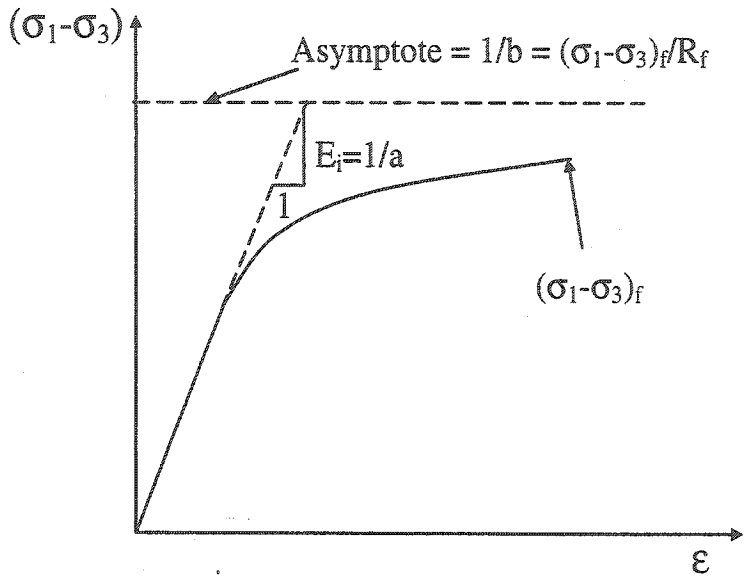

Figure 2.4 Hyperbolic stress-strain curve by Duncan and Chang (1970)

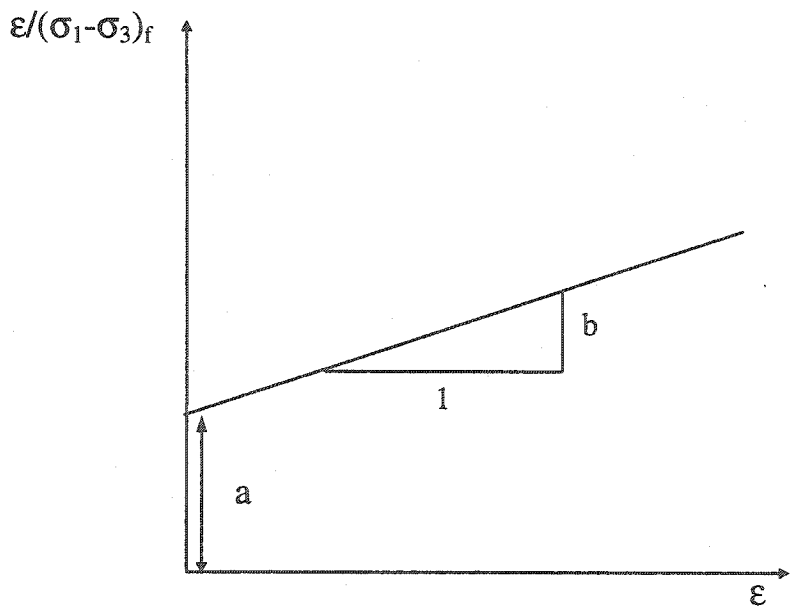

Figure 2.5 Theoretically-transformed curve of hyperbolic stress-strain curve

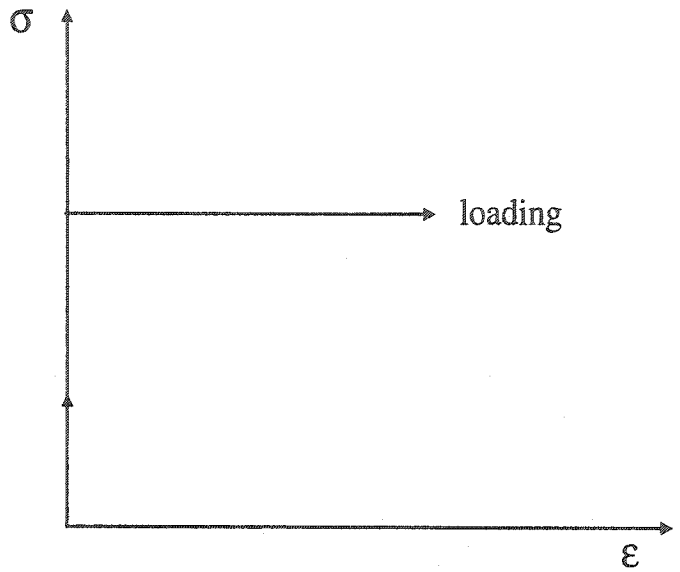

Figure 2.6 Typical stress-strain relation of a rigid perfectly plastic model

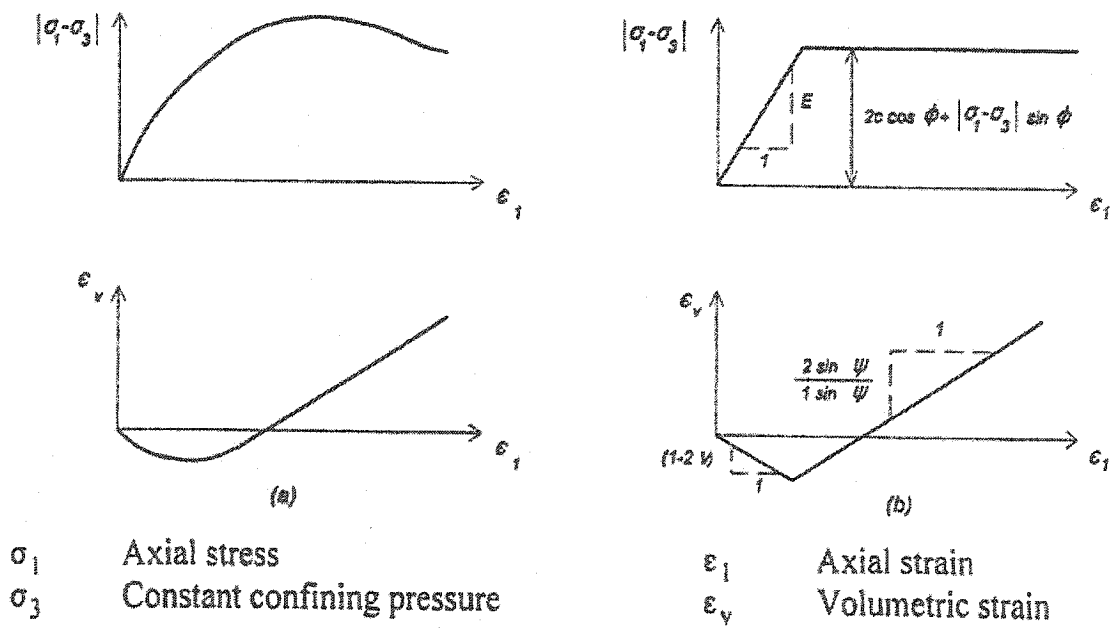

Figure 2.7 Mohr-Coulomb model idealized form (Plaxis, 1998)

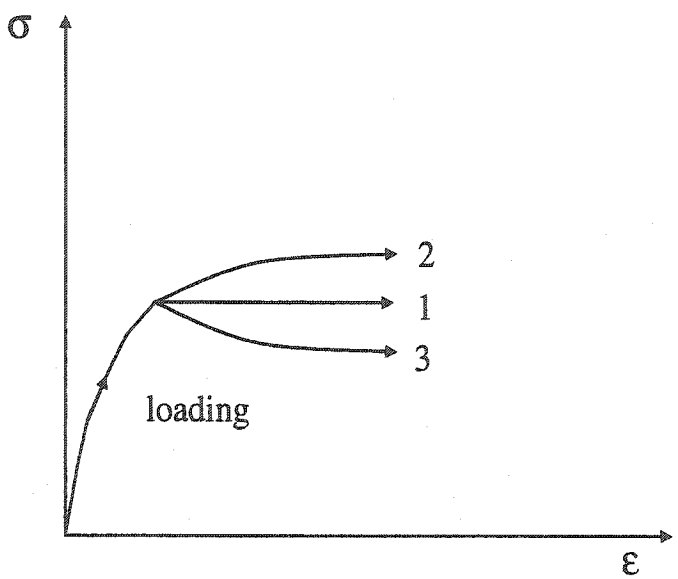

Figure 2.8 Typical stress-strain curves of an elasto-plastic model (1) perfectly plastic, (2) strain hardening, and (3) strain softening

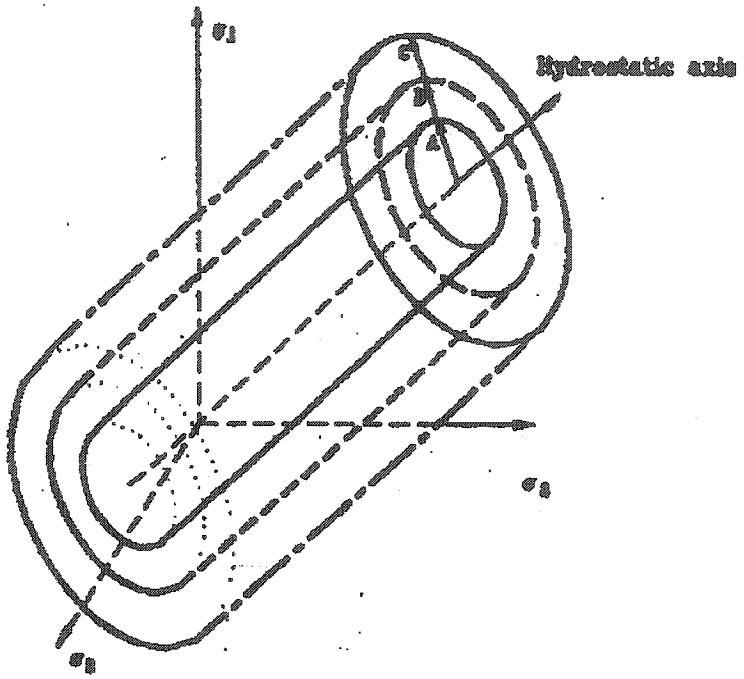

Figure 2.9 Isotropic hardening law

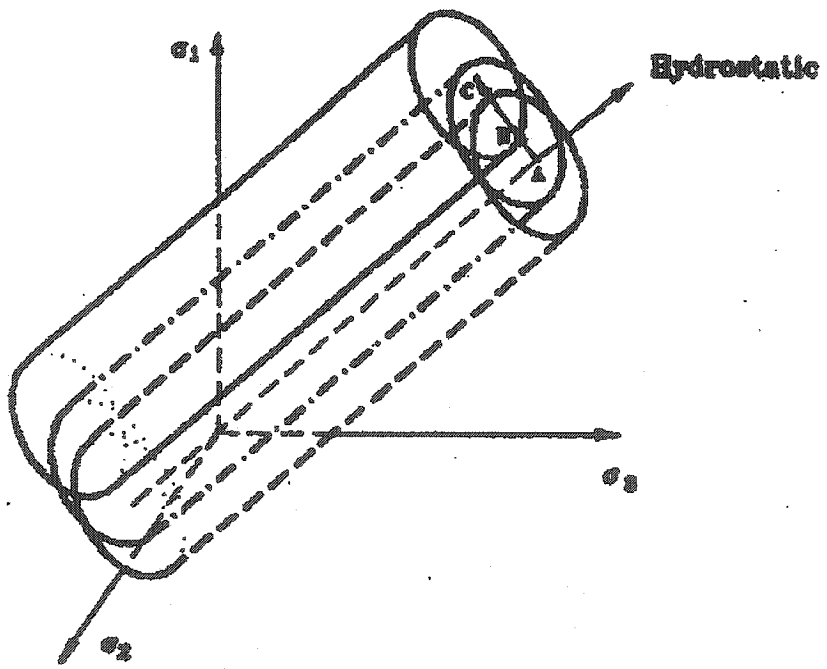

Figure 2.10 Kinematic hardening law

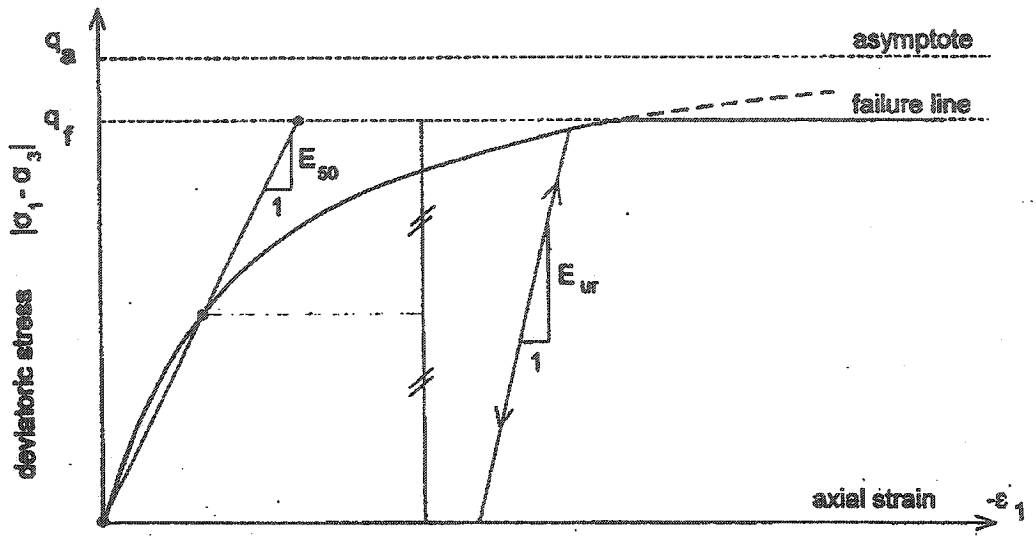

Figure 2.11 Hyperbolic stress-strain relation in primary loading for a standard drained triaxial test

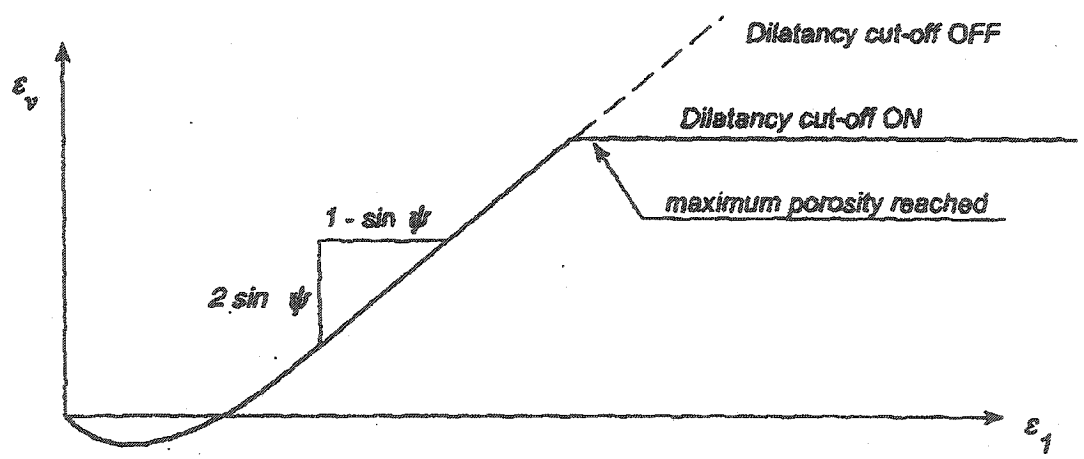

Figure 2.12 Volumetric strain-axial strain curve for a standard drained triaxial test considering dilatancy cut-off

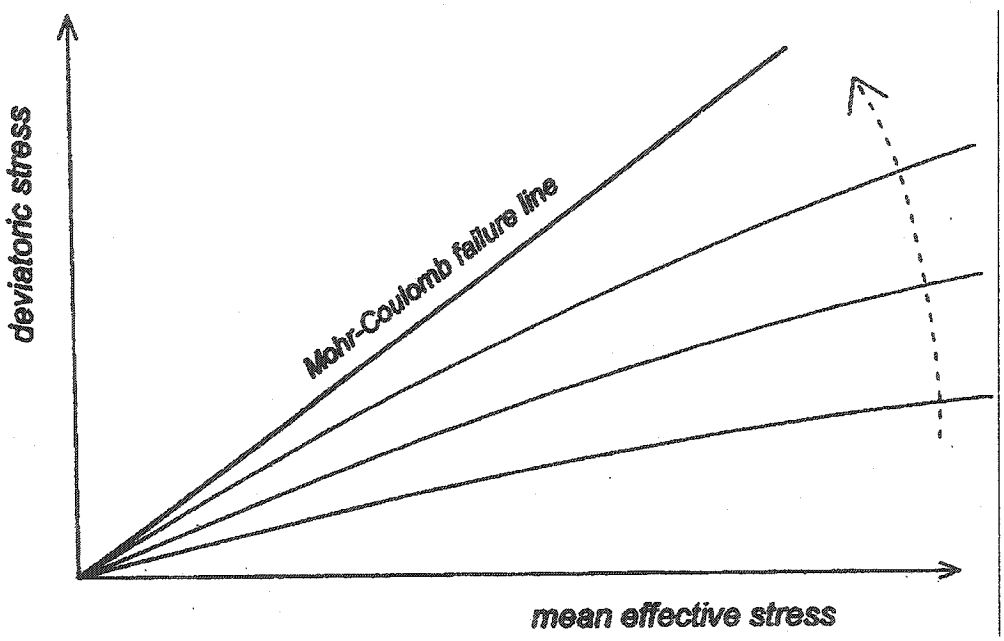

Figure 2.13 Successive yield loci for constant values of the hardening parameter γ^p

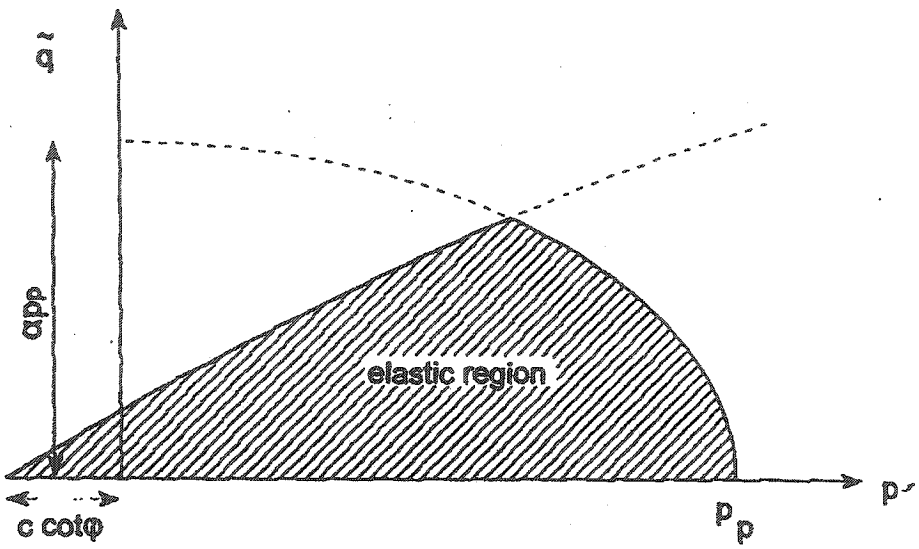

Figure 2.14 Shear and cap yield surface of the Hardening-Soil model in p-$\tilde{q}$ plane (Plaxis, 1998)

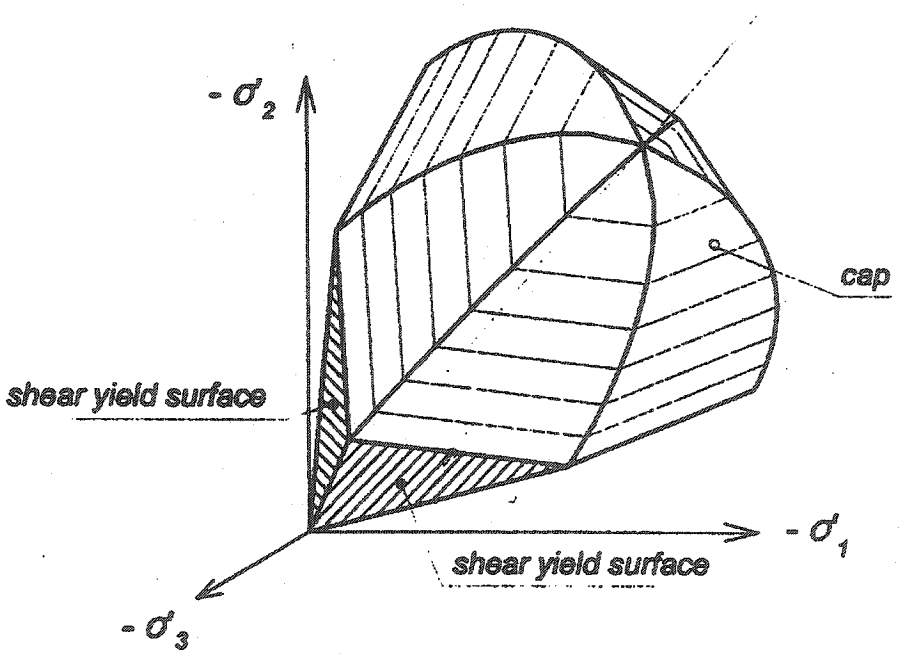

Figure 2.15 Shear and cap yield surface of the Hardening-Soil model in principal stress space (Plaxis, 1998)

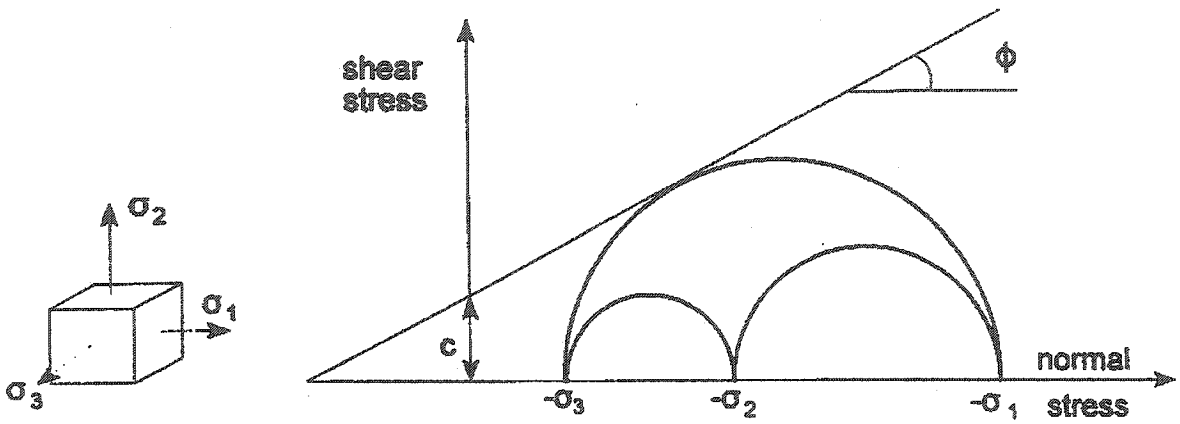

Figure 2.16 Mohr-Coulomb's stress circles at yield

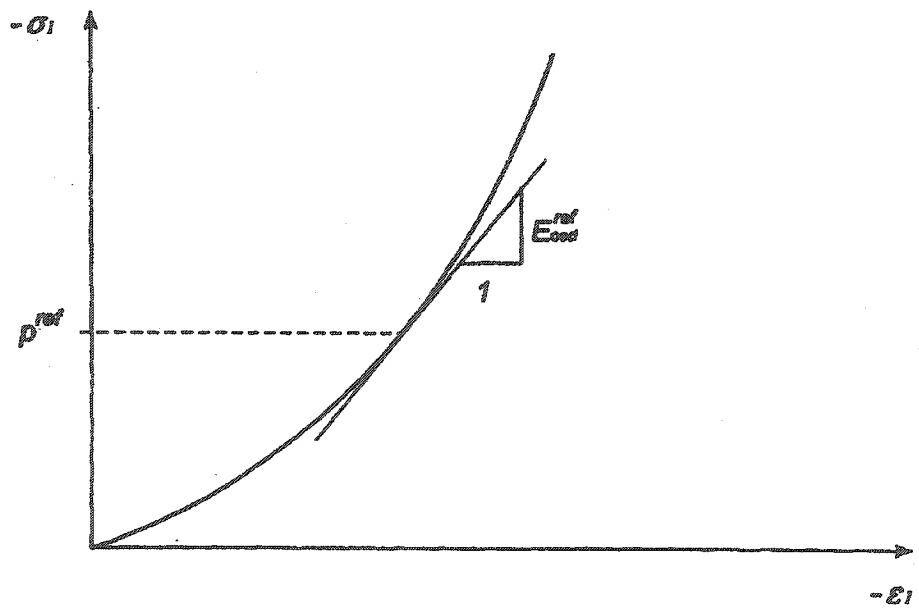

Figure 2.17 Definition of E_{oed}^{ref} for one-dimensional compression in oedometer test results

CHAPTER 3
PLAXIS: FINITE ELEMENT PROGRAM FOR THE ANALYSIS OF GEOMECHANICS PROBLEMS

3.1 Introduction

Plaxis is a finite element program designed to analyze the deformation and stability in geotechnical engineering projects. It can perform either plane strain or axisymmetric analyses. A plane strain analysis is chosen when a structure has a uniform cross section over a certain length. The displacements perpendicular to this cross section are assumed to be zero. An axisymmetric analysis is used for circular structures with a uniform radial cross section around the central axis, where the deformation and stress state are assumed to be identical in any radial direction.

A selection of five models is available to simulate the behaviour of soil and other structural materials depending on the degrees of accuracy required. They are the linear elastic model, the Mohr-Coulomb model, the Hardening-Soil model, the Soft Soil model, and the Soft Soil Creep model.

Plaxis is configured by four sub-programs: Input, Calculations, Output and Curves. The Input program is a user-friendly graphical program which enables a quick generation of complex finite element models. The Calculations program defines the construction stages and performs the actual calculations. A detailed graphical presentation of the computational results is then illustrated in the Output program. Finally, the Curves program generates load-displacement curves, stress-strain diagrams and stress paths that give an insight into the global and local behaviour of the soil.

A general description of Plaxis features is given below with emphasis on the features used in this study.

3.2 Constitutive models in Plaxis

3.2.1 Linear elastic model

The linear elastic model is based on Hooke's law of linear elasticity. It is primarily used to model the behaviour of structural material rather than the soil behaviour. The simple model involves only two elastic parameters, that are Young's modulus, E, and Poisson's ratio, ν.

3.2.2 Mohr-Coulomb model

This elastic-perfectly plastic model is used as a first approximation of the soil behaviour in general. The computations of this model are very fast given that an average constant modulus is used for the soil. The model involves five parameters, that is Young's modulus, E, Poisson's ratio, ν, the cohesion, c, the friction angle, ϕ, and the dilatancy angle, ψ.

3.2.3 Hardening-Soil model

The elasto-plastic model, considering hardening plasticity, is used to simulate the behaviour of sands, gravel and overconsolidated clays. It accounts for stress-dependency of moduli, where the moduli increase with pressure. The limiting states of stress are described by the cohesion, c, the friction angle, ϕ, and the dilatancy angle, ψ. The soil modulus is described by the triaxial loading modulus, E_{50}, the unloading modulus, E_{ur}, and the oedometer loading modulus, E_{oed}.

3.2.4 Soft-Soil model

This is a Cam-Clay type model which can be used to simulate the behaviour of soft soils like normally consolidated clays and peat. The model performs best in situations of primary compression.

3.2.5 Soft-Soil creep model

This is a second order model formulated in the framework of viscoplasticity. The model can be used to simulate the time-dependent behaviour of soft soils.

3.3 Input program

The Input program is used to create a finite element model and specify the material properties and boundary conditions. To set up a finite element model, a two-dimensional "geometry model" composed of points, lines and other components must be drawn. The generation of a finite element mesh is automatically performed by Plaxis based on the input of the "geometry model". The final part of the input comprises the generation of water pressures and initial effective stresses to set the initial state.

3.3.1 Types of elements

There are two types of triangular elements available in Plaxis, the 6-node triangular element and the 15-node triangular elements. The 15-node element is more accurate, giving a smoother stress distribution in the soil, however, the calculation process is very time-consuming. When numerous elements are required, the 6-node element is an efficient selection.

3.3.2 Geometry

The generation of a finite element model starts with a geometry model, consisting of points, lines and clusters, representing the problem of interest. Points and lines are entered by the user, whereas clusters are generated by the program. Second, structural objects or special conditions are assigned to the geometry model.

Wall and plates

A beam in Plaxis is a structural object used to model slender structures with a flexural rigidity and a normal stiffness. Therefore, since the beam represents a real plate in the out-of-plane direction, it is used to model walls and plates.

Beams are composed of beam elements with two degrees of freedom for displacement and one for rotation. The input parameters required to describe the beam are the flexural rigidity, EI, and the axial stiffness, EA.

Geotextiles

Geotextiles are used to model soil reinforcement that has no compressive resistance The normal stiffness is input as a parameter to calculate the tensile force in the material.

Node to node anchors

Node-to-node anchors are used to model a spring tie between two points. They are a two-node elastic spring element that can undergo tension and compression. The input parameter is a constant spring stiffness.

Fixed end anchors

Fixed-end anchors are similar to node-to-node anchors, except one end of the spring is fixed.

Tunnels

Tunnels are used to represent circular and non-circular tunnels in the ground. It is built of arcs having a radius and a radial angle increment.

Interface

Soil-structure interfaces are modelled in Plaxis by applying an interface geometry line. The interface behaviour is modelled in Plaxis by an elasto-plastic model. The Mohr-Coulomb failure criterion differentiates the elastic displacements from the plastic slip. The interface exhibits elastic behaviour when the shear stress, τ, is:

$$|\tau| < \sigma_n \tan\delta + c_a \tag{3.1}$$

where: σ_n is the normal stress

δ is the friction angle of the interface

c_a is the adhesion of the interface

The soil behaviour is plastic when both sides of Eq. 3.1 are equal.

The friction angle, cohesion, and dilatancy angle of the interface are obtained from the soil properties and a strength reduction factor, R_{int}, in the following manner.

$$c_a = R_{\text{int}} c_{soil} \tag{3.2}$$

and

$$\tan\delta = R_{\text{int}} \tan\phi_{soil} \tag{3.3}$$

$$\psi_i = 0 \text{ for } R_{int} < 1, \text{ otherwise } \psi_i = \psi_{soil} \tag{3.4}$$

When the interface is elastic, relative displacements perpendicular to the interface and parallel to the interface occur. The magnitudes of these displacements are:

$$\textit{Elastic normal displacement} = \frac{\sigma t_i}{E_{oed,i}} \tag{3.5}$$

and

$$\textit{Elastic distortion} = \frac{\tau t_i}{G_i} \tag{3.6}$$

where: $E_{oed,i}$ is the one-dimensional compression modulus of the interface
G_i is the shear modulus of the interface
t_i is the virtual thickness of the interface

The shear and compression moduli are related by the expressions:

$$E_{oed,i} = 2G_i \frac{1-\nu_i}{1-2\nu_i} \qquad G_i = R_{\text{int}}^2 G_{soil} \le G_{soil} \qquad \nu_i = 0.45 \tag{3.7}$$

The virtual thickness as stated by Plaxis (1998) is an imaginary dimension used to obtain the material properties of the interface and is defined as the virtual thickness factor times the average element size. The average element size is determined by the global coarseness setting for the mesh generation.

Prescribed displacement

Prescribed displacements are imposed on geometry lines to control their displacements. During calculations, the magnitude of the prescribed displacement is the product of the input value and the load multiplier entered in the Calculations program, *Mdispl*.

Tractions

Tractions are distributed loads applied to geometry lines. During calculations, the magnitude of traction loads is the product of the input value and the load multiplier, *MloadA* and *MloadB*.

Point forces

Point forces are concentrated forces that act on a geometry point and represent a line load in the out-of-plane direction. During calculations, the magnitude of point forces is the product of the input value and the load multiplier, *MloadA* and *MloadB*.

Mesh generation

Manual mesh generation is very time-consuming. Plaxis saves precious time by automatically generating the finite element mesh based on the geometry model. A global coarseness can be applied and a local mesh coarseness parameter is available to refine the mesh in areas where it is expected to have large stress concentrations and large displacements. The local coarseness parameter is set by the local element size factor for each geometry point. Also, the mesh can be refined around specific structural objects, interfaces, and individual soil clusters.

3.4 Calculations program

The Calculations program executes three types of finite element calculations, namely a Plastic calculation, a Consolidation analysis and an Updated mesh analysis. The calculation process is divided into calculation phases to separately perform cases such as activating a load system or prescribed displacement, simulating a construction stage,

introducing a consolidation period, or calculating a safety factor. The calculation phase is then divided into calculation steps, to apply the load in small increments, to correctly simulate the non-linear behaviour of soil. Plaxis has an automatic load stepping procedure that determines the proper load increments.

3.4.1 Types of calculation

Plastic calculation

This calculation executes an elastic-plastic deformation analysis. Its stiffness matrix is based on the original generated mesh. Therefore, this calculation is appropriate for cases where only small deformations are expected.

Consolidation analysis

A consolidation analysis analyzes the development and dissipation of excess pore pressures as a function of time. It is applied when the material of the model includes saturated clay-type soils.

Updated mesh analysis

This analysis performs a plastic calculation. The stiffness matrix is based on the deformed geometry, as opposed to the Plastic calculation, by updating the mesh. It is appropriate to use this calculation when large deformations, as for soft soils, are expected to occur.

3.4.2 Types of load steps

The non-linear behaviour of soil is accurately modelled by applying small load increments. To achieve this, the calculation in Plaxis is performed by one of three load step procedures. For plastic calculations a selection can be made between Manual control and Load advancement (ultimate level or number of steps). For consolidation analysis the Automatic time stepping procedure is to be used.

Manual control

This procedure allows the user to manually input the magnitude of the load step. It is crucial to ensure that the step size is not too large, otherwise too many iterations will be required for equilibrium and the solution might even diverge.

Load advancement

Small load increments require many calculation steps while large increments need excessive iterations to reach equilibrium, both of which are time-consuming. Plaxis features an automatic load step procedure that optimizes the step size to obtain an efficient calculation process. The Load advancement ultimate level and the Load advancement number of steps use the automatic loading step procedure, presented below from the Plaxis user manual.

When the first calculation step is applied, a series of iterations are carried out in order to reach equilibrium. There are three possible outcomes of this particular process. These outcomes are:

1. If the solution reaches equilibrium within a number of iterations that is less than the desired minimum control parameter, then the calculation step is assumed to be too small. In this case, the size of the load increment is multiplied by two and further iterations are applied to reach equilibrium.

2. If the solution fails to converge within the desired maximum number of iterations, then the calculation step is assumed to be too large. In this case, the size of the load increment is reduced by a factor of two and the iteration procedure is continued.

3. If the number of required iterations lies between the desired minimum and the desired maximum, then the size of the load increment is assumed to be satisfactory. After the iterations are complete, the next calculation step begins. The initial size of this calculation step is made equal to the size of the previous successful step.

Ultimate level

This option terminates the calculation when one of the following three cases is satisfied: (1) the number of additional calculation steps is reached, (2) a user-specified load level is applied, or (3) a failure load is reached.

Number of steps

In this option the number of additional calculation steps is always fully performed, even if failure is reached during the calculation. Hence, the load level is only determined at the end of the calculation.

Automatic time stepping

When performing a consolidation analysis, the Automatic time stepping procedure selects appropriate time steps. The time steps are increased if too few iterations are required per step, or decreased when excessive iterations are required due to an increasing amount of plastic deformation.

3.4.3 Selection of displacement and stress points

Nodal points and stress points, at desired locations on the generated mesh, can be selected to generate load-displacement curves, stress paths and stress-strain diagrams.

3.5 Output program

The Output program gives a graphical output of the deformations and the stresses in the soil and interface, as well as the forces in structural elements.

3.5.1 Deformations

Deformations are visualized by a deformed mesh superimposed on the initial geometry and by the total or incremental displacements and strains (horizontal and vertical) displayed as vectors, contour lines or shaded areas. Compression is negative.

3.5.2 Stresses

The total and effective stresses can be illustrated as principal stresses, where the length and direction of each line in the plot represents the magnitude and the direction of the principal stress. Also, they can be presented as contour lines or shaded areas of the mean stress and relative shear stress. Compression is negative.

Relative shear stress

The relative shear stress indicates the proximity of the stress point to the failure envelope and is equal to τ/τ_{max}, where τ is the shear stress and τ_{max} is the maximum value of shear stress for the case where the Mohr's circle is expanded to touch the Coulomb failure envelope.

3.6 Curve program

The Curves program generates load or time versus displacement curves, stress-strain diagrams and stress or strain paths. These curves can be further used to analyze the local behaviour of the soil.

CHAPTER 4
MODELLING OF SAND BEHAVIOUR BY THE HARDENING-SOIL MODEL

4.1 Experimental drained triaxial tests

4.1.1 Soil description

The soil samples consisted of a medium size crushed quartz sand. The grain size distribution of the sand is illustrated in Figure 4.1 and the general properties are described in Table 4.1. The minimum void ratio was determined according to ASTM standard D4252-91 and the maximum void ratio according to D4253-93.

Table 4.1 Soil properties

Soil type	Mean grain size, D_{50} (mm)	Minimum unit weight, γ_{min} (kN/m^3)	Maximum unit weight, γ_{max} (kN/m^3)	Minimum void ratio, e_{min}	Maximum void ratio, e_{max}	Uniformity coefficient C_u
Medium crushed quartz sand	0.6	13.12	16.06	0.65	1.02	2.06

4.1.2 Experimental data and strength parameters

Three consolidated drained triaxial tests were performed under a series of confining pressures, σ_3 = 100 kPa, 200 kPa, and 300 kPa. The sand samples were medium dense with relative densities of 46.8% for σ_3 = 100 kPa, 44.6% for σ_3 = 200 kPa, and 42.4% for σ_3 = 300 kPa. During the test, readings of the axial load, the axial displacement and the volume change were taken. The tests were conducted until the axial strain reached approximately 12%.

The deviatoric stress versus axial strain curves for the three drained triaxial tests under various confining pressures are presented in Figure 4.2. It is observed from these curves that the experimental ultimate deviatoric stresses are 330 kPa at σ_3 = 100 kPa, 605 kPa at σ_3 = 200 kPa, and 897 kPa at σ_3 = 300 kPa.

The volumetric strain versus axial strain curves for the three drained triaxial tests are presented in Figure 4.3. The sand sample under σ_3 = 100 kPa, was compressing until the axial strain of 1.5% was reached and henceforth, began dilating. On the other hand, the sand samples under σ_3 = 200 kPa and 300 kPa, compressed without any dilation. The sample at σ_3 = 200 kPa reached a constant volumetric strain of 1.14% at 5.59% axial strain and the sample at σ_3 = 300 kPa reached a constant volumetric strain of 2.87% at 10.89% axial strain.

The Mohr circles corresponding to failure, based on the ultimate deviatoric stresses, are sketched in Figure 4.4. The angle of the failure envelope represents the internal friction angle of the medium crushed quartz sand and was measured to be 37.0°. The intercept of the failure envelope line with the shear stress axis represents the cohesion. There is no cohesion, as is typical for sands.

An alternative method to determine the internal friction angle and cohesion of a soil, other than the Mohr circles, is by plotting the p-q graph where $p = (\sigma_{1f}+\sigma_3)/2$ and $q = (\sigma_{1f}-\sigma_3)/2$. The line joining the points corresponding to various stress states is called the K_f-line. The angle of the K_f-line, ψ_{p-q}, is related to the internal friction angle by $\sin\phi = \tan\psi_{p-q}$. The cohesion is related to the intercept of the K_f-line with the y-axis. As is shown in Figure 4.5, the internal friction angle of the medium crushed quartz sand was found to be 37.0° and there is no cohesion.

4.2 Determination of Hardening-soil model parameters from triaxial tests

Dilatancy angle, ψ

The dilatancy angle, ψ, is determined from the volumetric strain versus axial strain curve of the drained consolidated triaxial test. When the soil sample no longer compresses, the part of the curve corresponding to dilation, according to the Hardening-soil model, becomes linear. The slope of this linear section of the curve is defined in terms of the dilatancy angle by $2\sin\psi/(1-\sin\psi)$ as shown in Figure 2.12.

From Figure 4.3, the dilatancy angle of the sand sample is 4° at σ_3 = 100 kPa and 0° at σ_3 = 200 kPa and 300 kPa.

Secant modulus, E_{50}^{ref}

The first step to determine the reference secant modulus for drained triaxial test, E_{50}^{ref}, for a reference confining pressure, p^{ref}, is to calculate the ultimate deviatoric stress, q_f, using Eq. 2.15 and a friction angle of 37°. Accordingly, the ultimate deviatoric stress was found to be 302 kPa at σ_3 = 100 kPa, 605 kPa at σ_3 = 200 kPa, and 907 kPa at σ_3 = 300 kPa. Subsequently, as illustrated in Figure 2.11, a point on the deviatoric stress versus axial strain curve is placed at half the value of the ultimate deviatoric stress. A line joining this point and the point (0,0) is drawn. The slope of this line is the reference secant modulus for a reference confining pressure.

As measured from Figure 4.6, the secant modulus of the sand sample was calculated to be 41,970 kPa for a reference confining pressure of 100 kPa, 23,434 kPa for p^{ref} = 200 kPa, and 22,670 kPa for p^{ref} = 300 kPa.

Other parameters

The tangent modulus for primary oedometer loading, E_{oed}^{ref}, is set equal to E_{50}^{ref} by default in Plaxis. Hence, E_{oed}^{ref} = 41,970 kPa for p^{ref} = 100 kPa, 23,434 kPa for p^{ref} = 200 kPa, and 22,670 kPa for p^{ref} = 300 kPa.

The unloading/reloading modulus, E_{ur}^{ref}, is set equal to $3E_{50}^{ref}$ by default in Plaxis. Therefore, E_{ur}^{ref} = 125,910 kPa for p^{ref} = 100 kPa, 70,302 kPa for p^{ref} = 200 kPa, and 68,010 kPa for p^{ref} = 300 kPa.

The power for stress-level dependency of modulus, m, is typically set to 0.5 for sands (Plaxis, 1998). Poisson's ratio for unloading/reloading, ν_{ur}, is typically set by default to 0.2 in Plaxis. The failure ratio, R_f, by default in Plaxis is 0.9.

Summary of model parameters

Table 4.2 summarizes the model parameters for the Hardening-soil model for various confining pressures of the experimental consolidated drained triaxial tests.

Table 4.2 Summary of model parameters for Hardening-Soil model

	Set 1	Set 2	Set 3
p^{ref} (kPa)	100	200	300
c (kPa)	0	0	0
ϕ (degree)	37	37	37
ψ (degree)	4	0	0
E_{50}^{ref} (kPa)	41,970	23,434	22,670
E_{oed}^{ref} (kPa)	41,970	23,434	22,670
m	0.5	0.5	0.5
E_{ur}^{ref} (kPa)	125,910	70,302	68,010
ν_{ur}	0.2	0.2	0.2
R_f	0.9	0.9	0.9

4.3 Comparison of experimental results and model predictions

In this section, the three sets of parameters listed in Table 4.2 will be used to model the sand behaviour under drained triaxial conditions. The resulting deviatoric stress versus axial strain curves and volumetric strain versus axial strain curves will then be compared to the experimental drained triaxial test results. The set of model parameters that best models, on average, the experimental triaxial test results will be used for further analysis.

4.3.1 Deviatoric stress versus axial strain curves

Each set of parameters is used to model the behaviour of sand in drained triaxial conditions for three confining pressures of σ_3 = 100 kPa, 200 kPa, and 300 kPa. The secant modulus, E_{50}, is calculated using Eq. 2.16 for increments of deviatoric stress, q, beginning from 0 kPa up to the ultimate deviatoric stress, q_f. Corresponding axial strain, ε_1, is determined using Eq. 2.14. The deviatoric stress versus axial strain curves using the Hardening-soil model, are plotted in Figure 4.7 for parameter set 1 from Table 4.2, in Figure 4.8 for set 2, and in Figure 4.9 for set 3. The experimental deviatoric stress versus axial strain curves are also plotted on the same graphs for comparison.

Parameter set 1 based on the test results corresponding to the confining pressure of 100 kPa does not predict well the experimental results for a confining pressure of 200 kPa and 300 kPa. The sand sample was denser than the sand samples for a confining pressure of 200 kPa and 300 kPa, which results in a steeper slope than the observed results. Parameter set 2 gives good model predictions in comparison to the experimental results. Parameter set 3 also gives good results, however, the ultimate deviatoric stress is reached at an axial strain larger than the observed results.

Therefore, based on the deviatoric stress versus axial strain curves, it seems that parameter set 2 would be most suitable to model the behaviour of the soil.

4.3.2 Volumetric strain versus axial strain curves

The secant modulus, E_{50}, and the axial strain, ε_1, for increments of deviatoric stresses, q, are calculated as indicated in section 4.3.1. The total volumetric strain, ε_v, is the addition of the elastic component, ε_v^e, and the plastic component, ε_v^p. The elastic component is the sum of the elastic normal strains, ε_1^e, ε_2^e, and ε_3^e, which are determined using Eq. 2.24. The incremental plastic component is related by a factor of $\sin\psi_m$ to the incremental plastic shear strain, γ^p, as stated in Eq. 2.26. The total plastic shear strain is obtained from Eq. 2.20 for drained triaxial tests and is divided into increments for corresponding deviatoric stress increments. The critical state angle, ϕ_{cv}, and the mobilized friction angle, ϕ_m, are determined using Eqs. 2.27a and 2.28, respectively. The mobilized dilatancy angle, ψ_m, is calculated by Eq. 2.27. The plastic volumetric strain increments are summed for each deviatoric stress to give the plastic volumetric strain component.

The resulting volumetric strain versus axial strain curves using the Hardening-soil model, are shown in Figure 4.10 for parameter set 1 from Table 4.2, in Figure 4.11 for set 2, and in Figure 4.12 for set 3. The experimental volumetric strain versus axial strain curves are also plotted on the same graphs for comparison.

Parameter set 1 based on the confining pressure of 100 kPa does not predict well the experimental results for confining pressures of 200 kPa and 300 kPa. The sand sample of this set was denser than the sand samples for a confining pressure of 200 kPa and 300 kPa. As a result, this set models the volumetric strain for the other confining pressures by predicting that the samples will dilate after a certain axial strain, which is not the case for the observed results. Parameter sets 2 and 3 also do not produce results that match the experimental results very well, which shows that the model can be further improved.

Parameter set 2 gives slightly better predictions on average for the three confining pressures.

4.3.3 Model parameters for the Hardening-soil model

The model parameter set 2 from Table 4.2 is illustrated to be the best out of the three sets to represent the sand behaviour, based on the experimental drained triaxial tests. Henceforth, these model parameters will be used in the analysis of interfaces using the Plaxis finite element code.

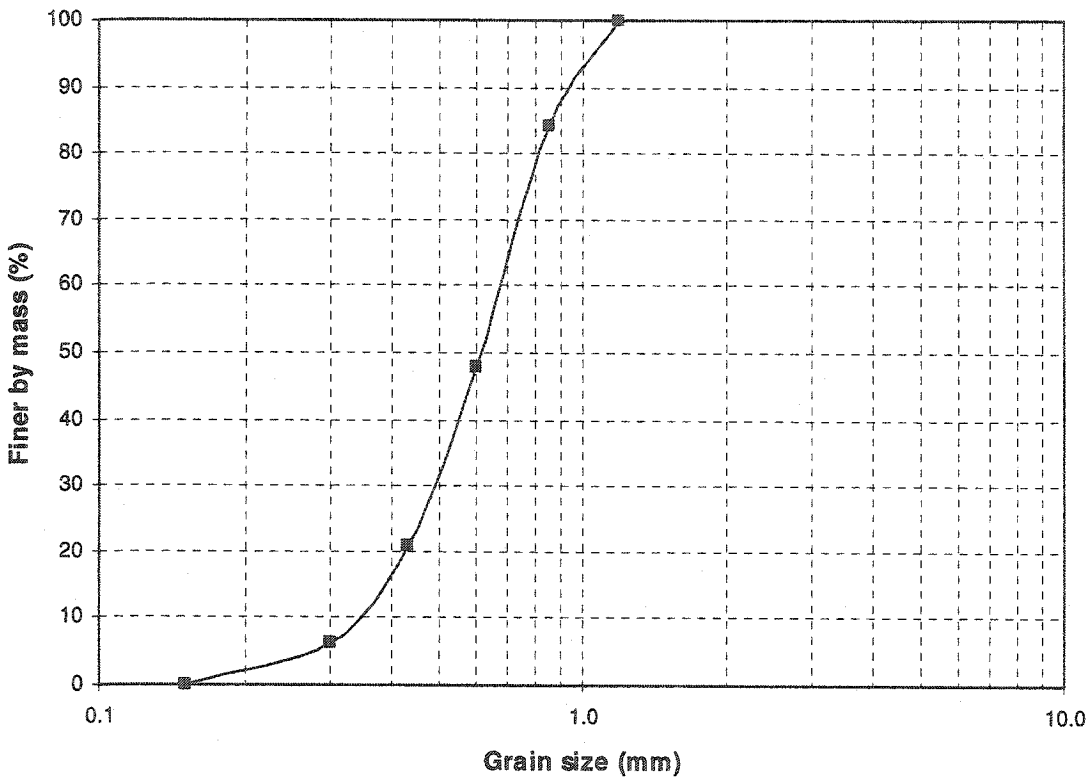

Figure 4.1 Grain size distribution of medium crushed quartz sand

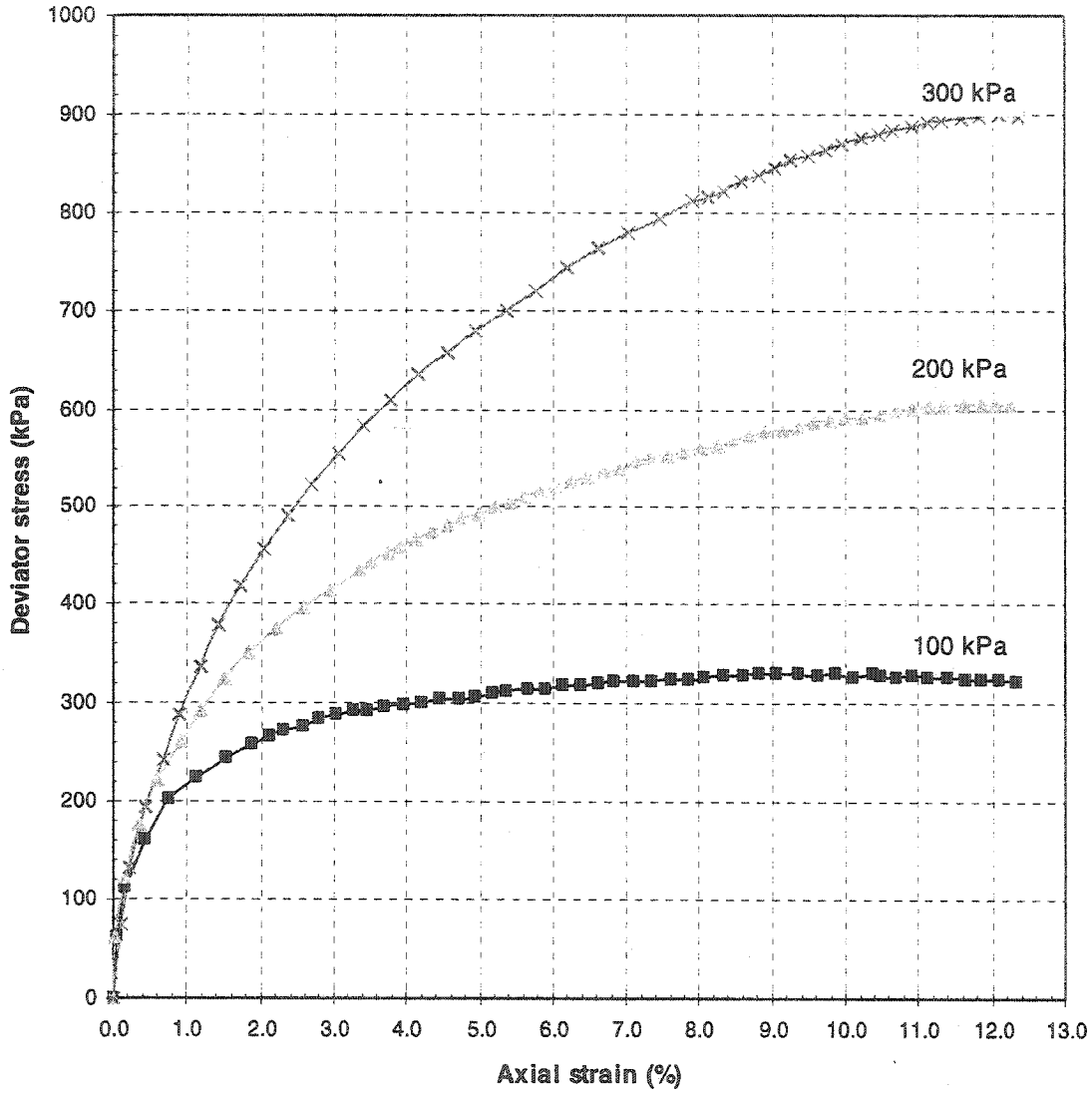

Figure 4.2 Experimental stress-strain curves for consolidated drained triaxial tests at various confining pressures

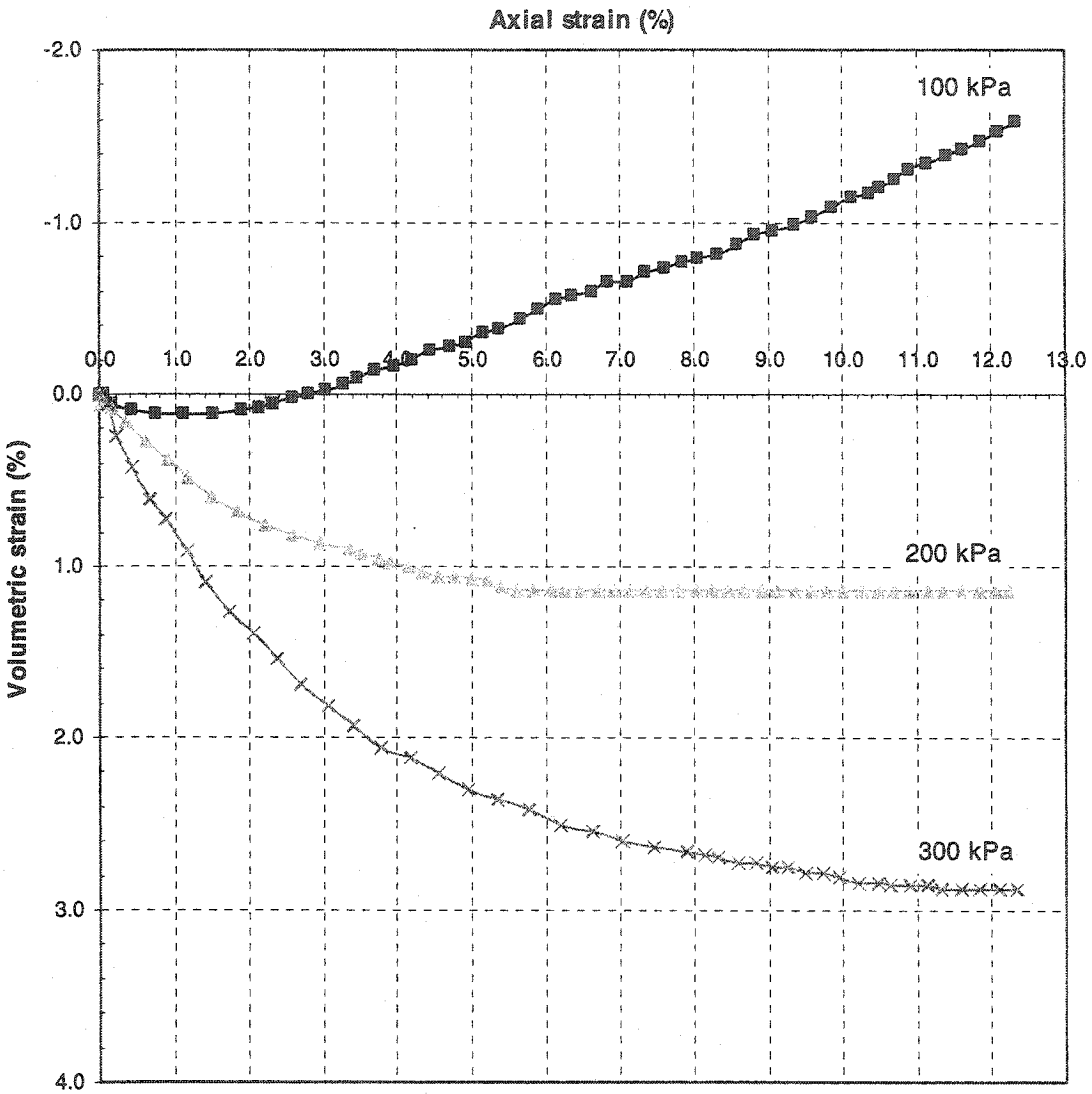

Figure 4.3 Experimental volumetric-axial strain curve for drained triaxial tests at various confining pressures

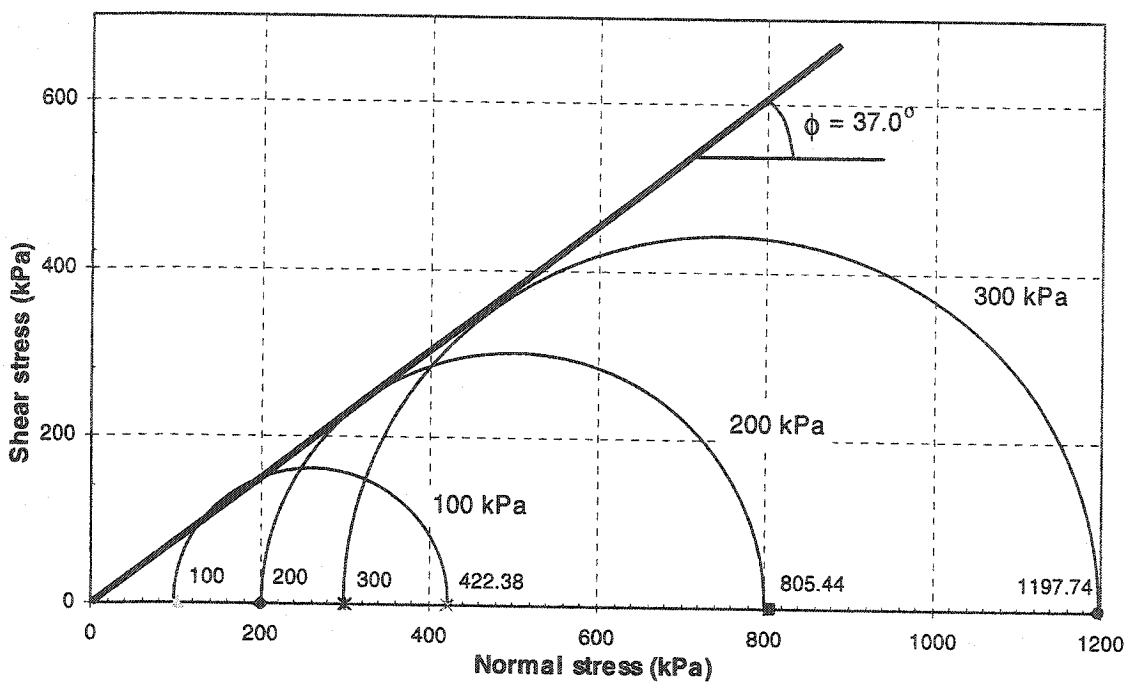

Figure 4.4 Mohr circles at failure for drained triaxial tests at various confining pressures

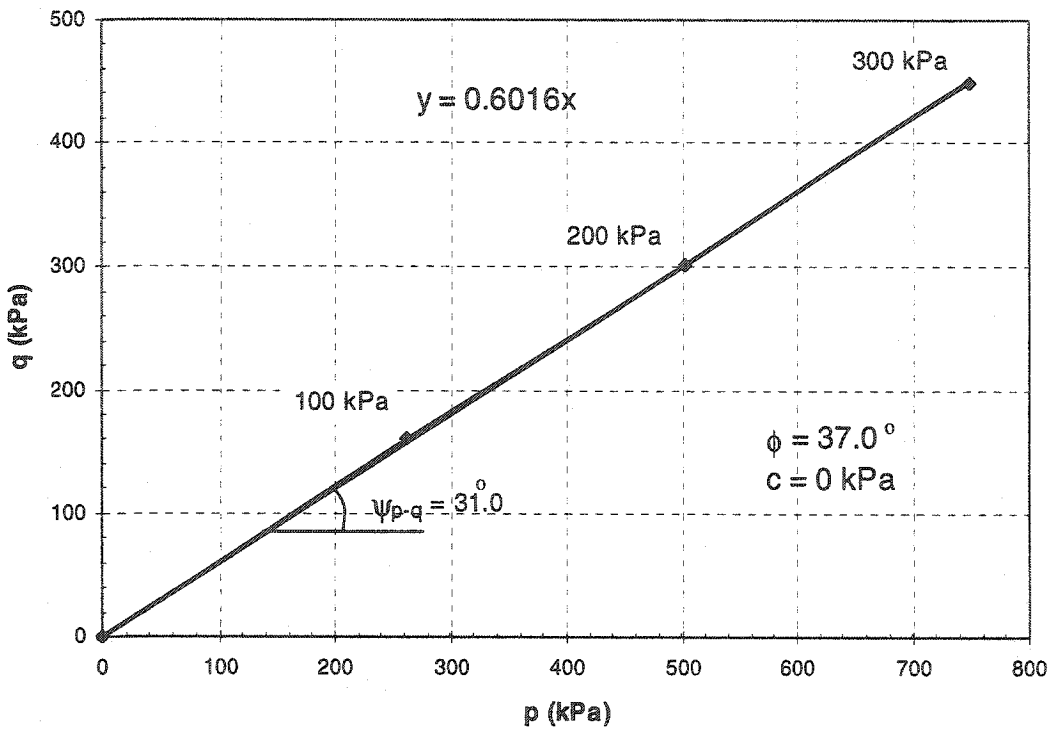

Figure 4.5 p-q graph representing the failure envelope for drained triaxial tests at various confining pressures

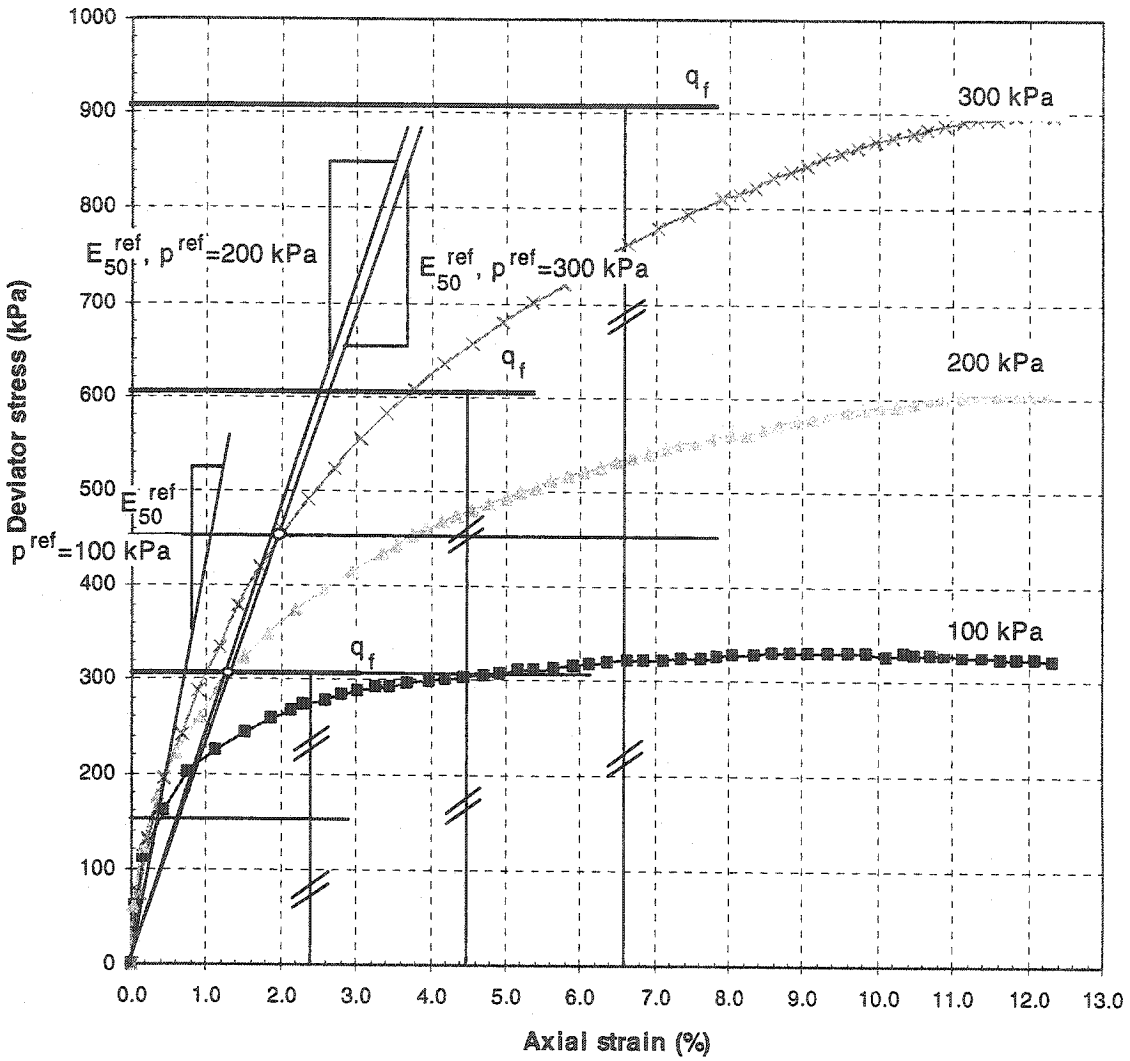

Figure 4.6 Graphical determination of the secant stiffness, E_{50}^{ref}, at various reference confining pressures

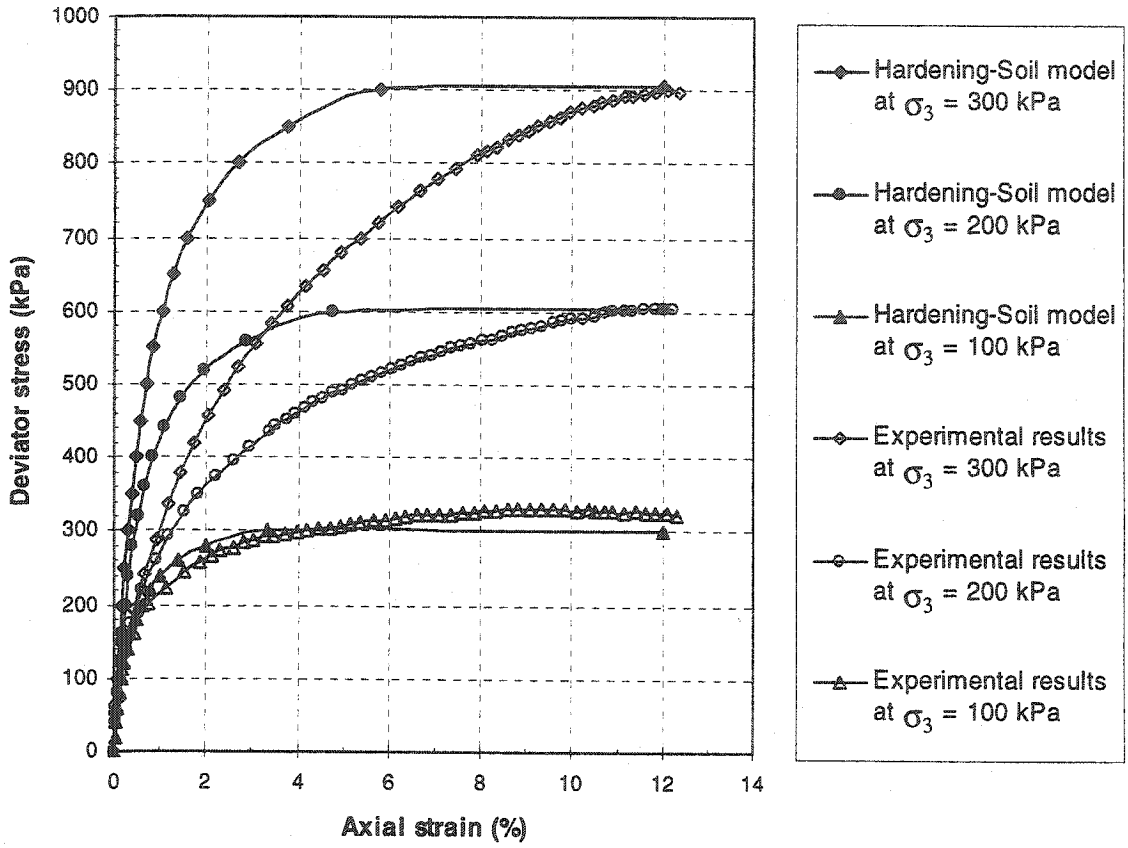

Figure 4.7 Comparison of deviator stress versus axial strain curves, between results of the Hardening-soil model and the experimental drained triaxial tests for parameter set 1 from Table 4.2

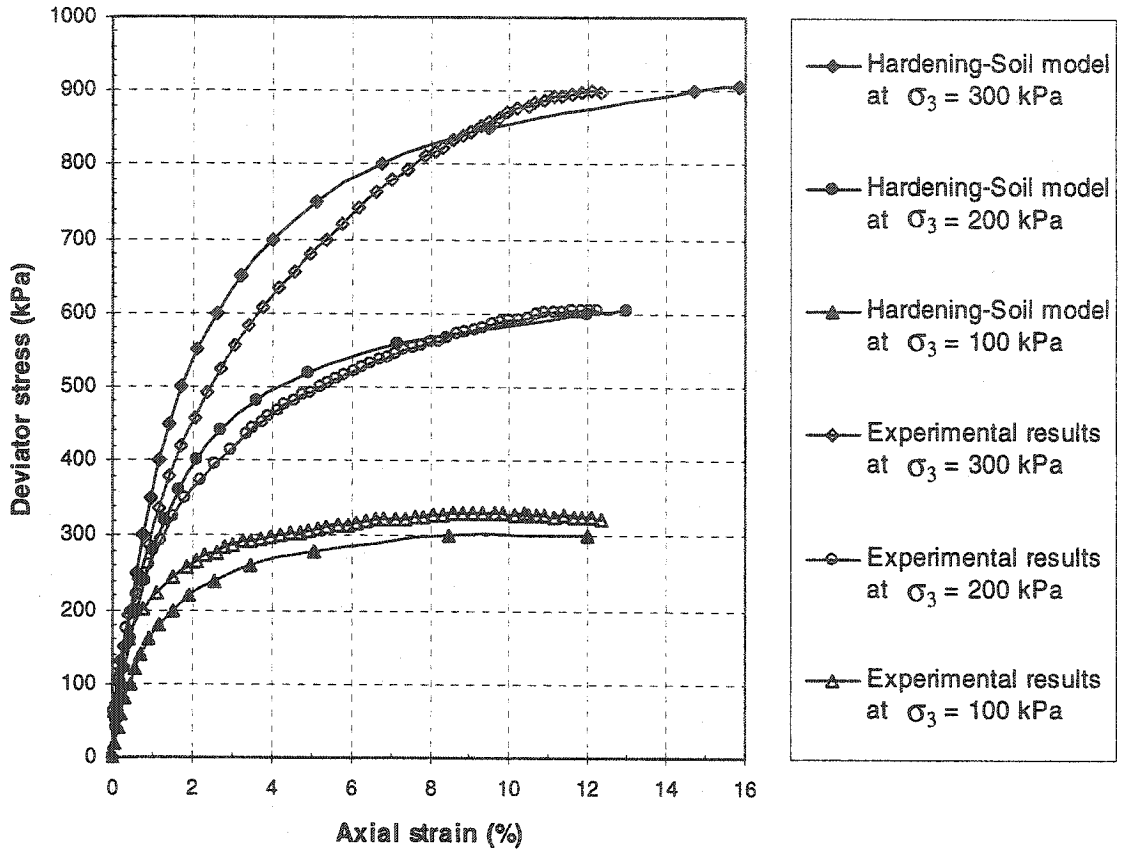

Figure 4.8 Comparison of deviator stress versus axial strain curves, between results of the Hardening-soil model and the experimental drained triaxial tests for parameter set 2 from Table 4.2

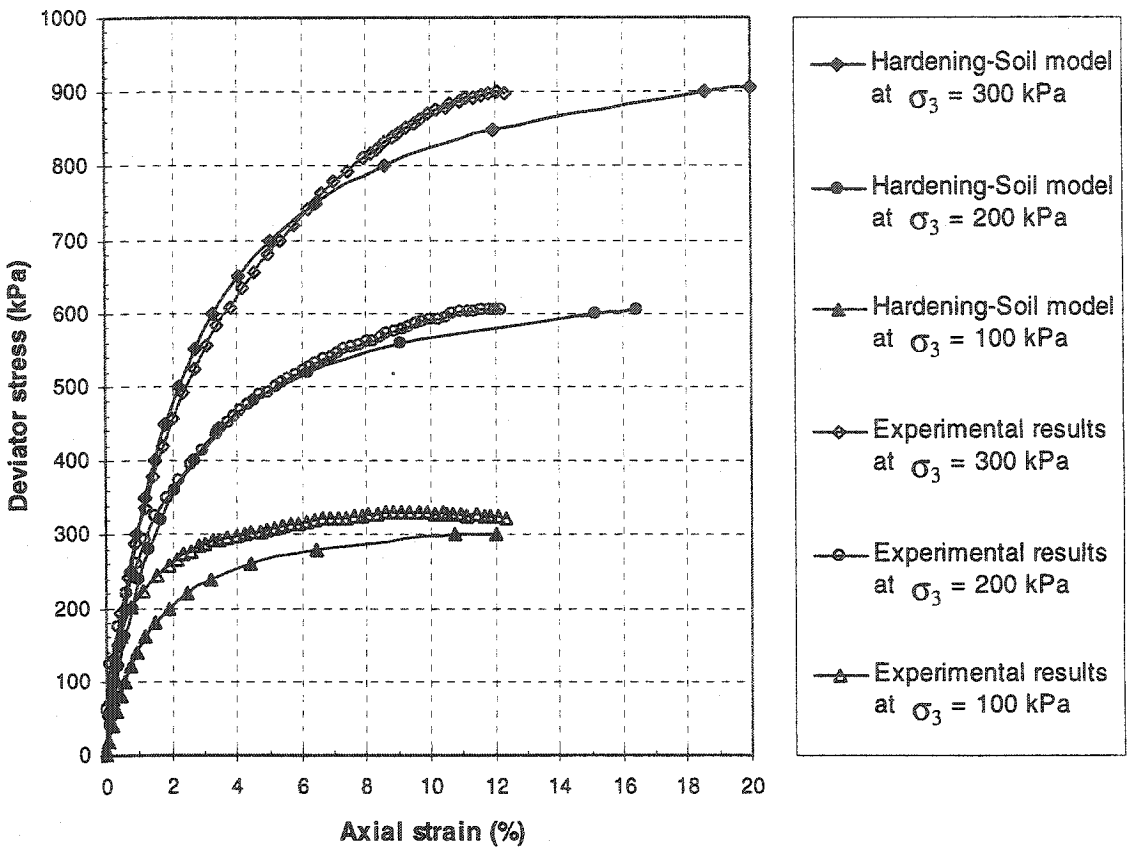

Figure 4.9 Comparison of deviator stress versus axial strain curves, between results of the Hardening-soil model and the experimental drained triaxial tests for parameter set 3 from Table 4.2

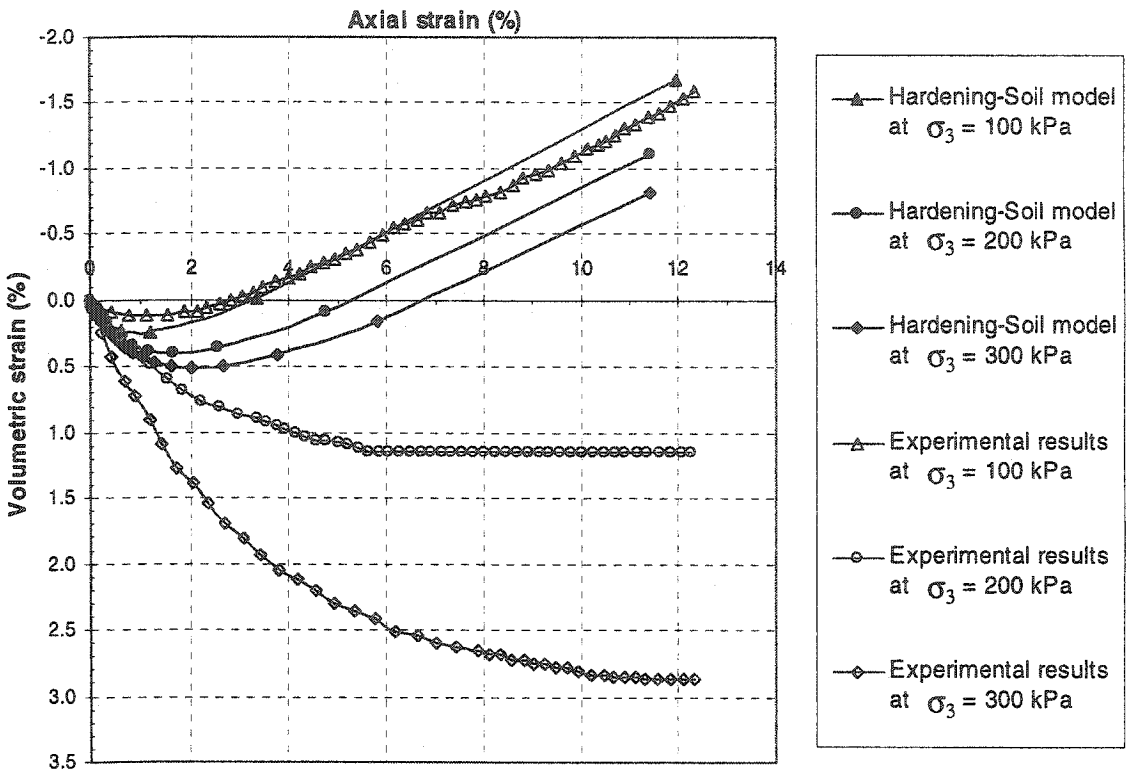

Figure 4.10 Comparison of volumetric strain versus axial strain curves, between results of the Hardening-soil model and the experimental drained triaxial tests for parameter set 1 from Table 4.2

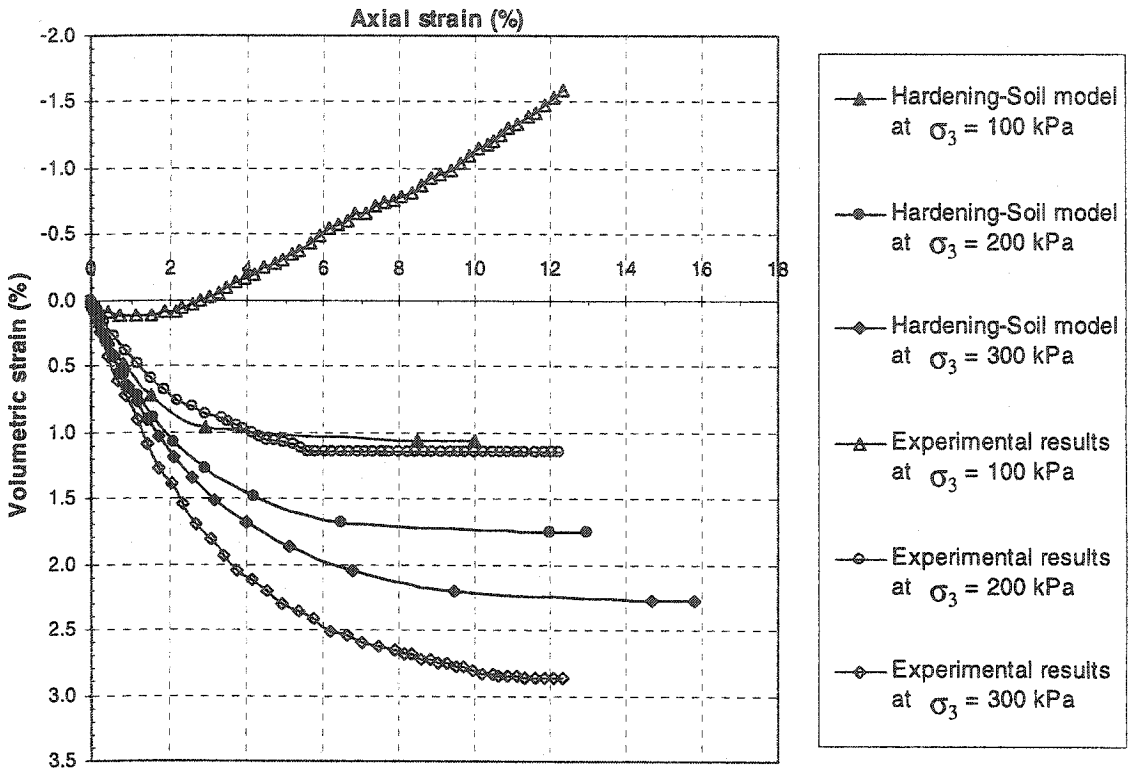

Figure 4.11 Comparison of volumetric strain versus axial strain curves, between results of the Hardening-soil model and the experimental drained triaxial tests for parameter set 2 from Table 4.2

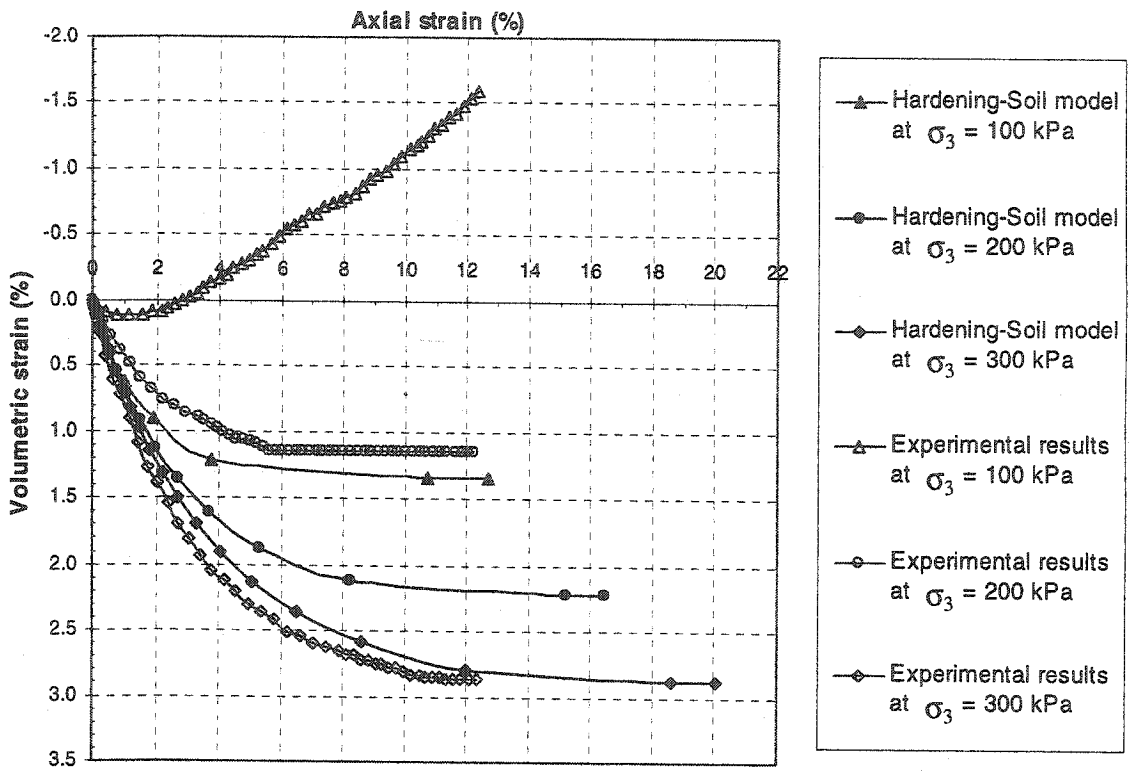

Figure 4.12 Comparison of volumetric strain versus axial strain curves, between results of the Hardening-soil model and the experimental drained triaxial tests for parameter set 3 from Table 4.2

CHAPTER 5
EXPERIMENTAL OBSERVATIONS OF SAND-CONCRETE INTERFACE BEHAVIOUR

5.1 Sand and concrete interface tests

To characterize interface behaviour and determine the shear strength parameters, direct shear type tests were conducted. Three tests were performed on sand-concrete interfaces over a range of constant normal stresses.

5.1.1 Test apparatus

A 3-D interface testing device, C3DI, developed and described by Evgin and Fakharian (1996) was used for testing. The apparatus is schematically illustrated in Figure 5.1. The main components of the apparatus are the loading system, the data acquisition system, and the soil containers. The operation of the C3DI is automated by a computer controlled system, BENCHMATE.

The loading system of C3DI consists of a vertical loading unit, a horizontal loading unit, and a reaction frame. The vertical loading unit is a pneumatic actuator which applies the normal load in the y-direction. The horizontal loading unit comprises of an X-Z loading table controlled by two ball screw stepper motors capable of applying monotonic loads, as well as displacement or load controlled cyclic shears in the x and z-directions simultaneously. In this study, displacement-controlled tests were performed in the x-direction with a displacement rate of 1 mm/min. The reaction frame is capable to withstand 2.5 times the maximum applicable normal and tangential loads.

The data acquisition system includes two transducers that measure the applied loads in the x and y-directions and five LVDTs that monitor the displacement in the x and z-direction. In this study, two load transducers and two LVDTs were used to monitor the experiment.

The load transducers were used to measure the normal load in the y-direction and the tangential load in the x-direction. One LVDT was used to measure the tangential displacement in the x-direction, which represents the displacement of the interface plate. The other LVDT was used to measure the displacement in the y-direction representing the height change of the sample.

The soil containers of the apparatus can be either direct shear type or simple shear type. In this study, a direct shear type soil container was used. The direct shear type container is a 25 mm thick, hollow square box, with inside are of 100 mm x 100 mm. The bottom of the aluminium container is sealed with foam to minimize the leakage of sand during shearing. A 1 mm thick sheet of Teflon is glued to the bottom of the foam in order to minimize the friction between the box and the interface plate (structural material). The container is placed on a 300 mm x 300 mm interface plate. The size of the interface plate assures that the interface contact area remains constant during shearing.

5.1.2 Test materials

Soil

The soil used in the study was medium crushed quartz sand. The sand properties are described in Table 4.1.

Structural material

The structural material used in this investigation was concrete, whose mix design is shown in Table 5.1. The concrete plates, shown in Figure 5.2, were produced by casting the concrete directly into a form. The concrete plates were cured for two weeks, in a humidity room under constant temperature of 21°, to allow for the development of adequate strength.

The average roughness of the concrete plate, R_{max}, was 27 μm for five sampling locations and at a length of L = 15 mm.

Table 5.1 Concrete mix design

Materials	Quantity (kg)
Water	1.0
Cement	1.3
Aggregates	5.4

5.1.3 Sample preparation

The direct shear type container was centered on the concrete plate. The sand was carefully scooped and rained smoothly and uniformly into the container with a minimal height. This method resulted in loose to medium dense sand. The relative density of the sand samples ranged between 40-50%. The top surface was then levelled using a suction device. The concrete plate was then fixed to the C3DI loading table. The loading piston of the interface testing device was slowly lowered to touch the sand surface. The LVDTs were then placed on the box to measure displacement.

5.1.4 Test procedure

Once the sample was prepared and placed in the testing device as described in section 5.1.3, the normal load was applied and the initial normal displacement was measured. Before starting the shearing, all LVDTs were reset to zero.

Monotonic tests were performed with a constant normal stress. First, the normal load was applied. Subsequently, the concrete plate was displaced at a rate of 1 mm/min until the total displacement reached was 5 mm in the x-direction. Three interface tests were carried out at constant normal stresses of 100 kPa, 200 kPa, and 300 kPa.

5.1.5 Test results and observations

The relative density of the sand sample was 50.7%, 43.3%, and 46.2% for the 100 kPa, 200 kPa, and 300 kPa constant normal stress, respectively.

The shear stress versus tangential displacement curves for the three tests under various constant normal stresses are presented in Figure 5.3. It is observed from these curves that for a constant normal stress of 100 kPa, the maximum shear stress is 66 kPa which required a tangential displacement of 1.6 mm. For the 200 kPa constant normal stress, the maximum shear stress was 131 kPa attained at a tangential displacement of 2.3 mm, while for the 300 kPa constant normal stress, the maximum shear stress was 191 kPa attained at a tangential displacement of 3.0 mm. In the case of 100 kPa constant normal stress, it can be seen that the shear stress reached approximately 2/3 of its maximum shear stress before a significant displacement. This is probably to some extent due to a higher relative density in comparison to the other sand samples.

The normal displacement versus tangential displacement curves are shown in Figure 5.4. It is observed that the sand samples were compressing until the maximum shear stress was attained. Afterwards, the sand began to dilate. As the constant normal stress increased, it can be seen that the rate of dilation, however, decreased. This behaviour is typical for interfaces between rough surfaces and medium dense sand as observed from various test results. Furthermore, the 100 kPa constant normal stress test is denser that the other two samples, which also contributes to the higher rate of dilation.

The ratio of shear stress to normal stress versus tangential displacement curves are presented in Figure 5.5. The maximum stress ratio was 0.71, 0.67, and 0.65 for the constant normal stress tests of 100 kPa, 200 kPa, and 300 kPa, respectively. It is seen that the stress ratio decreases as the normal stress increases. The high value for the 100 kPa constant normal stress test can partly be attributed to the higher relative density with respect to the sand samples in the other two tests.

Interface strength properties

Figure 5.6 plots the maximum shear stress versus the normal stress. It can be seen that the shear strength increases linearly with the normal stress. The interface friction angle is 32.2°. There is no adhesion between the sand and concrete.

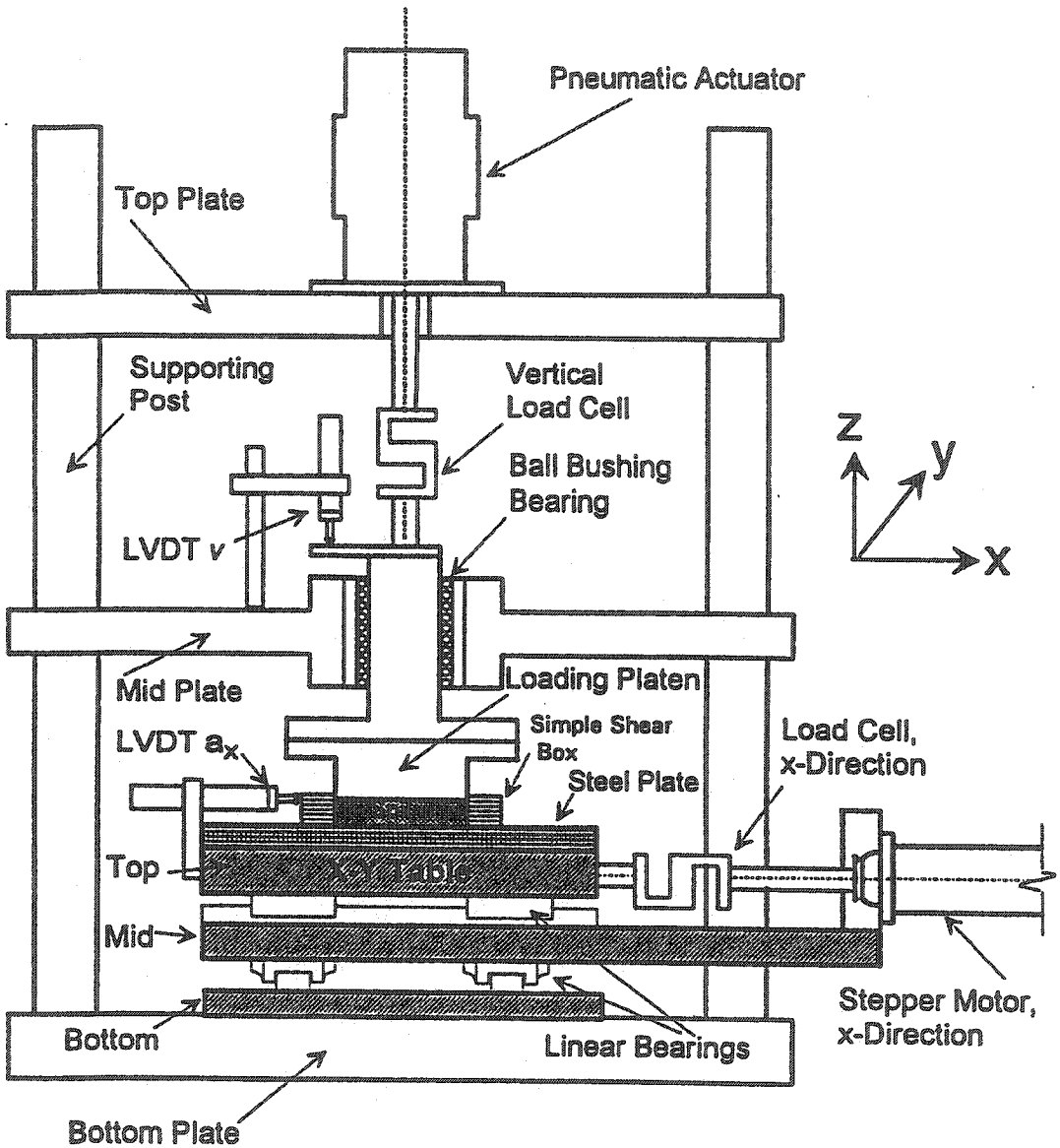

Figure 5.1 Schematic view of the C3DI interface testing device

Figure 5.2 Concrete plates for the direct shear interface test

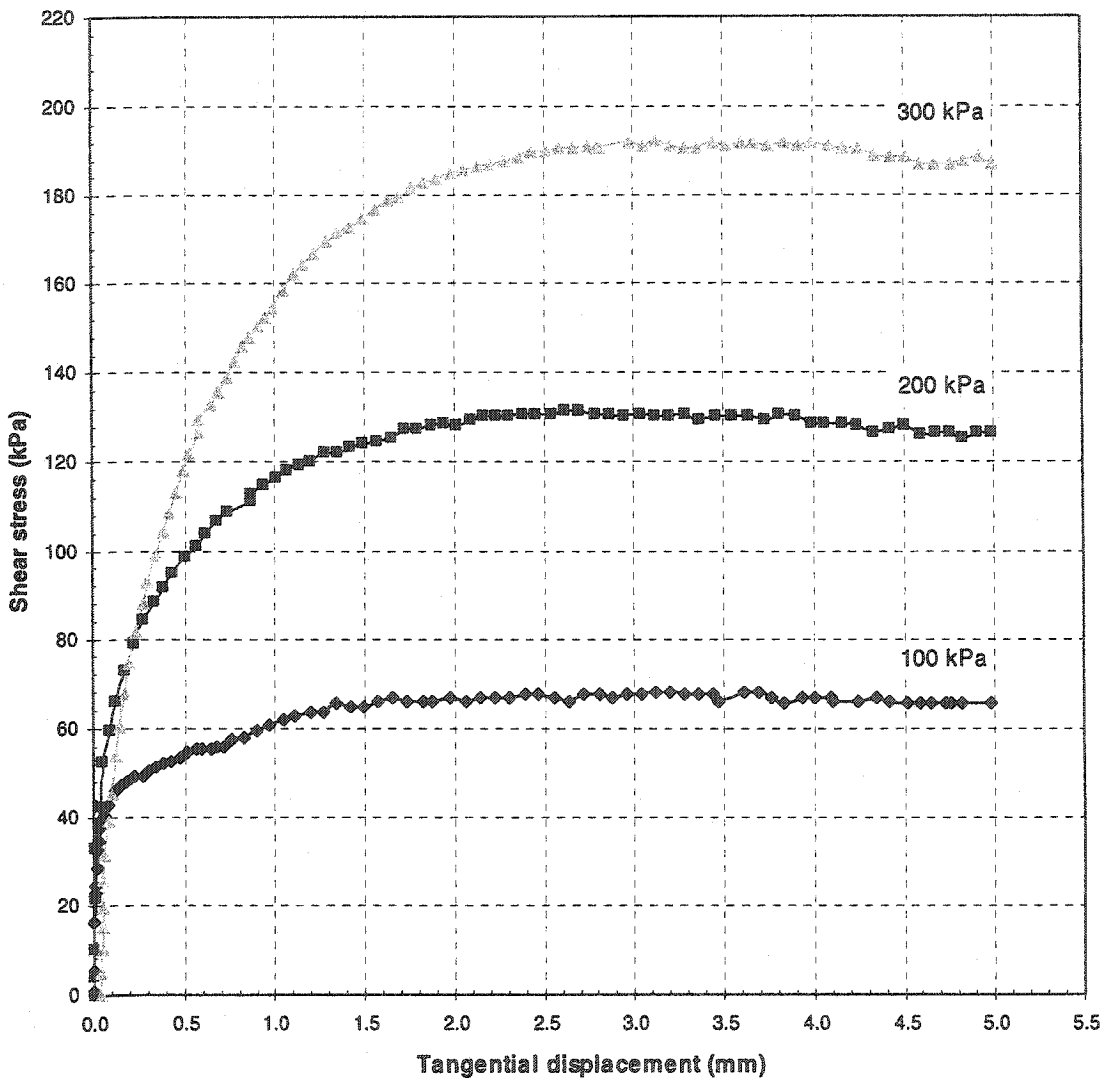

Figure 5.3 Shear stress versus tangential displacement curves of three constant normal stress interface tests

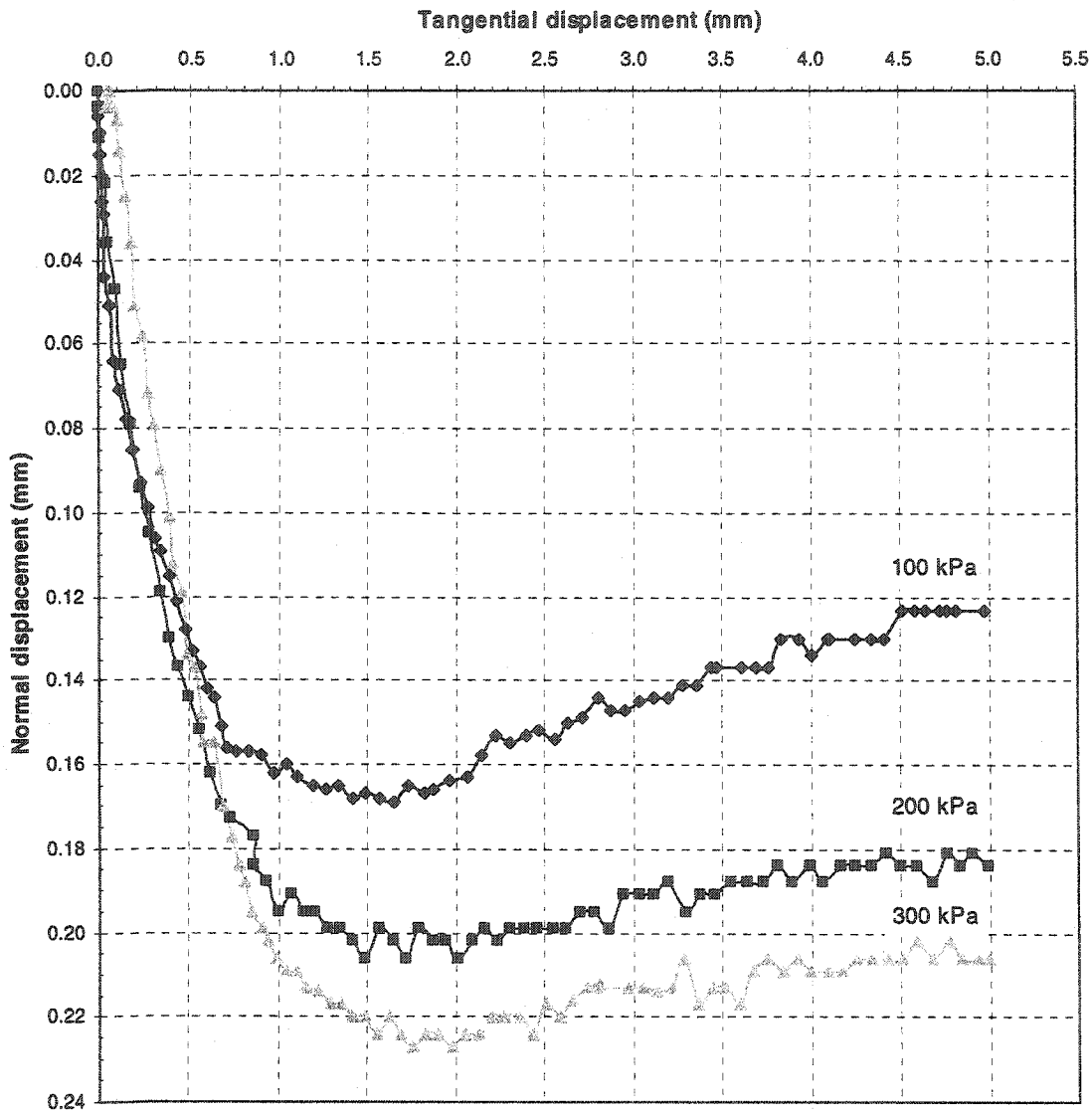

Figure 5.4 Normal displacement versus tangential displacement curves of three constant normal stress interface tests

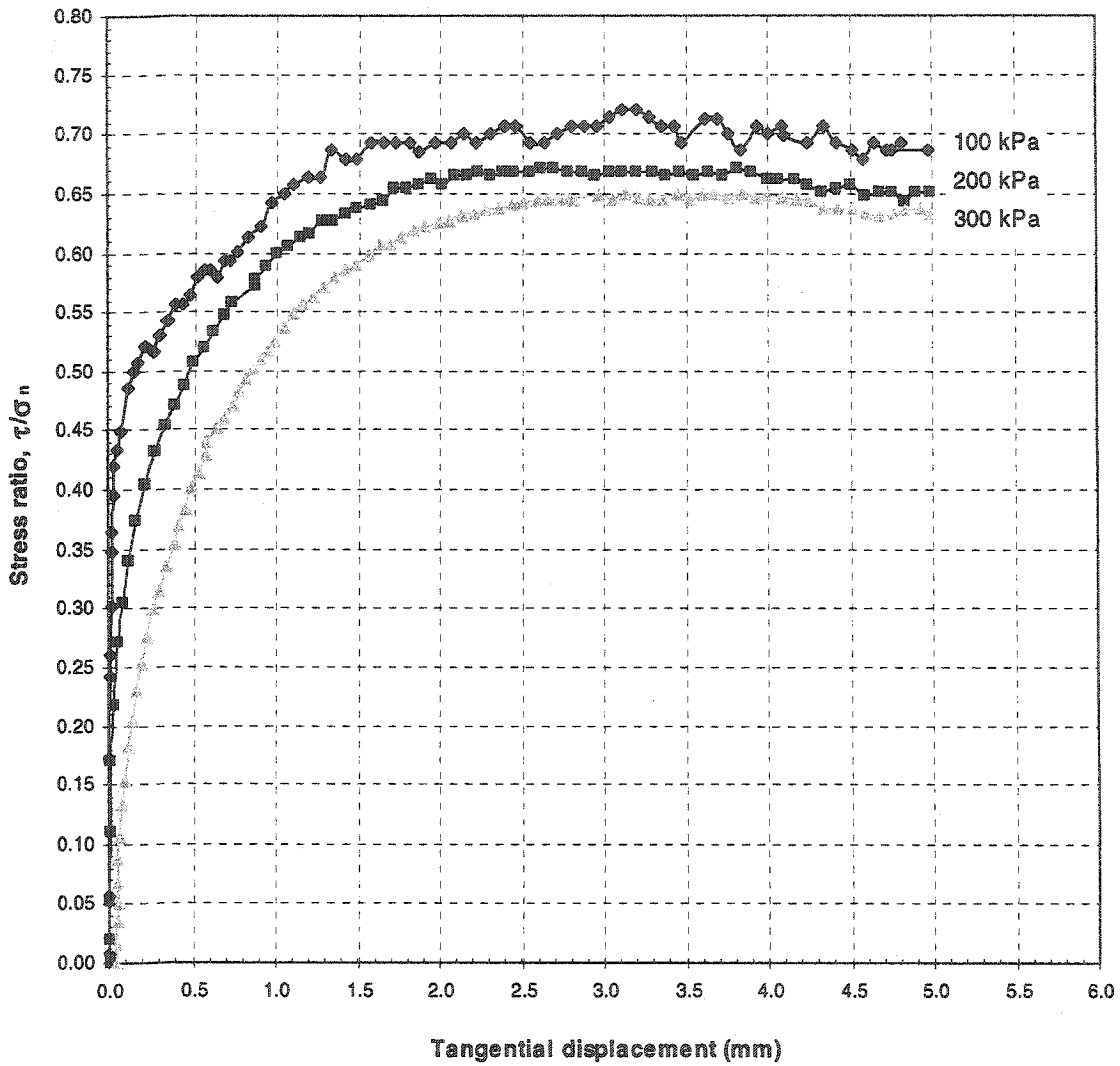

Figure 5.5 Shear to normal stress ratio versus tangential displacement curves of three constant normal stress interface tests

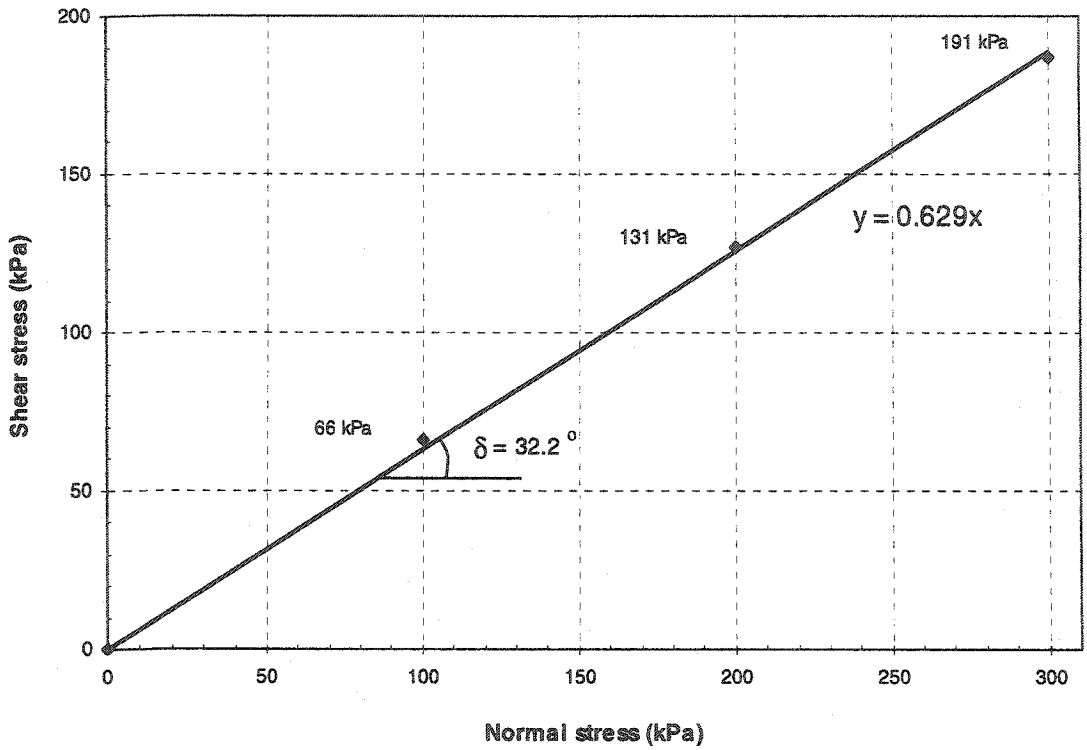

Figure 5.6 Shear stress at failure versus normal stress for the constant normal stress interface tests

CHAPTER 6
TWO-DIMENSIONAL FINITE ELEMENT ANALYSES OF INTERFACE BEHAVIOUR

In this chapter, three direct shear interface tests under a constant normal stress of 100 kPa, 200 kPa, and 300 kPa and a simple shear interface test under a constant normal stress of 300 kPa are simulated using the finite element program Plaxis. Various representations of the soil mass and interface layer are analysed to determine their effect on the predicted results of the interface behaviour. The model predictions of the shear stress, normal displacement, mean stress, relative shear, total volumetric strain, and stresses developed in the interface elements are presented and discussed. Subsequently, a comparison is made between the experimental results, presented in the previous chapter, and the modelled behaviour of the interface.

6.1 Finite element analyses of direct shear interface tests

Four analyses of different geometries are performed to determine the most suitable geometry representing the direct shear interface test. The four model predictions are compared to the experimental observations, presented in a previous chapter, as a basis for selection of the most suitable geometry for further analysis.

Once the geometry and input parameters are selected, detailed analyses are performed and compared to the observed experimental results presented in the previous chapter. The numerical values of the mean stress, relative shear stress, and total volumetric strain are presented, as well as the normal stresses and shear stresses that develop in the interface elements.

6.1.1 General settings

Plane strain model

The direct shear interface test is subjected to normal loads and tangential displacements in the y and x directions, respectively. The cross-sectional area of the soil sample remains constant along the z direction. Therefore, the strain normal to the x-y plane, ε_z, and the shear strains, γ_{xz} and γ_{yz} are zero. This state of strain is called plane strain. Hence, the direct shear test will be modelled by a plane strain model using the x-y coordinate system.

Elements

The analyses are performed using a six-node triangular element. It provides a second order interpolation for displacements. The element stiffness matrix is evaluated by numerical integration, using a total of three Gauss points (stress points).

Geometry and material properties

The geometry configuration has the same dimensions of the actual C3DI direct shear device described in a previous chapter. The main parts are the 27 mm x 100 mm steel cap, the 20 mm x 100 mm soil mass with a possible interface soil layer, and the 15 mm x 200 mm concrete plate. The steel cap and concrete plate are modelled using the linear elastic model while the soil mass and interface layer are modelled using the Hardening-Soil model. In order to select the geometry and input parameters that best match the experimental results presented in the previous chapter, four different cases are analysed.

In all four cases, an interface element is placed along the contact surface of the sand and the concrete plate to allow slippage. The roughness of the interface is modelled by selecting a suitable value for the strength reduction factor, R_{int}. This factor relates the friction angle of the interface to the friction angle of the soil mass.

In all four cases, the shear stress, at the bottom centre of the sand sample, and the normal displacement, at the bottom centre of the steel cap, are compared with the experimental results. Accordingly, the most suitable geometry is chosen for analyses.

Geometry #1

This case includes a soil mass without an interface soil layer as illustrated in Figure 6.1. The interface is only represented by the interface element, where R_{int} is 0.84. This value is obtained from Eq. 3.3, using the friction angle of sand, ϕ=37°, and the friction angle of the interface, δ=32.2°, which are based on the triaxial and interface tests, respectively. Table 6.1 summarizes the input parameters as obtained from previous chapters.

Table 6.1 Input parameters for Geometry #1

Material	p^{ref} (kPa)	c (kPa)	ϕ	ψ	E_{50}^{ref} (kPa)	E_{oed}^{ref} (kPa)	E_{ur}^{ref} (kPa)	R_{int}	ν_{ur}
Soil mass	200	0	37°	0°	23434	23434	70302	0.84	0.20
Concrete plate	-	-	-	-	$2x10^7$	-	-	-	0.15
Steel cap	-	-	-	-	$2x10^8$	-	-	-	0.15

Geometry #2

An interface layer, ten times the grain size (6 mm), is introduced to model the interface behaviour as illustrated in Figure 6.2. Below the interface layer, a layer of interface elements are used to allow slippage to take place. The material properties of the interface layer are the same as those of the soil mass except that the friction angle is 32.2°. The interface elements have R_{int}=1.00 since the friction angles of the interface layer and the interface elements are equal. Table 6.2 summarizes the input parameters as obtained from previous chapters.

Table 6.2 Input parameters for Geometry #2

Material	p^{ref} (kPa)	c (kPa)	ϕ	ψ	E_{50}^{ref} (kPa)	E_{oed}^{ref} (kPa)	E_{ur}^{ref} (kPa)	R_{int}	ν_{ur}
Interface layer	200	0	32.2°	0°	23434	23434	70302	1.0	0.20
Soil mass	200	0	37°	0°	23434	23434	70302	1.0	0.20
Concrete plate	-	-	-	-	$2x10^7$	-	-	-	0.15
Steel cap	-	-	-	-	$2x10^8$	-	-	-	0.15

Geometry #3

This case is similar to Geometry #2. However, to study the effect of the moduli on the modelling results, the secant modulus, tangent modulus, and unloading/reloading modulus were reduced approximately in half. The geometry is illustrated in Figure 6.3. Table 6.3 summarizes the input parameters as obtained from previous chapters.

Table 6.3 Input parameters for Geometry #3

Material	p^{ref} (kPa)	c (kPa)	ϕ	ψ	E_{50}^{ref} (kPa)	E_{oed}^{ref} (kPa)	E_{ur}^{ref} (kPa)	R_{int}	ν_{ur}
Interface layer	200	0	32.2°	0°	12000	12000	36000	1.0	0.20
Soil mass	200	0	37°	0°	23434	23434	70302	1.0	0.20
Concrete plate	-	-	-	-	$2x10^7$	-	-	-	0.15
Steel cap	-	-	-	-	$2x10^8$	-	-	-	0.15

Geometry #4

In order to reduce the effect of a sudden change in the friction angle between the interface elements and the soil mass in Geometry #2 and Geometry # 3, the following change is made in this case. The interface layer is given a soil friction angle equal to 34.6°, which is the average of the soil mass friction angle and the friction angle of interface elements. The strength reduction factor for the interface elements then becomes R_{int}=0.91, computed by Eq. 3.3. Figure 6.4 illustrates the geometry and Table 6.4 summarizes the input parameters as obtained from previous chapters.

Table 6.4 Input parameters for Geometry #4

Material	p^{ref} (kPa)	c (kPa)	ϕ	ψ	E_{50}^{ref} (kPa)	E_{oed}^{ref} (kPa)	E_{ur}^{ref} (kPa)	R_{int}	ν_{ur}
Interface layer	200	0	34.6°	0°	23434	23434	70302	0.91	0.20
Soil mass	200	0	37°	0°	23434	23434	70302	1.0	0.20
Concrete plate	-	-	-	-	$2x10^7$	-	-	-	0.15
Steel cap	-	-	-	-	$2x10^8$	-	-	-	0.15

Boundary conditions

On the right and left boundaries of the steel cap and soil mass, a horizontal displacement fixity was introduced to restrict movement in the x direction and allow a vertical displacement in the y direction only. A vertical displacement fixity was placed at the bottom boundary of the concrete plate to restrict movement in the y direction. Figure 6.1 shows these boundary conditions.

Traction and displacement

A uniformly distributed normal stress is applied along AA on the cap, as illustrated in Figure 6.1. This load simulates the constant normal stress applied during the direct shear interface test. Along the bottom of the concrete plate, a gradually increasing horizontal displacement of maximum 5 mm is specified to simulate the movement of the plate. Figure 6.1 illustrates the location of the displacement.

Comparison between modeling results and experimental results

Three finite element analyses were performed for each geometry case for a constant normal stress of 100 kPa, 200 kPa, and 300 kPa. To compare the shear stress versus tangential displacement predictions of the four geometries, the bottom centre point of the soil sample in each geometry was selected. Similarly, the bottom centre node of the steel cap was selected for all geometries, for comparison of the normal displacement versus tangential displacement predictions.

Figures 6.5, 6.6, and 6.7 plot the predicted shear stress versus tangential displacement of the four cases and the experimental results from the previous chapter for an applied constant normal stress of 100 kPa, 200 kPa, and 300 kPa, respectively. Geometry #1 gave a more or less linear relation for shear stress versus tangential displacement, before the ultimate shear stress is reached. Although, the ultimate shear stress is similar to the actual experimental results, the predicted values of tangential displacement deviated from the experimental results as the shear stress approached the shear strength of the interface.

Geometry #2 also resulted in an approximately linear relation for shear stress versus tangential displacement before the ultimate shear stress is reached, however, at a specific tangential displacement, there is a sudden drop followed by an increase in shear stress value. An analysis using geometry #3 was performed to study the effect of the moduli on the interface behaviour. The goal was to see if by reducing the moduli, a better result can be obtained than the linear shear stress-displacement relation obtained from Geometry #1 and #2. The analysis shows that the shear stress-displacement relation has a curvature, therefore, the results improved in comparison to a linear relation. However, the curve is shifted away from the experimental results and thus, predicts unreal tangential displacements for a given shear stress. Also, there is a sudden decrease and increase in shear stress at a tangential displacement before the ultimate shear stress is reached. Geometry #4 produced a linear shear stress versus tangential displacement relation. However, it overestimated the ultimate shear stress.

Figures 6.8, 6.9, and 6.10 plot the predicted normal displacement versus tangential displacement of the four cases and the experimental results for an applied constant normal stress of 100 kPa, 200 kPa, and 300 kPa, respectively. The analyses for all geometry cases underestimate the normal displacement in comparison to the experimental results. Geometry #1 and Geometry #4 produce very similar predictions. The results of Geometry #2 are not similar to the experimental results. While Geometry #3 also shows a different behaviour than that observed in the experiments. Hence, in comparing the normal displacement predictions to experimental results, none of the geometries produced good predictions.

In summary, it is assumed that Geometry #1 produces more consistent predictions for the experimental shear stress versus tangential displacement, as well as the experimental normal displacement versus tangential displacement relations than the other geometries. Therefore, it will be used for further detailed analyses.

Mesh generation

In Plaxis, the mesh is automatically generated. However, an option is available to refine the mesh at locations where stress concentrations and large deformations are expected. In this study, a medium size mesh was generated for the full geometry and then, the steel cap, soil mass and interface elements were further refined to give a fine mesh. A schematic presentation of the mesh is presented in Figure 6.11.

6.1.2 Calculation

There is a choice of three types of calculations in Plaxis. The *Plastic Calculation* is most suitable for the following analyses, because the analyses include elastic-plastic behaviour. The *Load Advancement Ultimate Level* algorithm available in Plaxis is the second calculation method to choose. It determines the load step size automatically and terminates the calculation when one of the following criteria is satisfied:

- The maximum number of additional calculation steps has been performed.
- The total specified load and displacement has been applied.
- A collapse load has been reached. Collapse occurs when the applied load reduces in magnitude in two successive calculation steps

The calculation is broken down into two phases. In the first phase, the constant normal stress is applied. The second phase includes the preservation of the constant normal stress and the application of tangential displacement to the concrete plate.

Selection of stress points and nodes for monitoring interface behaviour

Ten stress points are selected, as shown in Figure 6.11, where the development of stresses are examined. Ten nodal points are also selected, as illustrated in Figure 6.12, at locations where displacement response is required.

6.1.3 Results and discussion

Shear stress

The shear stress versus tangential displacement curves at specified locations, as illustrated in Figure 6.11, are presented in Figures 6.13, 6.14, and 6.15 for a constant normal stress of 100 kPa, 200 kPa, and 300 kPa, respectively. In the three analyses, it is observed that the shear stresses increase along the interface, from the left to the right vertical boundary. The shear stress at Point K, near the left vertical boundary of the box, suddenly decreases. This is due to the side effects where the soil is not allowed in the analysis to move horizontally because of the imposed boundary conditions while in reality, the soil is capable of moving horizontally. Furthermore, at the end of the analyses, the shear stress at Point T is continuously increasing and does not reach failure.

To compare the model predictions with the experimental results, an average shear stress acting along the whole length of the interface is calculated at every stage of analysis for all three constant normal stress tests. This average is obtained by adding the shear stress times the distance for points L, M, N, O, P, Q, R, and S and by dividing the total force by the total distance between these points. Accordingly, the predicted maximum shear stress for the constant normal stress of 100 kPa test is 62 kPa, while the experimental maximum shear stress is 66 kPa. Similarly, for the constant normal stress of 200 kPa and 300 kPa tests, the predicted values are 125 kPa and 187 kPa, respectively, and the experimental values are 131 kPa and 191 kPa, respectively. These results are plotted in Figure 6.16.

Even though the model gives good predictions of the average maximum shear stress along the interface, it does not predict well the tangential displacement corresponding to a shear stress as shown in Figure 6.16. Considering the test with normal stress equal to 300 kPa, the experimental tangential displacement is twice as much of the predicted value at 180 kPa shear stress. Similarly, for a given tangential displacement the predicted values of shear stress are either significantly smaller or larger than the measured values. The model predictions seem to be produced using an elastic, perfectly plastic model.

Normal displacement

The normal displacement versus tangential displacement curves at specified locations, as illustrated in Figure 6.12, are presented in Figures 6.17, 6.18, and 6.19 for a constant normal stress of 100 kPa, 200 kPa, and 300 kPa, respectively.

To compare the model predictions to the experimental results, the normal displacements at point C are used. Accordingly, the predicted maximum normal displacement for the constant normal stress of 100 kPa test is 0.025 mm, while the experimental maximum normal displacement is 0.170 mm. Similarly, for the constant normal stress of 200 kPa and 300 kPa tests the predicted values are 0.035 mm and 0.044 mm, respectively, and the experimental values are 0.208 mm and 0.226 mm, respectively. These results are plotted in Figure 6.20.

In summary, the model underestimates, up to roughly 6 times, the normal displacement for a given tangential displacement.

Mean stress

The mean stresses that develop in the direct shear box are presented in Figures 6.21, 6.22, and 6.23 for the constant normal stress tests of 100 kPa, 200 kPa, and 300 kPa, respectively. It is observed that the mean stresses are very low at the left boundary of the soil and they increase gradually towards the right side of the direct shear box, in the direction of the tangential displacement. The maximum mean stress occurs typically in the bottom right corner of the sand. For the 100 kPa constant normal stress test, the maximum mean stress is 190 kPa in compression and for the 200 kPa and 300 kPa constant normal stress tests, the mean stresses are 361 kPa and 574 kPa in compression, respectively.

Relative shear stress

The "relative shear stress", used in Plaxis, gives an indication of the proximity of the stress point to the failure envelope by dividing the shear stress reached by the maximum shear stress obtained from the Mohr-Coulomb failure envelope. In the direct shear interface test, it is seen from Figures 6.24, 6.25, and 6.26 that the soil in the bottom left side of the sample has reached the maximum shear stress. The relative shear stress ratio decreases gradually, within the soil mass, towards the right boundary of the box.

Total volumetric strain

The total volumetric strains for the tests with constant normal stress of 100 kPa, 200 kPa, and 300 kPa are illustrated in Figures 6.27, 6.28, and 6.29, respectively. Starting from the left side of the sample, the soil dilates at a decreasing rate towards the right side, in the direction of tangential displacement, and eventually compresses. In the 100 kPa constant normal stress analysis, the maximum volumetric strain is approximately 1.20% dilation at the left side and 0.7% compression at the right side of the soil mass. In the 200 kPa constant normal stress analysis, the maximum volumetric strain is 1.60% dilation at the left side and approximately 1.00% compression at the right side. In the 300 kPa constant normal stress analysis, the maximum volumetric strain is 2.20% dilation at the left side and 1.40% compression at the right side of the soil sample.

Stresses in interface elements

The normal stress and the shear stress along the interface for the 100 kPa constant normal stress analysis are plotted in Figures 6.30 and 6.31, respectively. The effects of the boundary conditions can be seen at both sides of the plots. The maximum normal stress is 129.90 kPa in compression and the maximum shear stress is 78.01 kPa. For the 200 kPa constant normal stress analysis, the normal stress and the shear stress along the interface are plotted in Figures 6.32 and 6.33, respectively. The maximum normal stress is 257.21 kPa and the maximum shear stress is 154.30 kPa. Finally, for the constant normal stress of 300 kPa test, Figure 6.34 illustrates the normal stress and Figure 6.35 shows the shear stress along the interface, where the maximum normal stress and shear stress are 390.20 kPa and 233.99 kPa, respectively.

6.2 Finite element analysis of a simple shear interface test

Two geometries are analysed to determine the best geometry representing the simple shear interface test. The selection of the most suitable geometry is made by comparing the two model predictions with the experimental observations by Li (2001). Once the geometry and input parameters are selected, a detailed analysis is performed and presented for a constant normal stress of 300 kPa test and compared to observed experimental results. The numerical values of mean stress, relative shear stress, and total volumetric strain are also presented, as well as the normal stresses and shear stresses that develop in the interface elements.

6.2.1 General settings

Plane strain model

The simple shear interface test is subjected to the same loads and displacements in the y and x directions, respectively, as the direct shear interface test. Hence, the cross-sectional area can be assumed constant along the z direction. The plane strain model will be used for the analysis.

Elements

The analysis is performed using a six-node triangular element. Plaxis uses a second order interpolation for displacements and the element stiffness matrix is evaluated by numerical integration using a total of three Gauss points (stress points).

Geometry and material properties

The geometry configuration is based on the actual dimensions of the sample in experiments performed by Li (2001). The main parts are the 27 mm x 100 mm steel cap, the 12 mm x 100 mm soil mass with a possible interface soil layer, and the 15 mm x 200 mm steel plate. The steel cap and steel plate are modelled using the linear elastic model

while the soil mass and interface layer are modelled using the Hardening-Soil model. Two geometry cases are analysed to study the effect of introducing an independent soil layer representing the interface, where the thickness of the layer is determined experimentally by Li (2001).

In both cases, an interface element is placed along the contact surface of the sand and the steel plate to allow for slippage. The roughness of the interface is modelled by selecting a suitable value for the strength reduction factor, R_{int}. The shear stress in the interface, at the bottom centre of the simple shear type soil container, and the normal displacement, at the bottom centre of the steel cap, are compared with the experimental observations by Li (2001). Accordingly, the most suitable geometry is chosen to perform the detailed analysis.

Geometry #1

This case includes a soil mass without an interface soil layer as illustrated in Figure 6.36. The interface is only represented by the interface elements, where R_{int} is 0.66. This value is obtained from Eq. 3.3, using the friction angle of sand, ϕ=37°, and the friction angle of the interface experimentally determined from interface tests by Li (2001), δ=26.6°. Table 6.5 summarizes the input parameters as obtained from previous chapters.

Table 6.5 Simple shear test input parameters for Geometry #1

Material	p^{ref} (kPa)	c (kPa)	ϕ	ψ	E_{50}^{ref} (kPa)	E_{oed}^{ref} (kPa)	E_{ur}^{ref} (kPa)	R_{int}	ν_{ur}
Soil mass	200	0	37°	0°	23434	23434	70302	0.66	0.20
Steel plate	-	-	-	-	$2x10^8$	-	-	-	0.15
Steel cap	-	-	-	-	$2x10^8$	-	-	-	0.15

Geometry #2

An interface layer, 8 mm thick determined experimentally by Li (2001), is introduced to model the interface behaviour as illustrated in Figure 6.37. The interface elements are still present to allow slippage. The material properties of this layer are the interface properties and R_{int}=1.00 since the friction angle of the layer, ϕ=26.6°, is equal to that of the interface. Table 6.6 summarizes the input parameters as obtained from previous chapters.

Table 6.6 Simple shear test input parameters for Geometry #2

Material	p^{ref} (kPa)	c (kPa)	ϕ	ψ	E_{50}^{ref} (kPa)	E_{oed}^{ref} (kPa)	E_{ur}^{ref} (kPa)	R_{int}	ν_{ur}
Interface layer	200	0	26.6°	0°	23434	23434	70302	1.0	0.20
Soil mass	200	0	37°	0°	23434	23434	70302	1.0	0.20
Steel plate	-	-	-	-	$2x10^7$	-	-	-	0.15
Steel cap	-	-	-	-	$2x10^8$	-	-	-	0.15

Boundary conditions

A vertical displacement fixity is placed at the bottom boundary of the steel plate. To simulate the stack of plates, a uniformly distributed horizontal stress is applied at the vertical boundaries of the soil sample. The magnitude of the horizontal stress is equal to the vertical stress times K_o, where K_o = 1-sinϕ. Figure 6.36 shows these boundary conditions.

Traction and displacement

A uniformly distributed stress is applied between points AA along the cap. This normal stress applied at the boundary remains the same during the simple shear interface test. Along the bottom of the steel plate, a gradually increasing tangential displacement up to 5 mm is applied to simulate the movement of the steel plate. Figure 6.36 illustrates the location of the applied stresses and the displacements.

Comparison between the modelling results and experimental results

A finite element analysis was performed for each geometry case for a constant normal stress of 300 kPa. To compare the shear stress versus the tangential displacement predictions, the bottom centre stress point in the soil sample was selected for each geometry. Similarly, the same nodal point was selected for both geometries, at the bottom centre of the steel cap, for comparison of the normal displacement versus the tangential displacement predictions.

Figure 6.38 plots the predicted shear stress versus tangential displacement of the two cases and the experimental results from Li (2001). The results of Geometry #2 are unstable with respect to the shear stresses as the tangential displacement increases. It does not reach a constant ultimate shear stress as the observed experimental results. Hence, Geometry #1 better models the experimental results than does Geometry #2.

Figure 6.39 plots the predicted normal displacement versus tangential displacement of the two cases and the experimental results. Geometry #1 underestimates the experimental normal displacement. Geometry #2 predicts that the soil mass undergoes continuous normal displacement during the test, however, the experimental results show that the normal displacement no longer changes at approximately 3.5 mm.

Geometry #1 is chosen for the detailed analysis of the simple shear interface test.

Mesh generation

In Plaxis, the mesh is automatically generated. However, an option is available to refine the mesh at locations where stress concentrations and large deformations are expected. A fine mesh is generated in the sand and is further refined along the interface element. A schematic presentation of the mesh is shown in Figure 6.40.

6.2.2 Calculation

As in the direct shear interface tests, a *Plastic Calculation* is performed using the *Load Advancement Ultimate Level* algorithm, which determines the load step size automatically. The calculation is broken down into two phases. In the first phase, the constant normal stress and the horizontal stress at the sand boundaries are applied. The second phase maintains the constant normal stress and horizontal stress while the steel plate is displaced horizontally.

Selection of stress points and nodes for monitoring interface behaviour

Ten stress points are selected, as shown in Figure 6.40, to study the stress advancement at these locations. Ten nodal points are also selected, as illustrated in Figure 6.41, at locations where displacements are investigated.

6.2.3 Results and discussion

Shear stress

The shear stress versus tangential displacement curves at specified locations, as illustrated in Figure 6.40, are presented in Figure 6.42 for a constant normal stress of 300 kPa. It can be seen that the highest shear stresses occur at the left boundary of the sand box and gradually decrease towards the right boundary, in the direction of the tangential displacement.

The average of the shear stress curves is calculated to compare the model predictions and the experimental results. The average shear stress is obtained by adding the shear stress times the distance for points K, L, M, N, O, P, Q, R, S, and T and dividing by the length of the sand box. Figure 6.43 plots the average shear stress and the experimental results. Accordingly, the predicted maximum shear stress is 140 kPa in comparison to the experimental value of maximum shear stress of 149 kPa.

Similar to the direct shear interface test results, the model gives close predictions of the average maximum shear stress along the interface, but it is conservative. Initially, it underpredicts the shear stress for a given tangential displacement and subsequently, it overpredicts the shear stress. Plaxis is not efficient in predicting the curvature of the shear stress versus tangential displacement curve. However, this can partly be the result of the fact that the interface elements in Plaxis are only modelled using the Mohr-Coulomb model, which is an elastic-perfectly plastic model.

Normal displacement

The normal displacement versus tangential displacement curves at the specified locations, as shown in Figure 6.41, are presented in Figure 6.44 for a constant normal stress of 300 kPa.

To compare the model predictions to the experimental results, the normal displacements at point C are used. Figure 6.45 shows the calculated normal displacement in comparison to the experimental results. The predicted maximum normal displacement is 0.064 mm while the experimental maximum normal displacement is 0.257 mm. Once again, the model underpredicts the normal displacement.

Deformed mesh

The deformed mesh illustrating the movement of the sand with respect to its initial position is shown in Figure 6.46. The model does not take into account the interface layer to predict the movement of the sand, consequently, the sand boundary is linearly sloping.

Mean stress

The mean stresses that develop in the simple shear box, for a constant normal stress of 300 kPa, are presented in Figure 6.47. It is observed that there is not a great difference among mean stresses in the sand sample. The maximum mean stress is 789 kPa in compression.

Relative shear stress

The "relative shear stress", used in Plaxis, gives an indication of the proximity of the stress point to the failure envelope by dividing the shear stress reached at a specific time by the maximum shear stress obtained from the Mohr-Coulomb failure envelope. In the simple shear interface test, it is seen from Figure 6.48 that the soil in the majority of the right hand side of the sample has reached the maximum shear stress. The relative shear stress ratio slightly decreases at the left hand side of the box.

Total volumetric strain

The shadings of the total volumetric strains for a constant normal stress of 300 kPa are illustrated in Figure 6.49. The left hand side of the soil mass compresses at a decreasing rate towards the right side, in the direction of tangential displacement, and eventually the soil dilates. The maximum volumetric strain is approximately 0.8% compressive at the left side and 0.8% dilative at the right side of the soil mass.

Stresses in interface elements

The normal stress and the shear stress along the interface for a constant normal stress of 300 kPa are plotted in Figures 6.50 and 6.51, respectively. It is seen that both the normal and shear stresses are largest at the left hand side of the sample. Moving from left to right, stresses level off until the centre of the sand interface is passed and eventually they start decreasing. The maximum normal stress is 683.07 kPa in compression and the maximum shear stress is 310.27 kPa, both occurring at the left boundary.

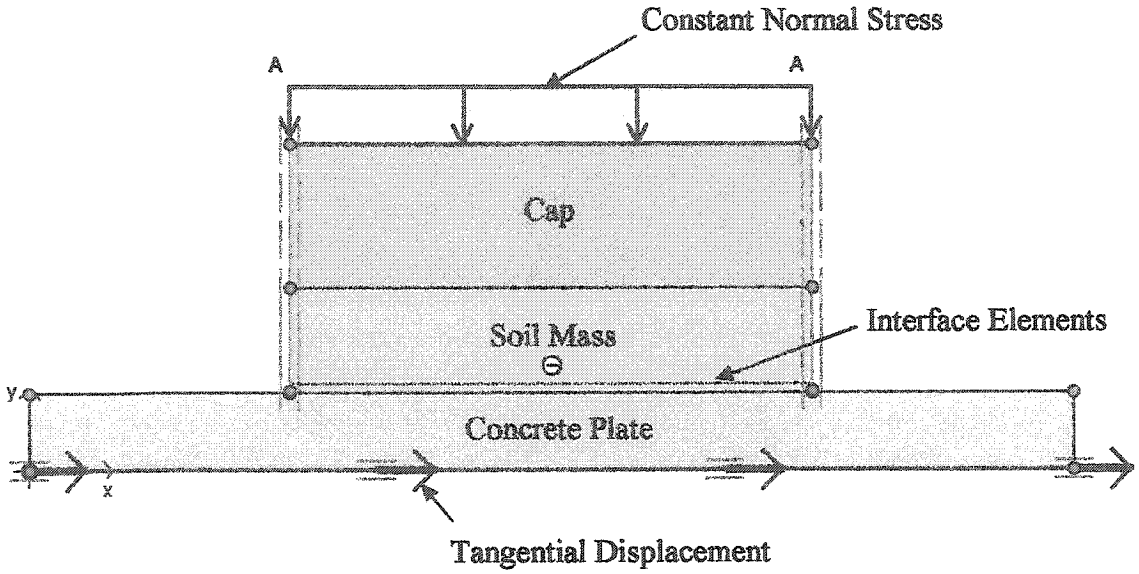

Figure 6.1 Geometry #1: No interface soil layer, interface represented by the Plaxis interface reduction factor, $R_{int} = 0.84$, resulting in an interface friction angle, $\delta = 32.2°$

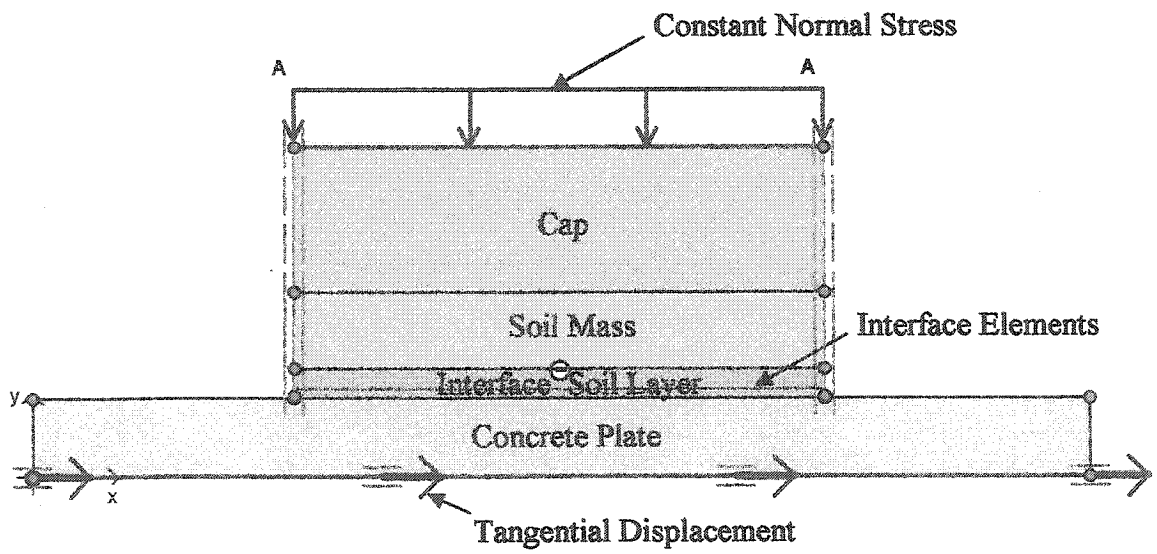

Figure 6.2 Geometry #2: Interface represented by an independent soil layer where R_{int}=1.0, ϕ=32.2° and there is no reduction in the moduli, E_{50}, E_{oed}, and E_{ur}

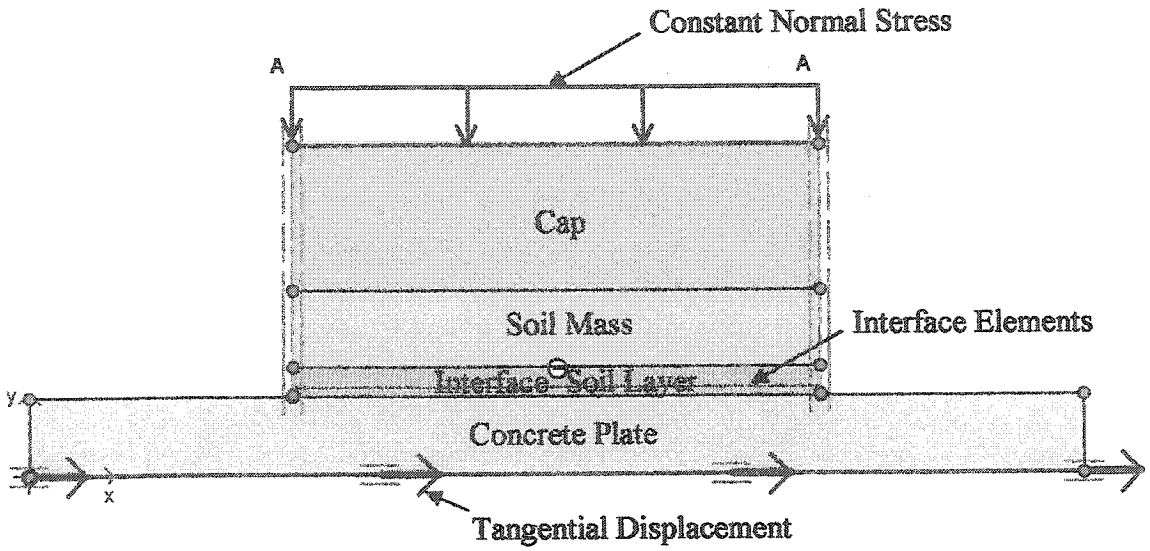

Figure 6.3 Geometry #3: Interface represented by an independent soil layer where R_{int}=1.0, ϕ=32.2° and the moduli, E_{50}, E_{oed}, and E_{ur} are reduced by approximately 0.5 times

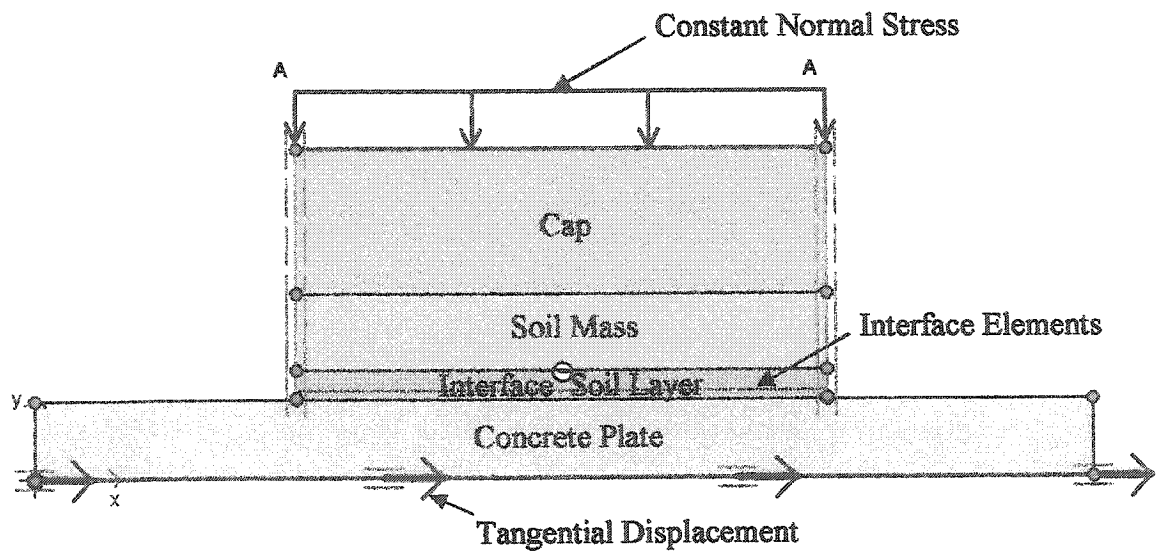

Figure 6.4 Geometry #4: Interface represented by an independent soil layer where R_{int}=0.91, resulting in an interface friction angle δ = 32.2°, ϕ=34.6° and there is no reduction in the moduli, E_{50}, E_{oed}, and E_{ur}

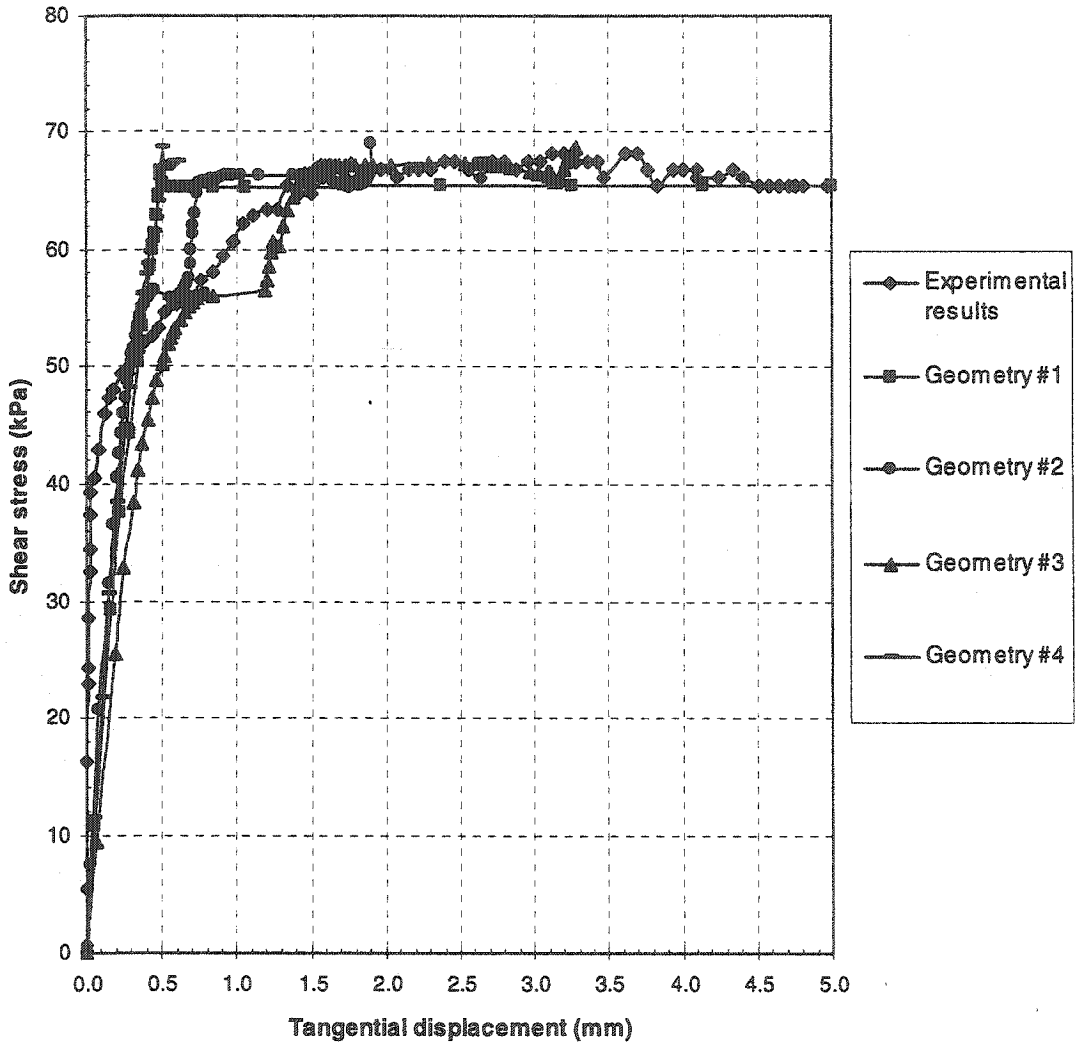

Figure 6.5 Plaxis results for shear stress versus tangential displacement curves for the geometries in Figures 6.1 to 6.4 in comparison to the experimental results, constant normal stress = 100 kPa

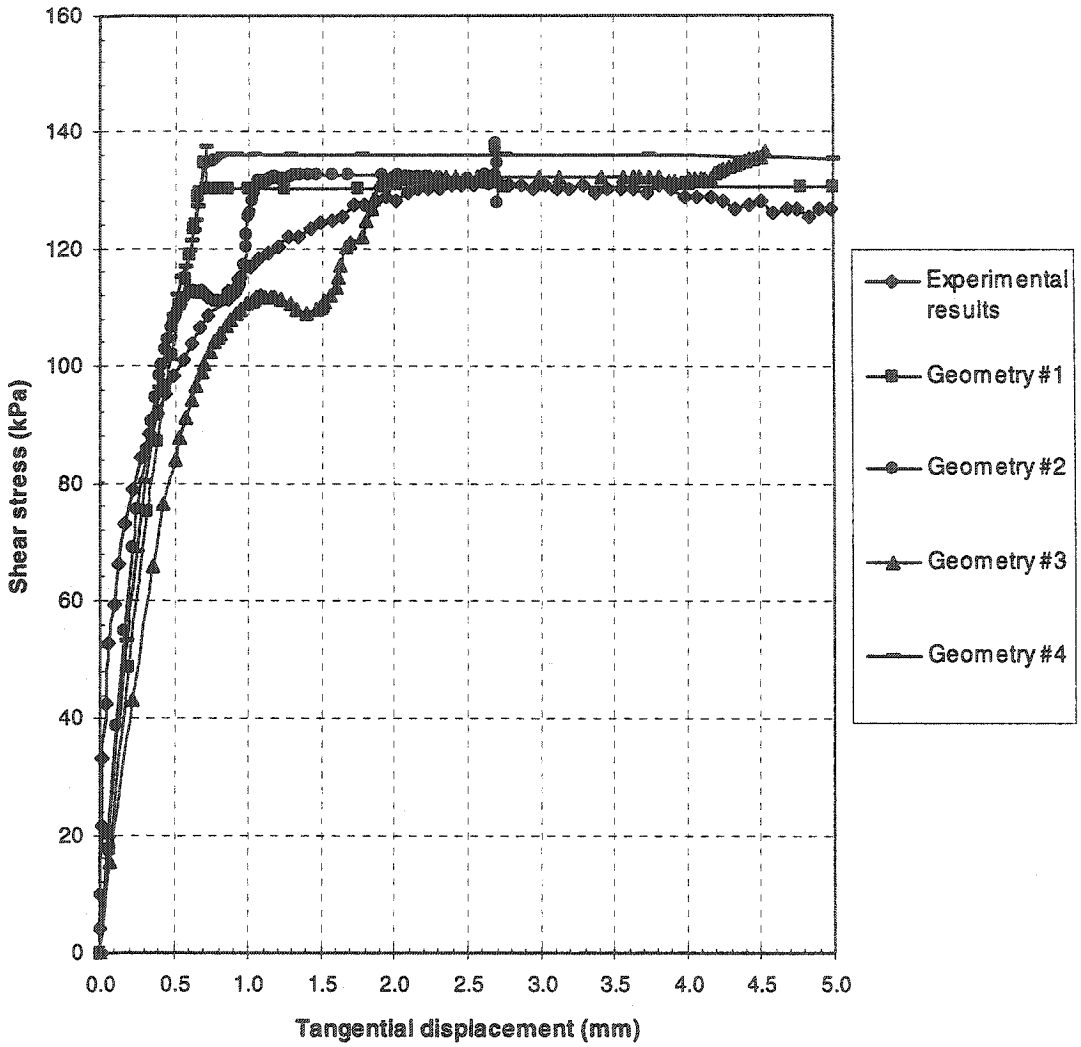

Figure 6.6 Plaxis results for shear stress versus tangential displacement curves for the geometries in Figures 6.1 to 6.4 in comparison to the experimental results, constant normal stress = 200 kPa

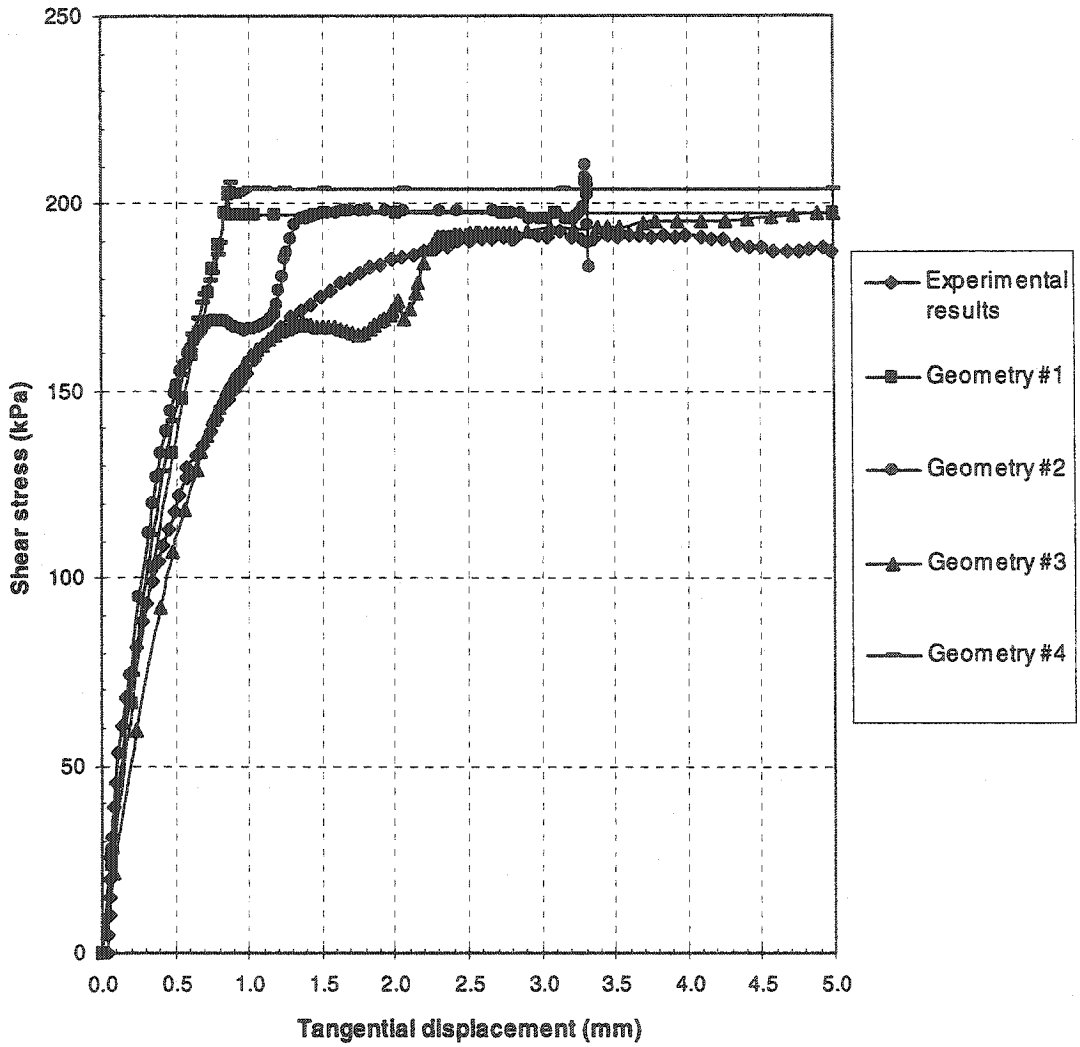

Figure 6.7 Plaxis results for shear stress versus tangential displacement curves for the geometries in Figures 6.1 to 6.4 in comparison to the experimental results, constant normal stress = 300 kPa

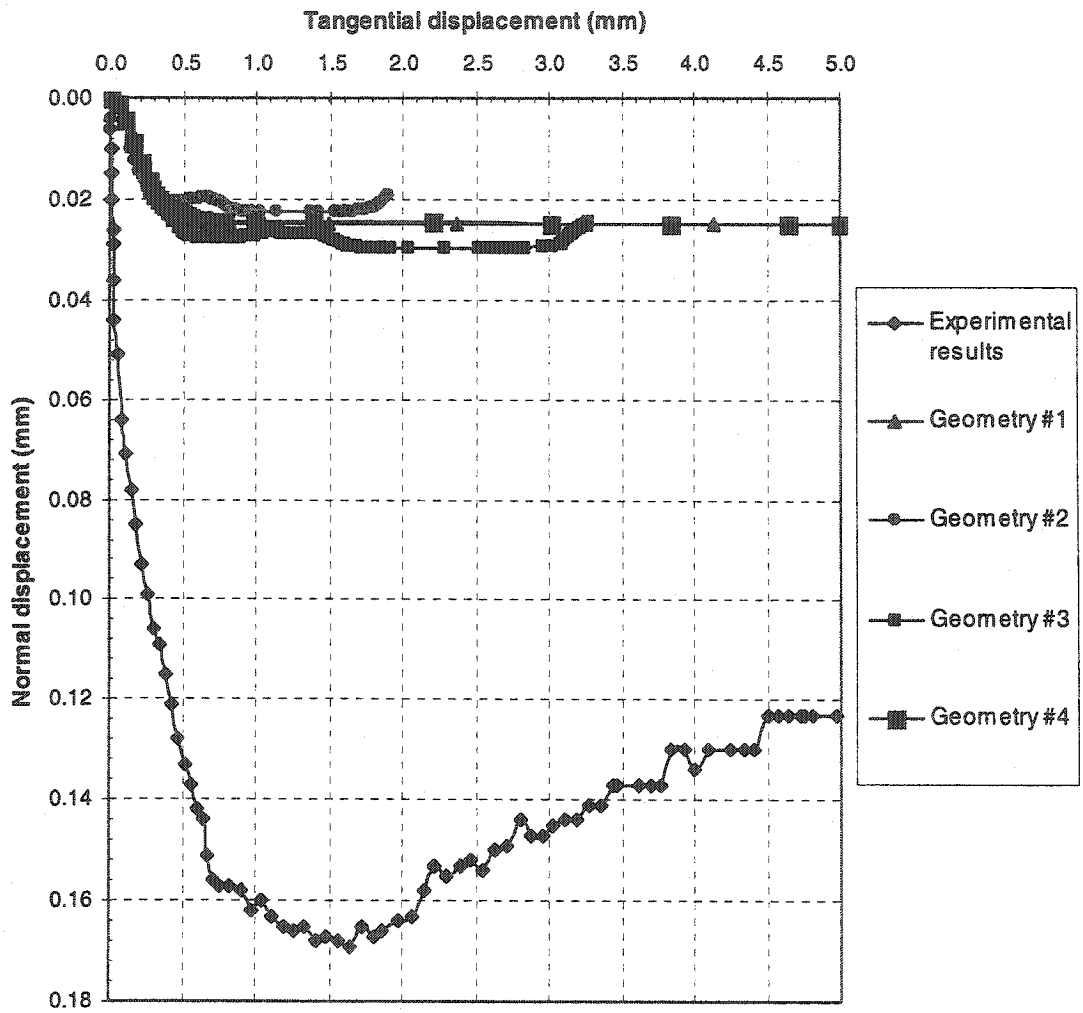

Figure 6.8 Plaxis results for normal displacement versus tangential displacement curves for the geometries in Figures 6.1 through 6.4 in comparison to the experimental results, constant normal stress = 100 kPa

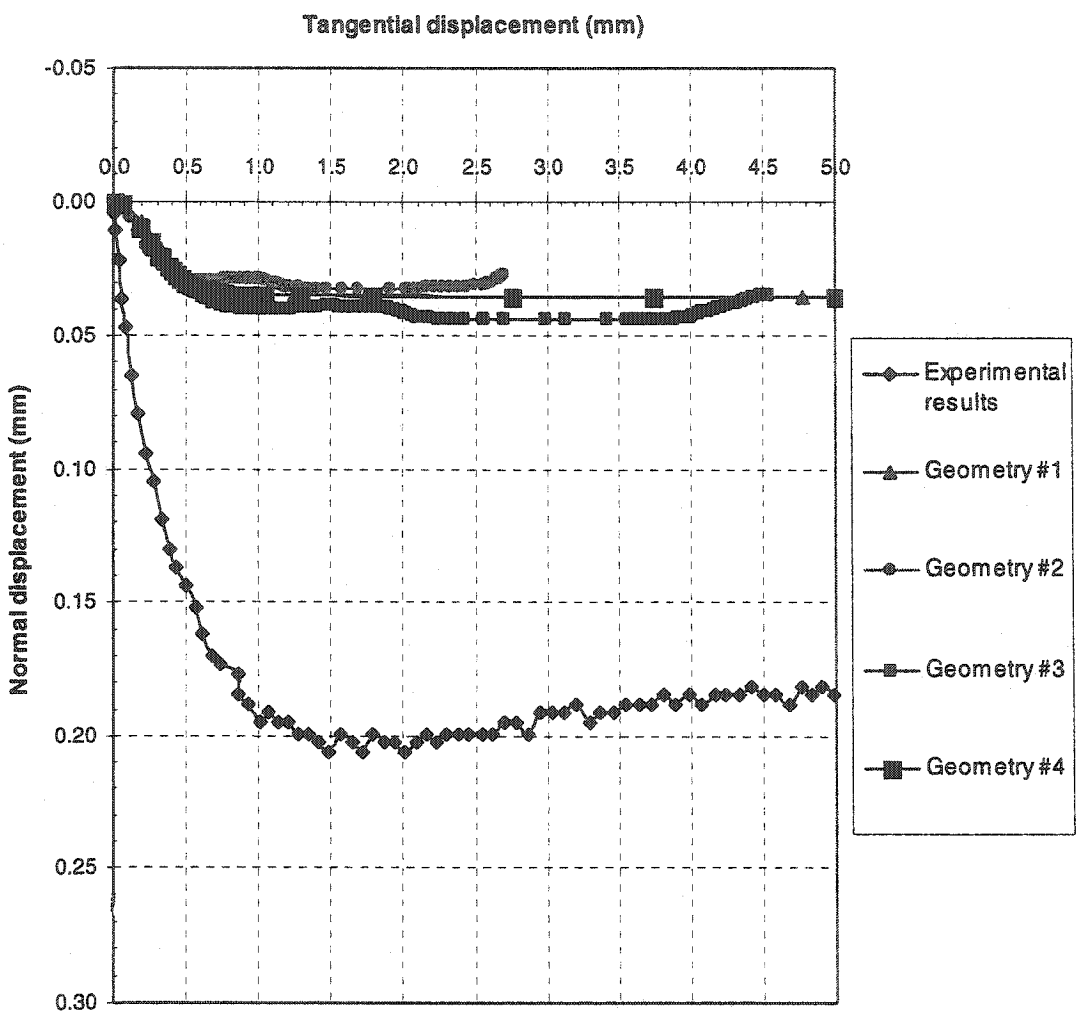

Figure 6.9 Plaxis results for normal displacement versus tangential displacement curves for the geometries in Figures 6.1 through 6.4 in comparison to the experimental results, constant normal stress = 200 kPa

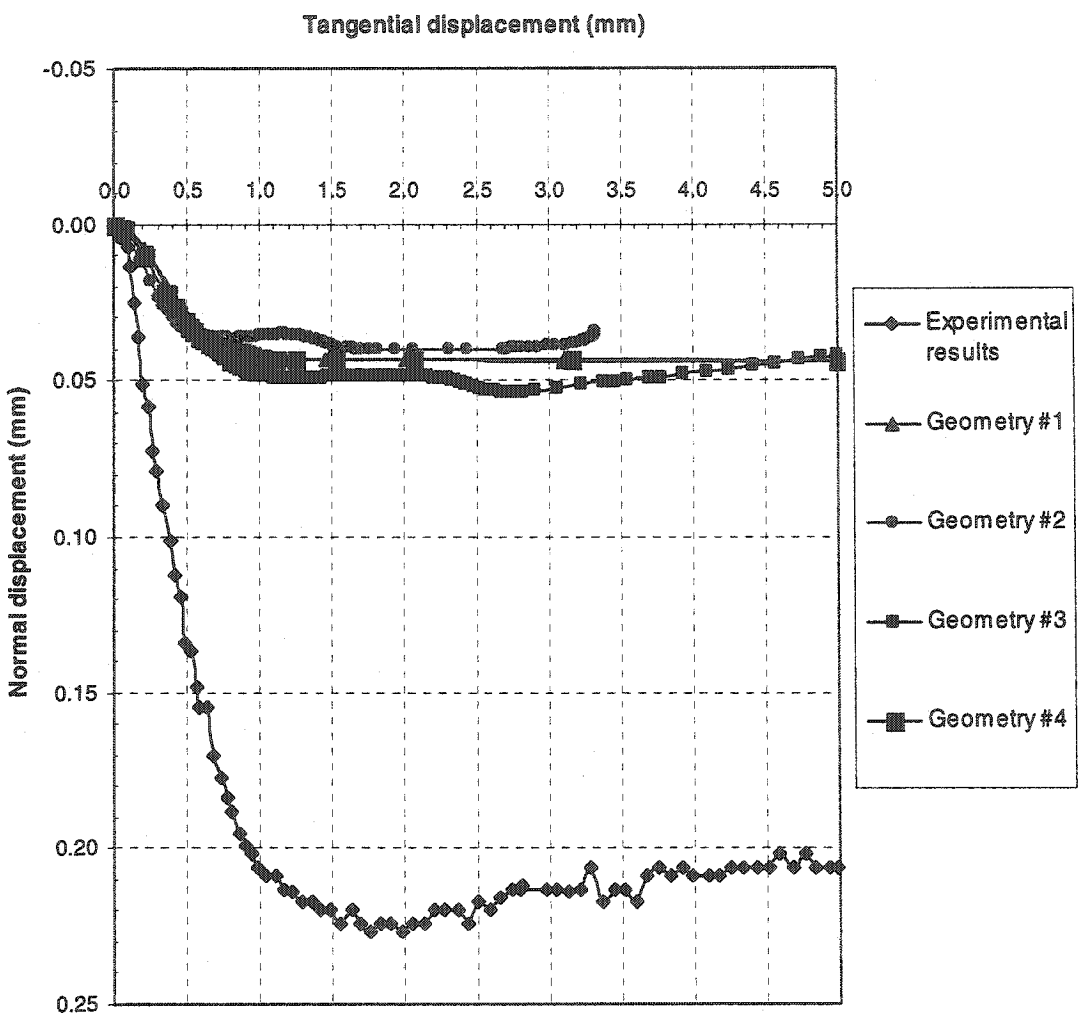

Figure 6.10 Plaxis results for normal displacement versus tangential displacement curves for the geometries in Figures 6.1 through 6.4 in comparison to the experimental results, constant normal stress = 300 kPa

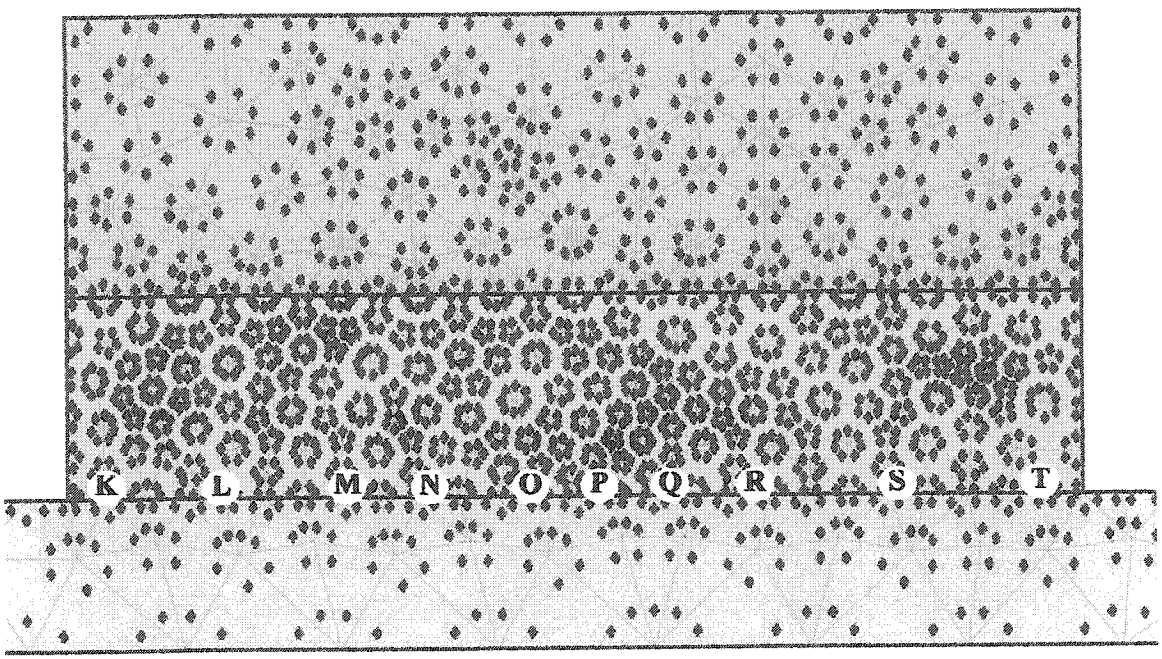

Figure 6.11 Schematic presentation of the locations of stress points

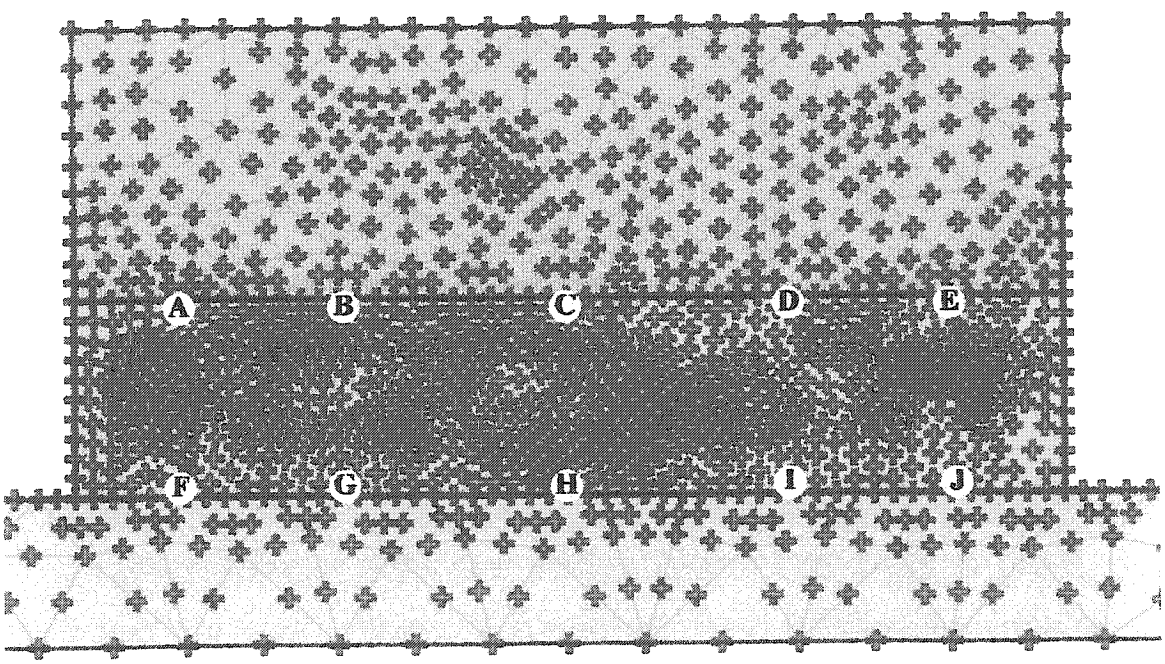

Figure 6.12 Schematic presentation of the locations of nodal points

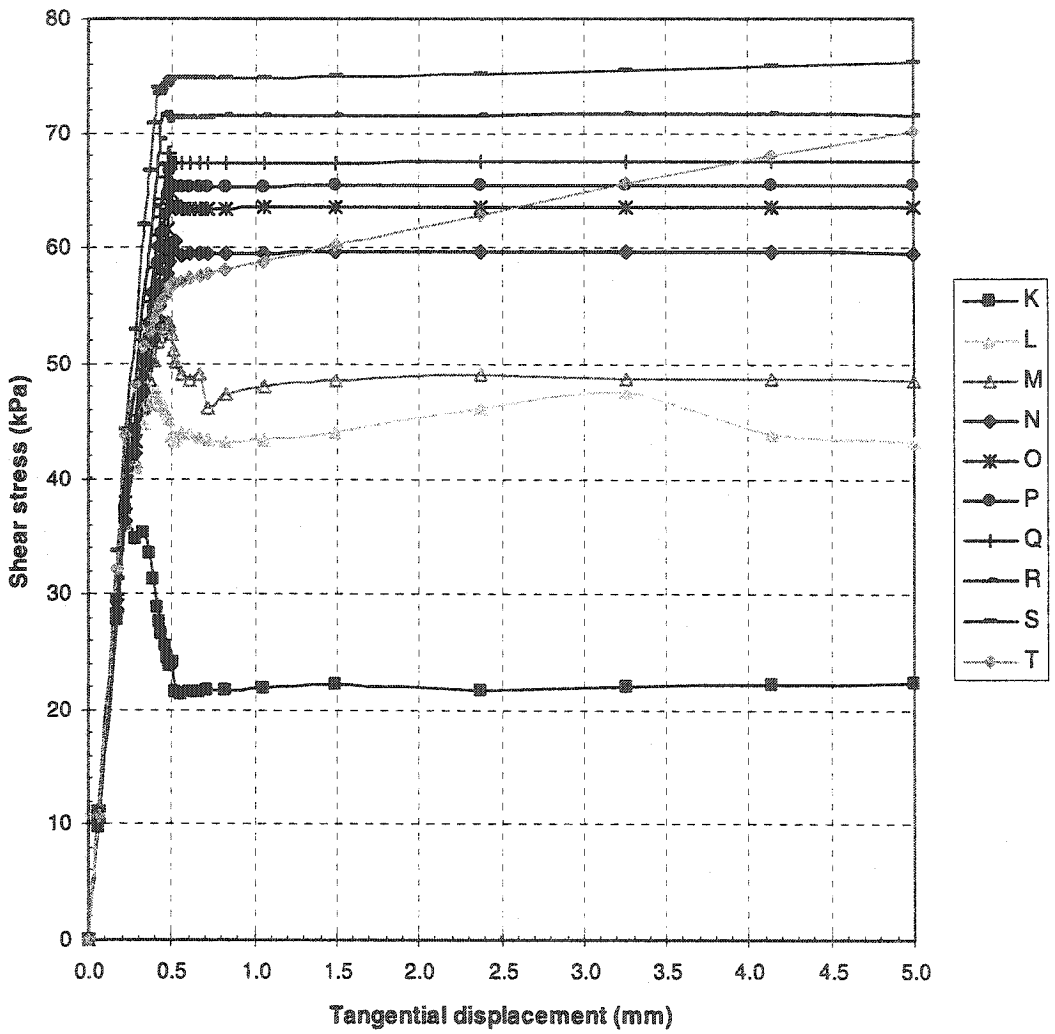

Figure 6.13 Shear stress versus tangential displacement curves at different locations on the interface, as illustrated in Figure 6.11, constant normal stress = 100 kPa

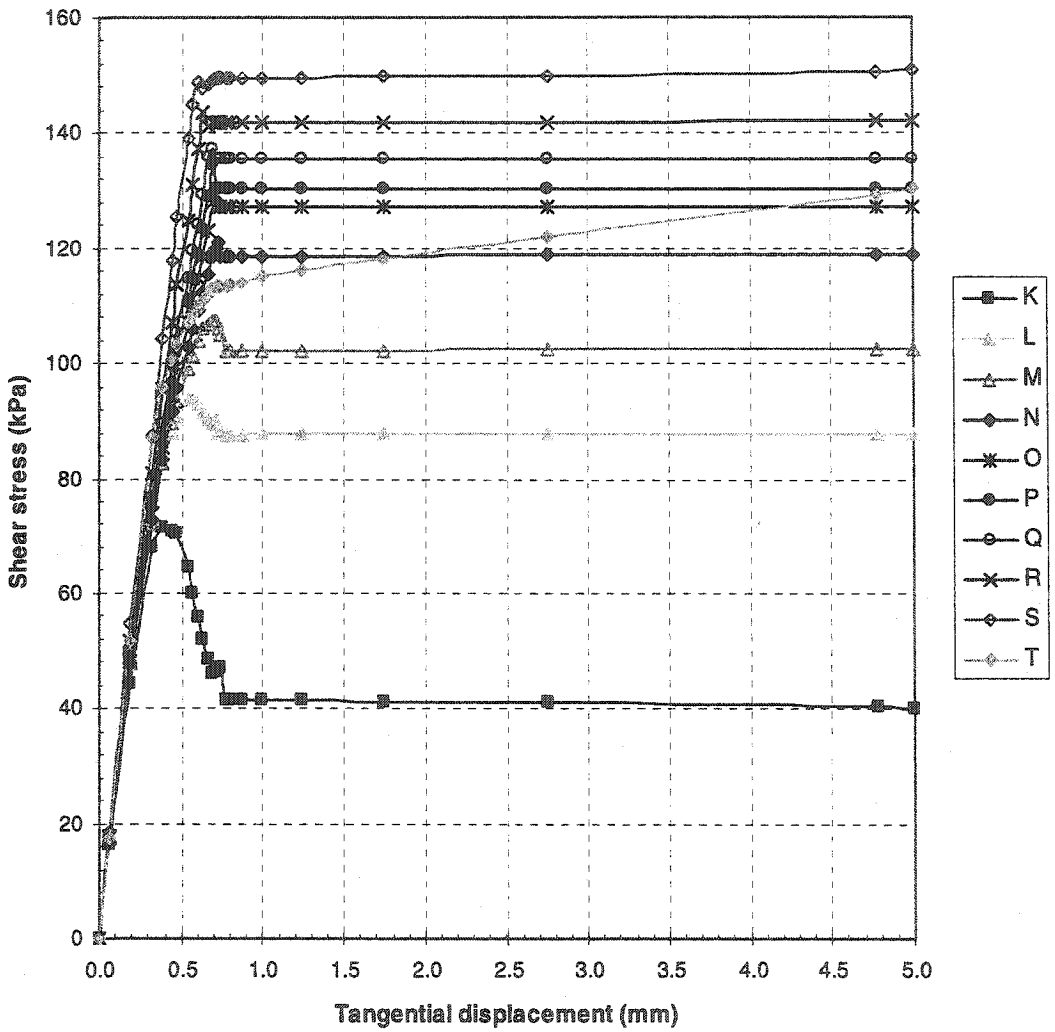

Figure 6.14 Shear stress versus tangential displacement curves at different locations on the interface, as illustrated in Figure 6.11, constant normal stress = 200 kPa

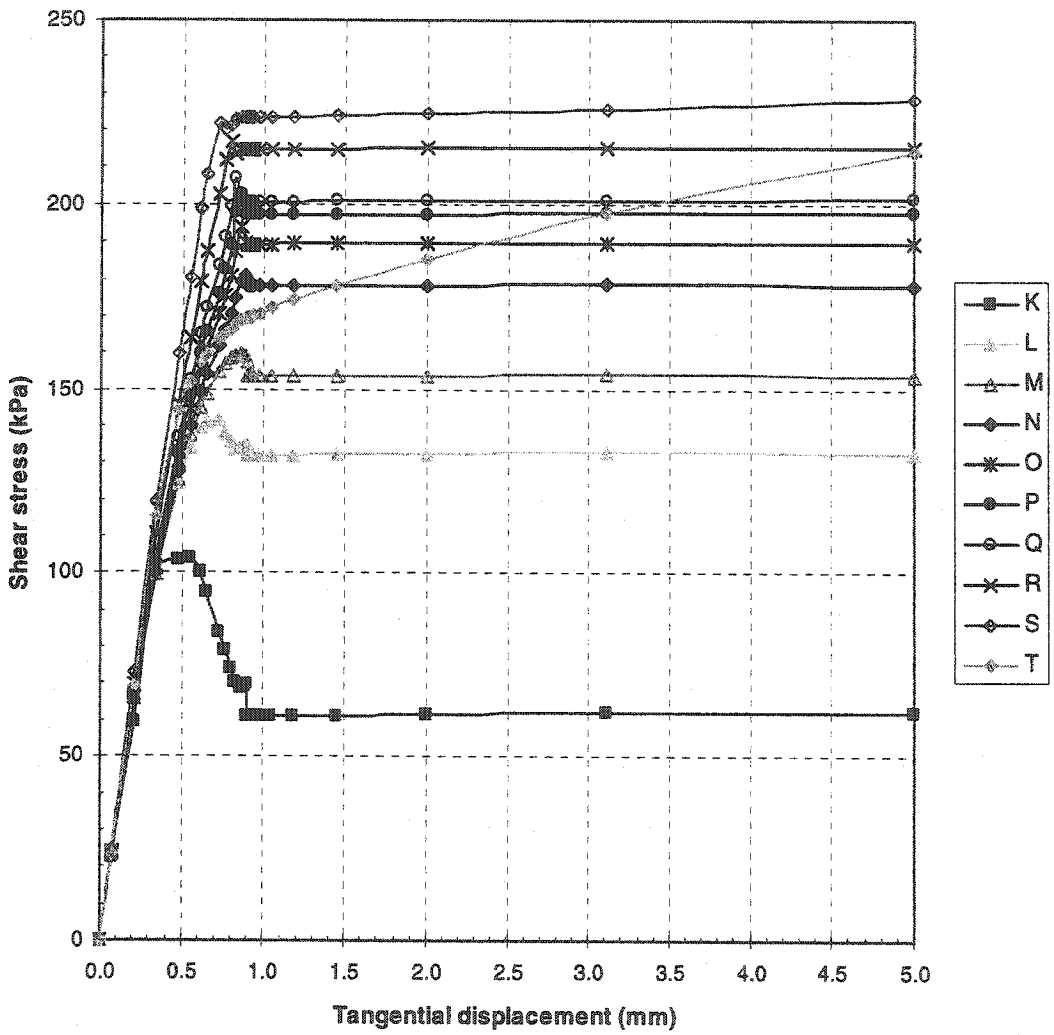

Figure 6.15 Shear stress versus tangential displacement curves at different locations on the interface, as illustrated in Figure 6.11, constant normal stress = 300 kPa

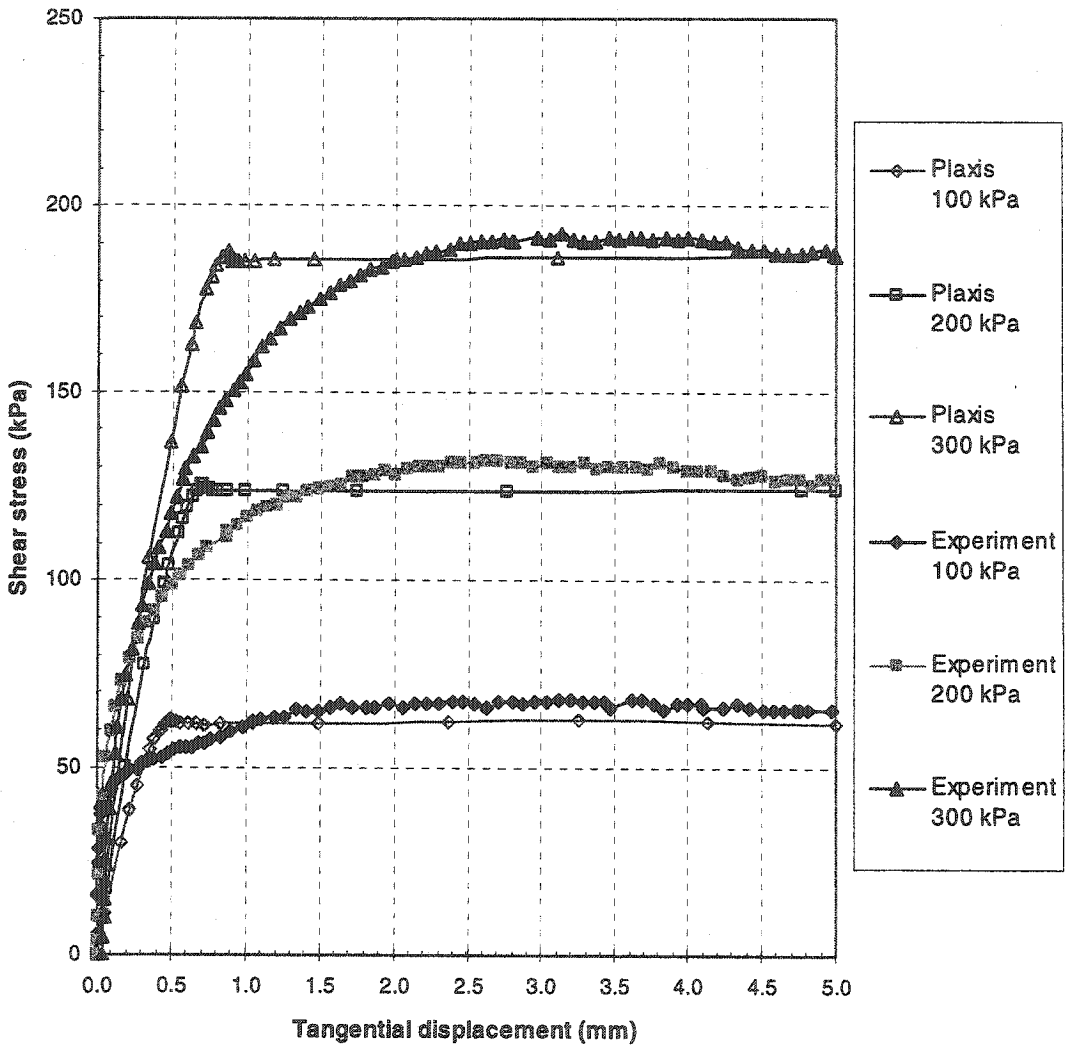

Figure 6.16 Comparison of experimental results and Plaxis results of average shear stress versus tangential displacement curves

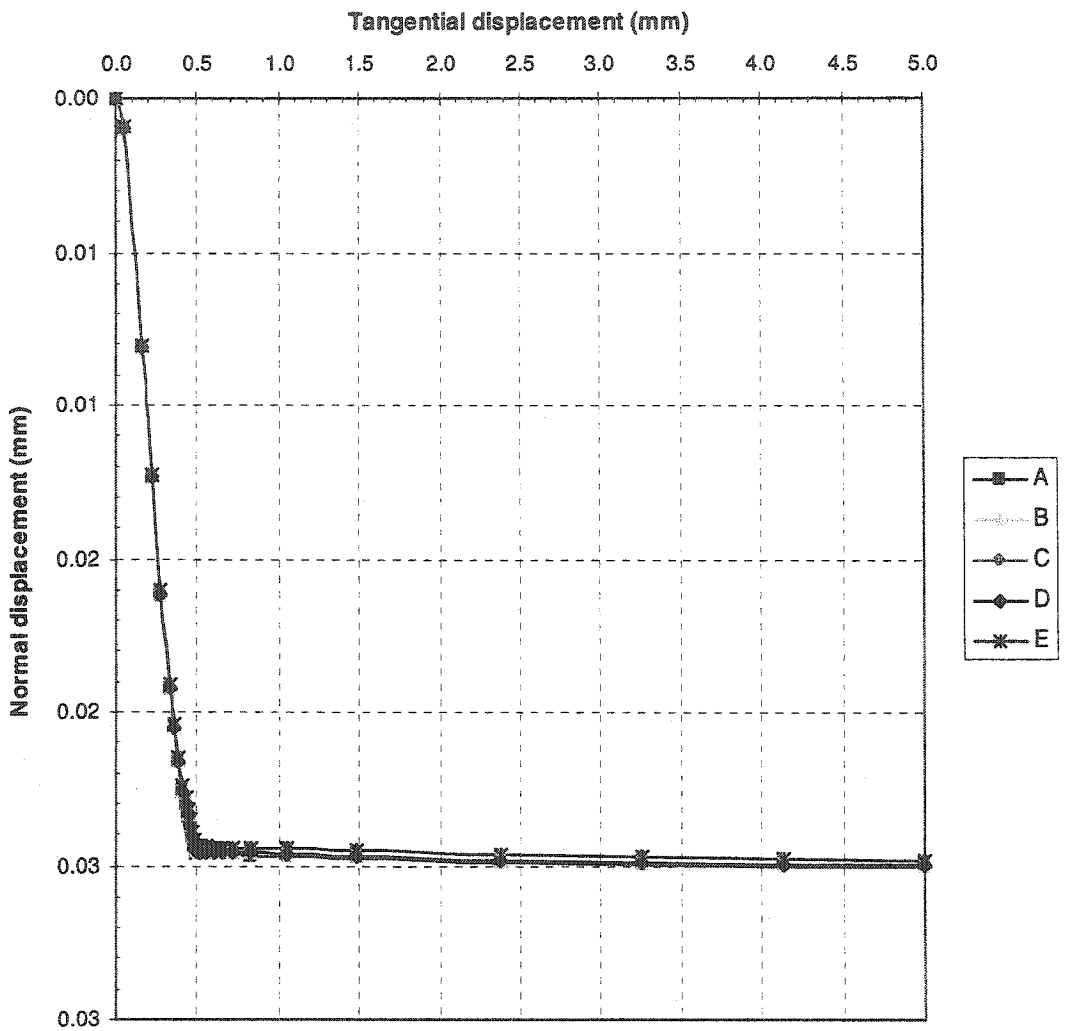

Figure 6.17 Normal displacement versus tangential displacement curves at different locations on the loading cap, as illustrated in Figure 6.12, constant normal stress = 100 kPa

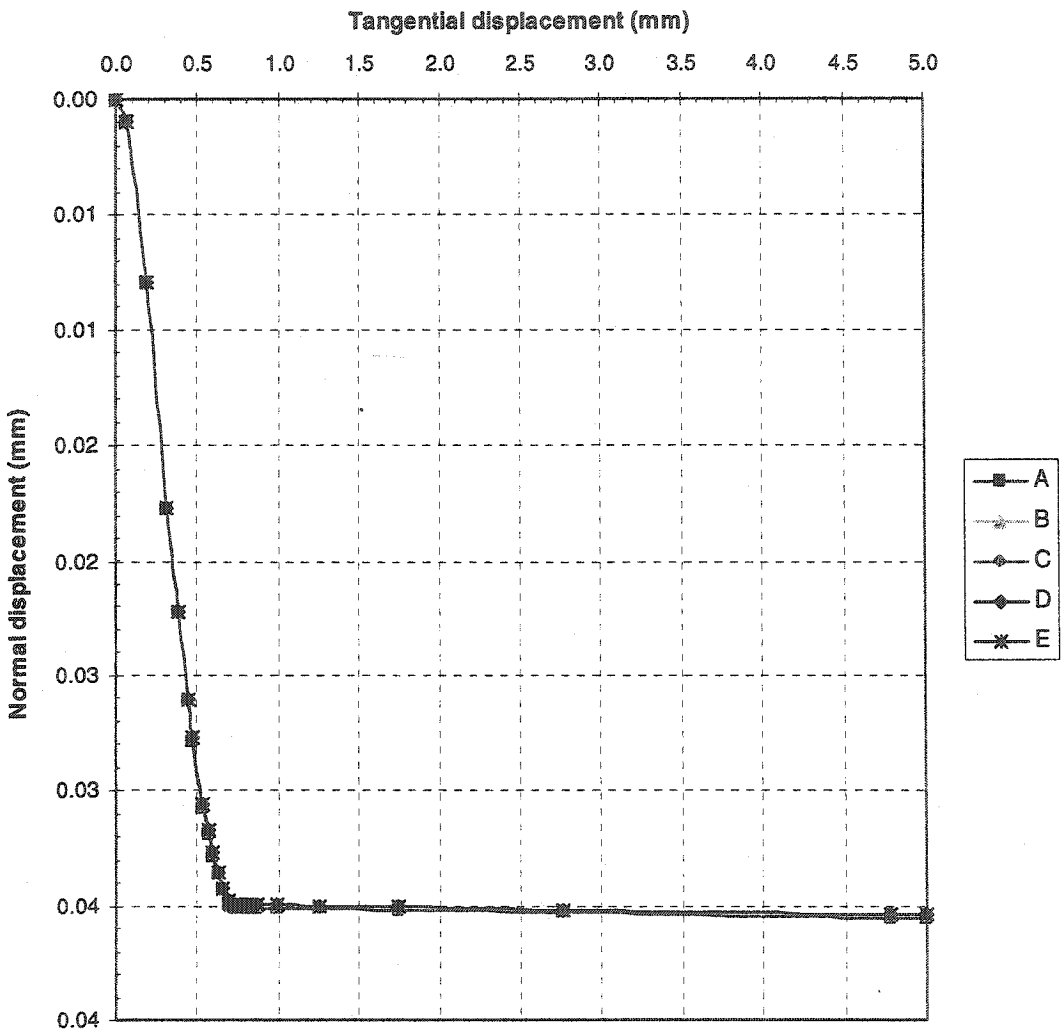

Figure 6.18 Normal displacement versus tangential displacement curves at different locations on the loading cap, as illustrated in Figure 6.12, constant normal stress = 200 kPa

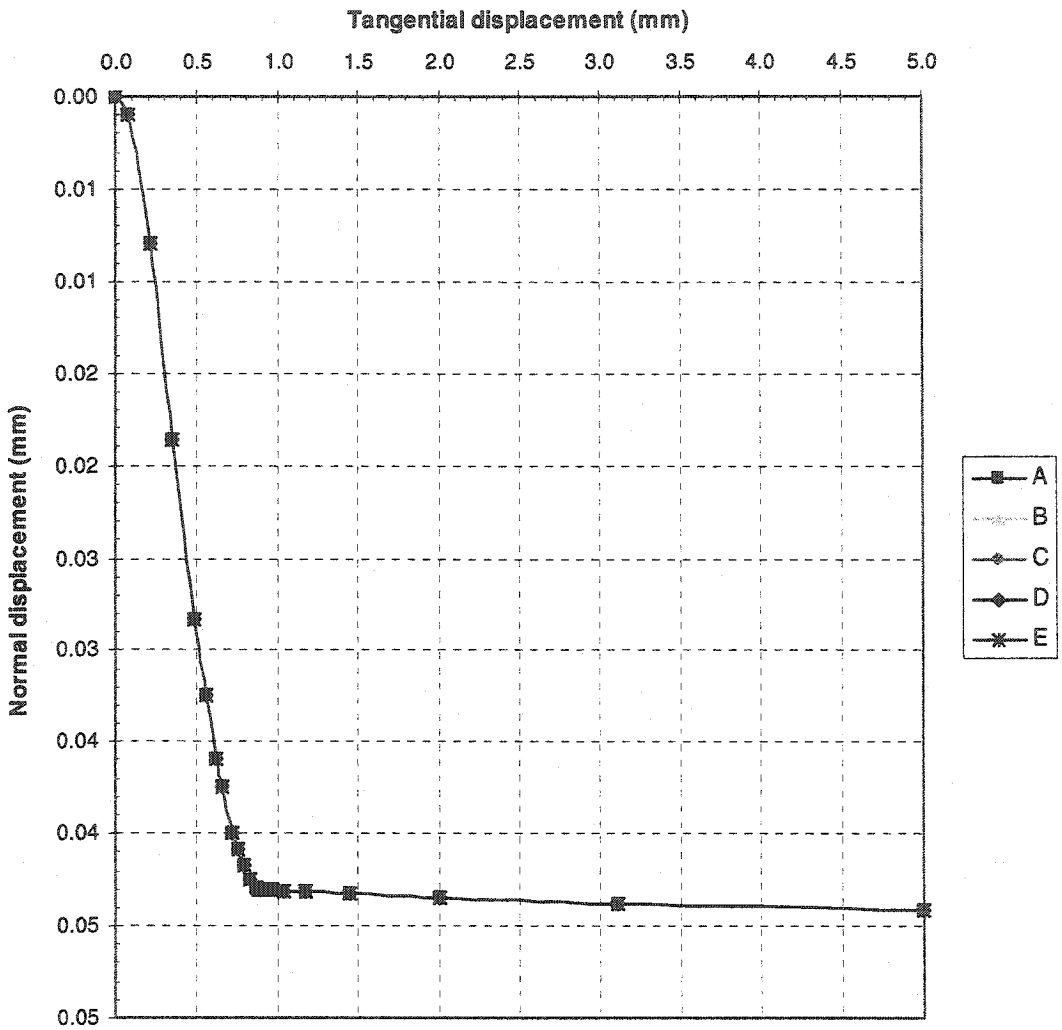

Figure 6.19 Normal displacement versus tangential displacement curves at different locations on the loading cap, as illustrated in Figure 6.12, constant normal stress = 300 kPa

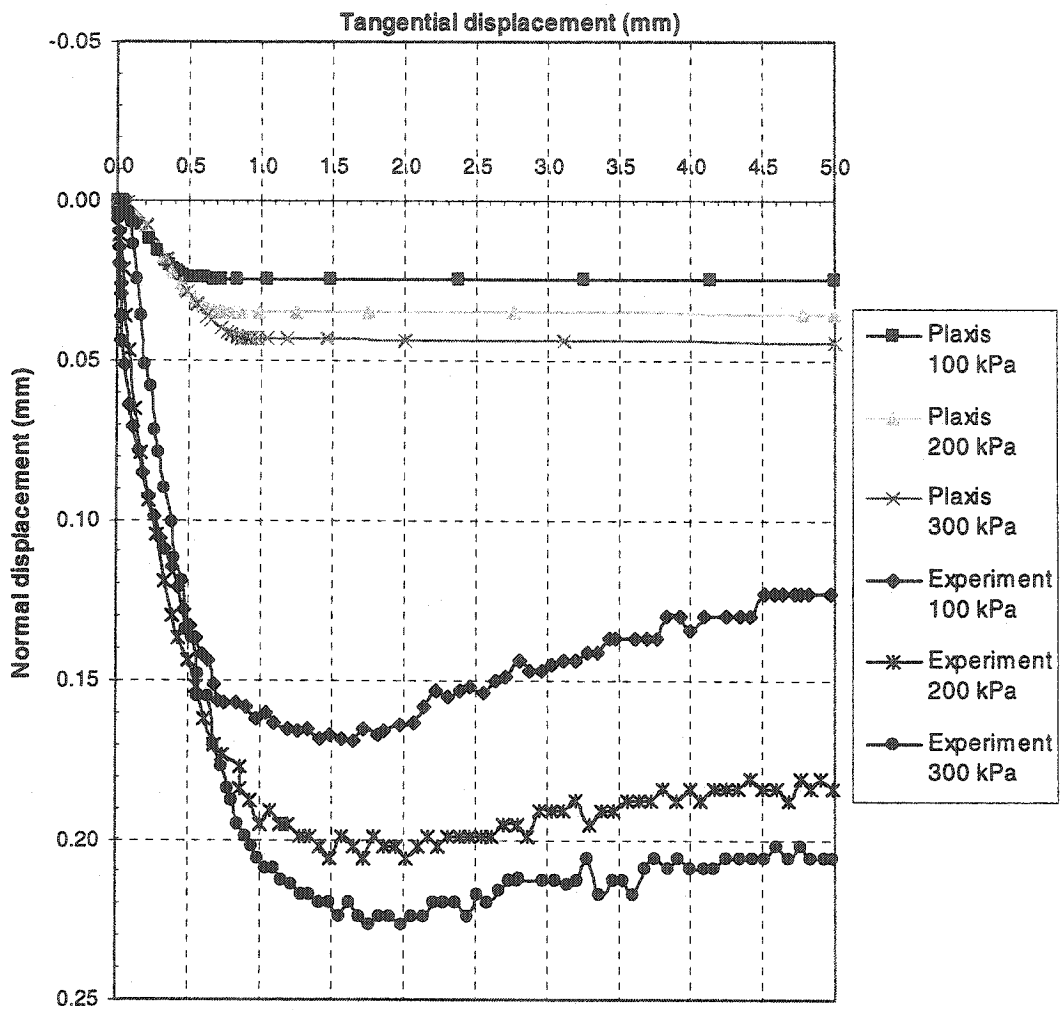

Figure 6.20 Comparison of experimental results and Plaxis results of average normal displacement versus tangential displacement curves

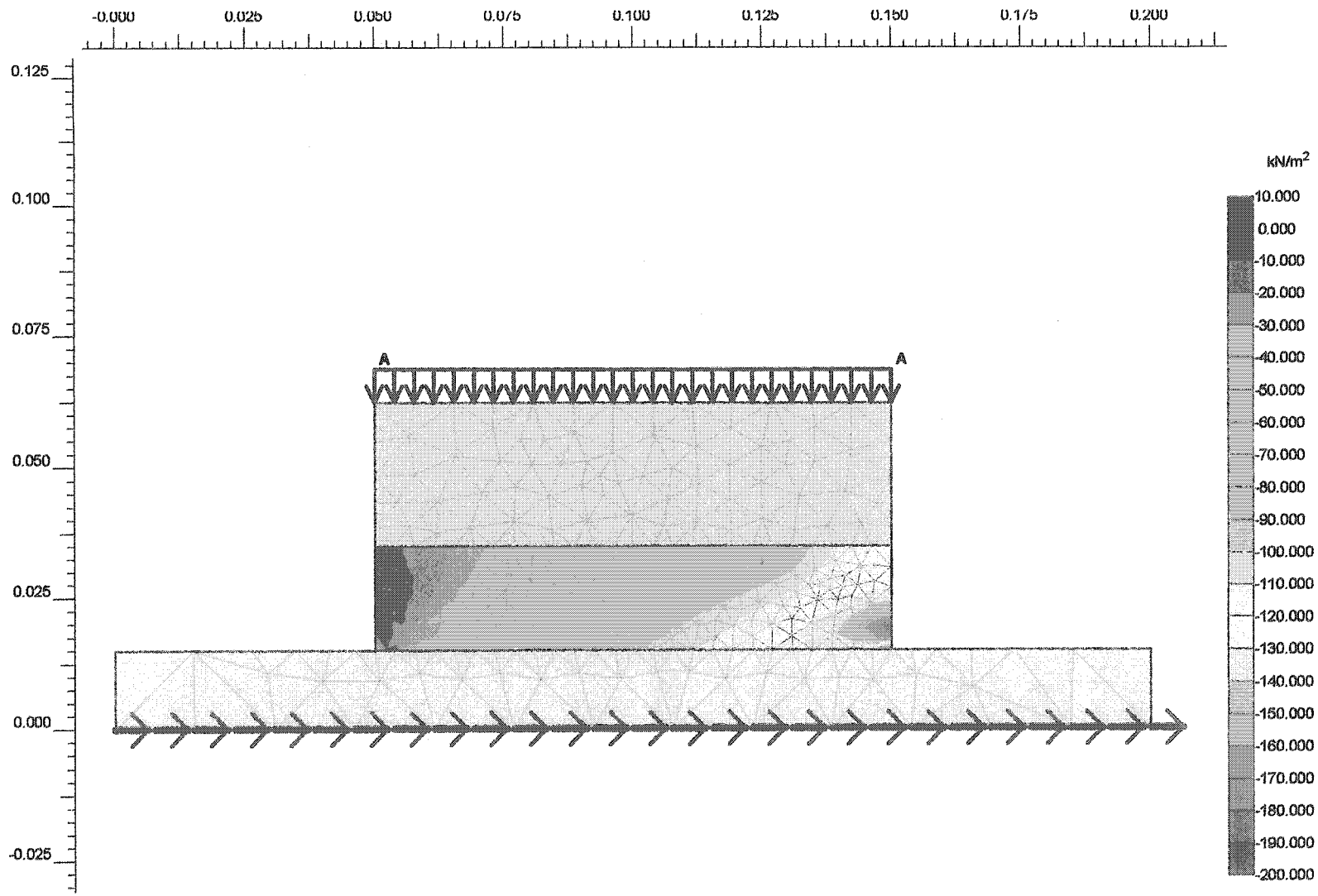

Figure 6.21 Mean stress shading for an applied constant normal stress = 100 kPa. Compression is negative.

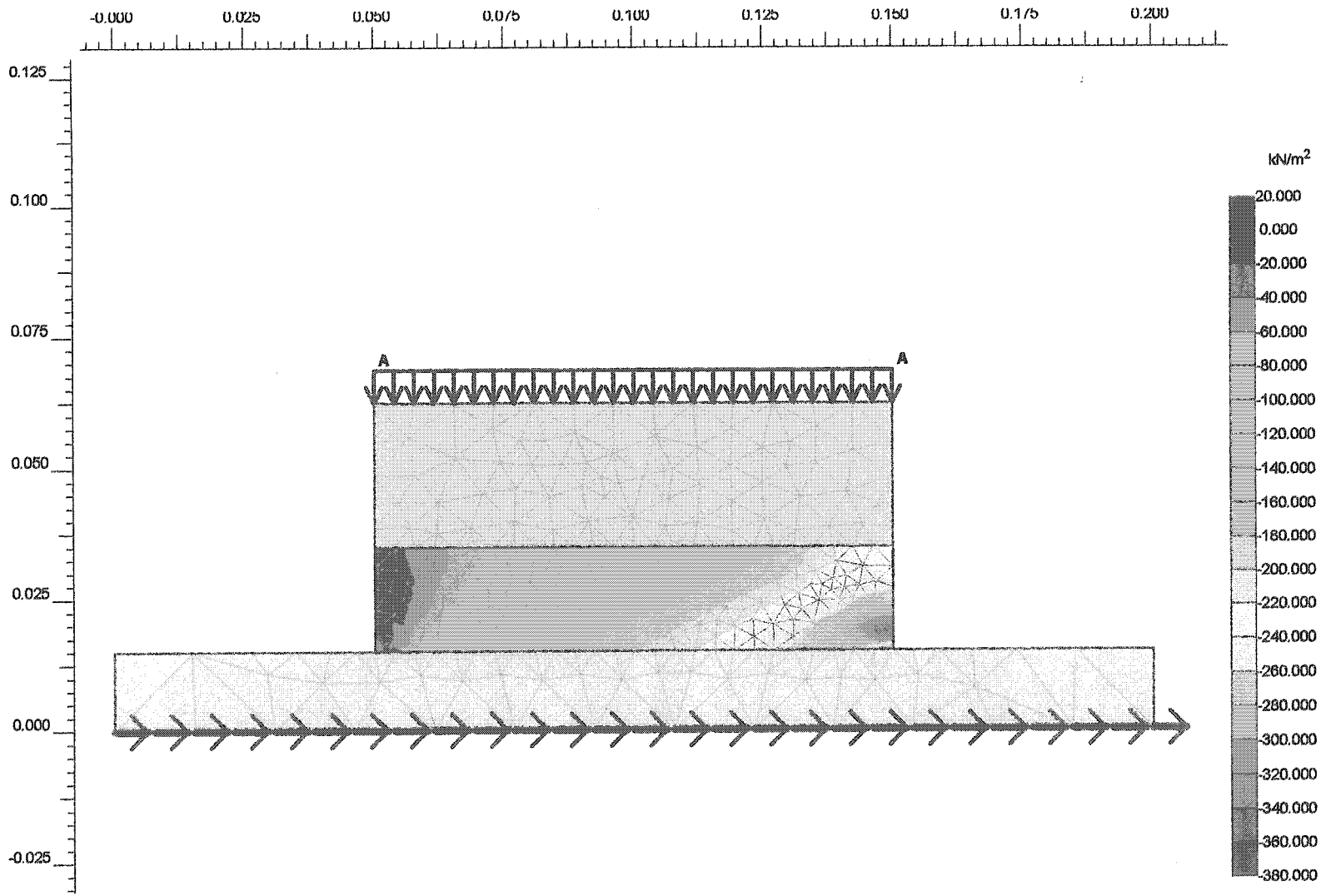

Figure 6.22 Mean stress shading for an applied constant normal stress = 200 kPa. Compression is negative.

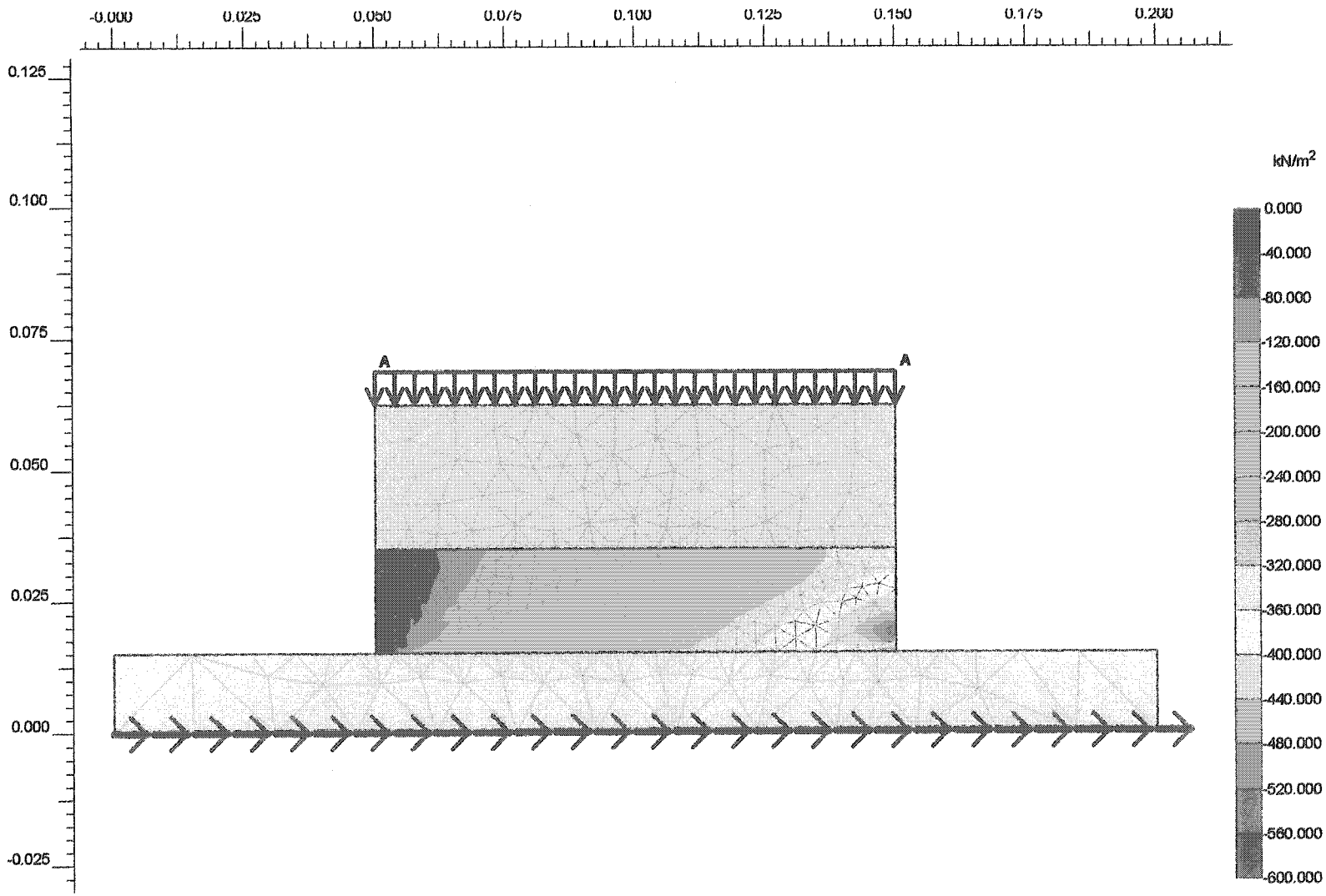

Figure 6.23 Mean stress shading for an applied constant normal stress = 300 kPa. Compression is negative.

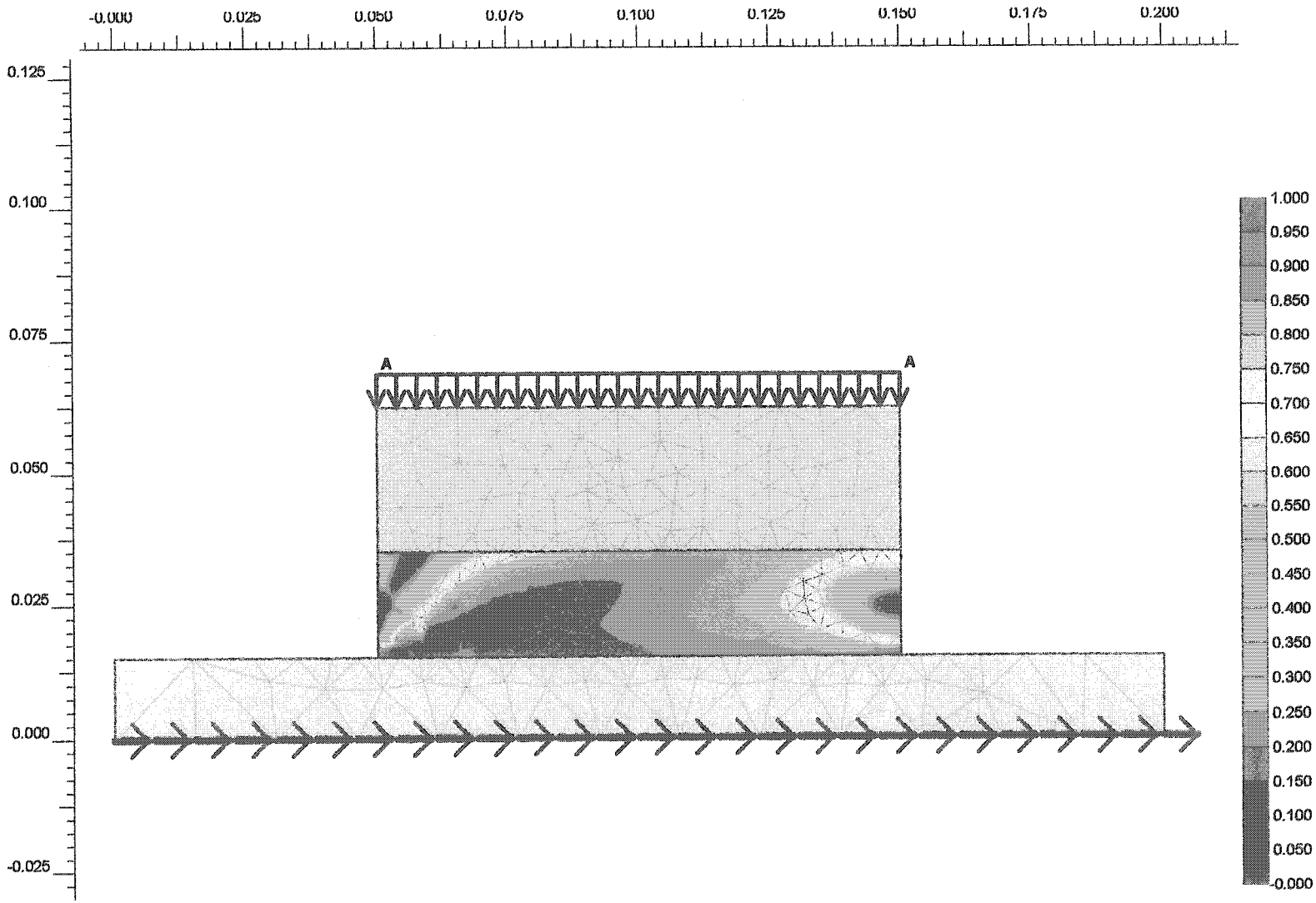

Figure 6.24 Relative shear shading for an applied constant normal stress = 100 kPa

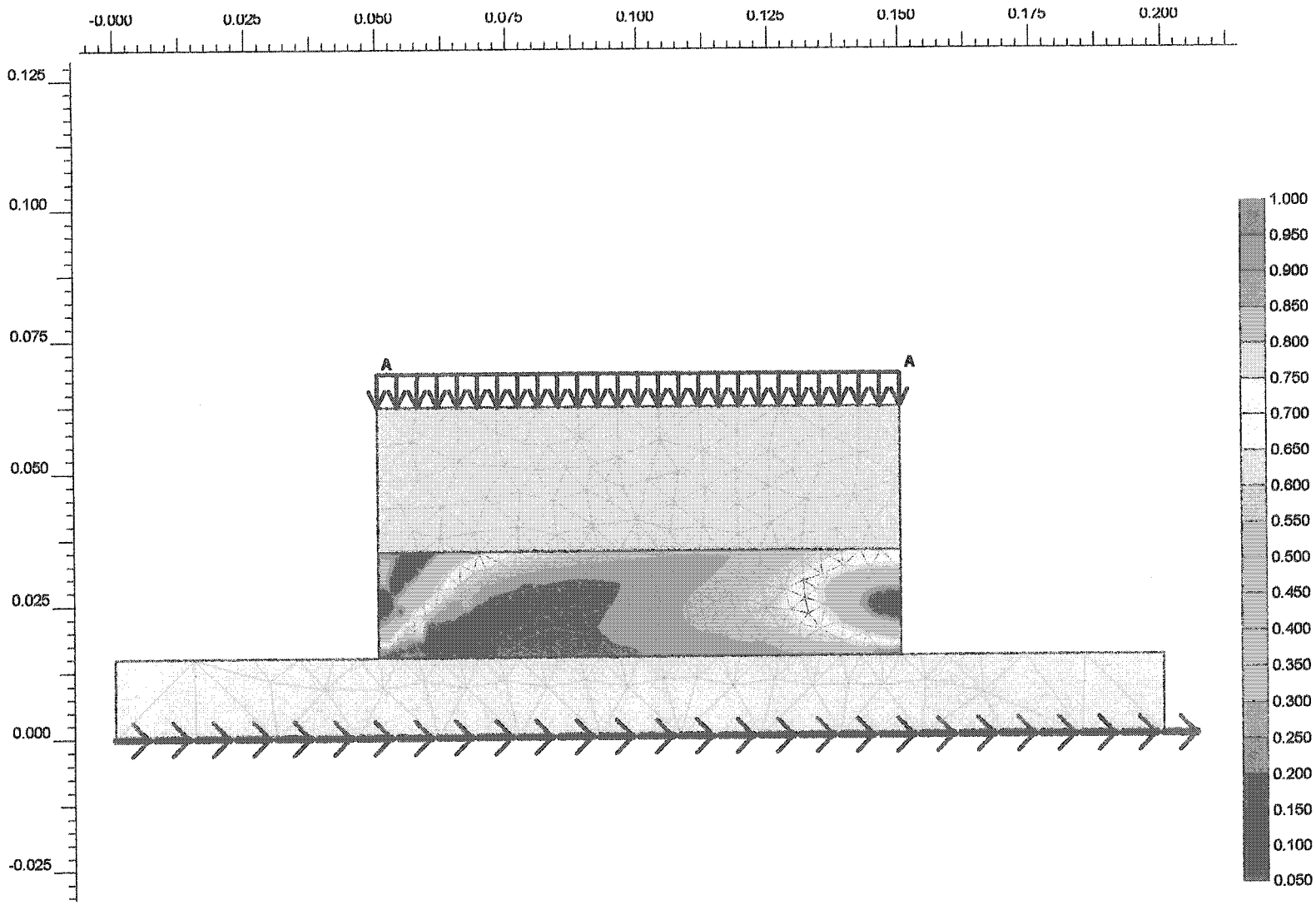

Figure 6.25 Relative shear shading for an applied constant normal stress = 200 kPa

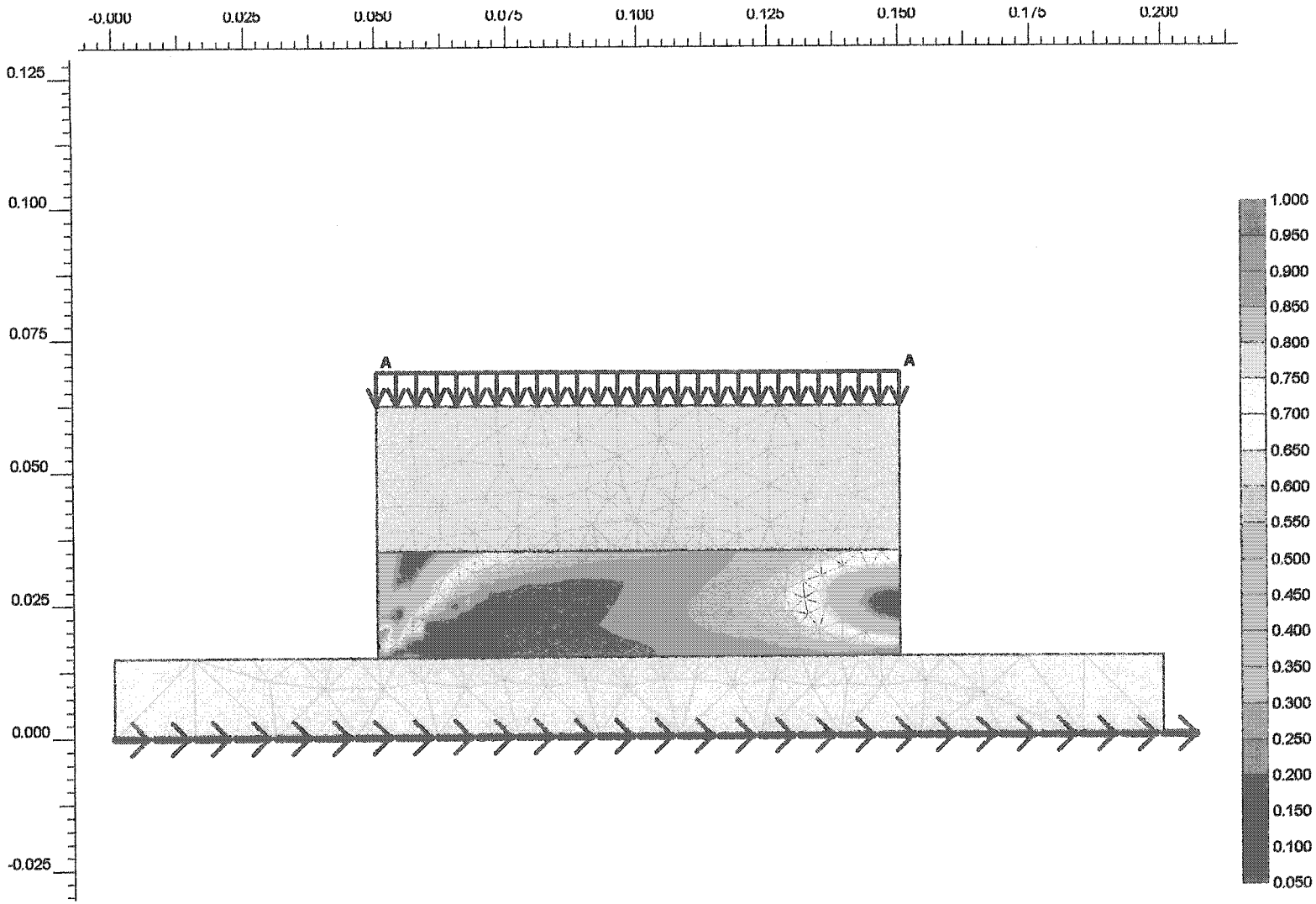

Figure 6.26 Relative shear shading for an applied constant normal stress = 300 kPa

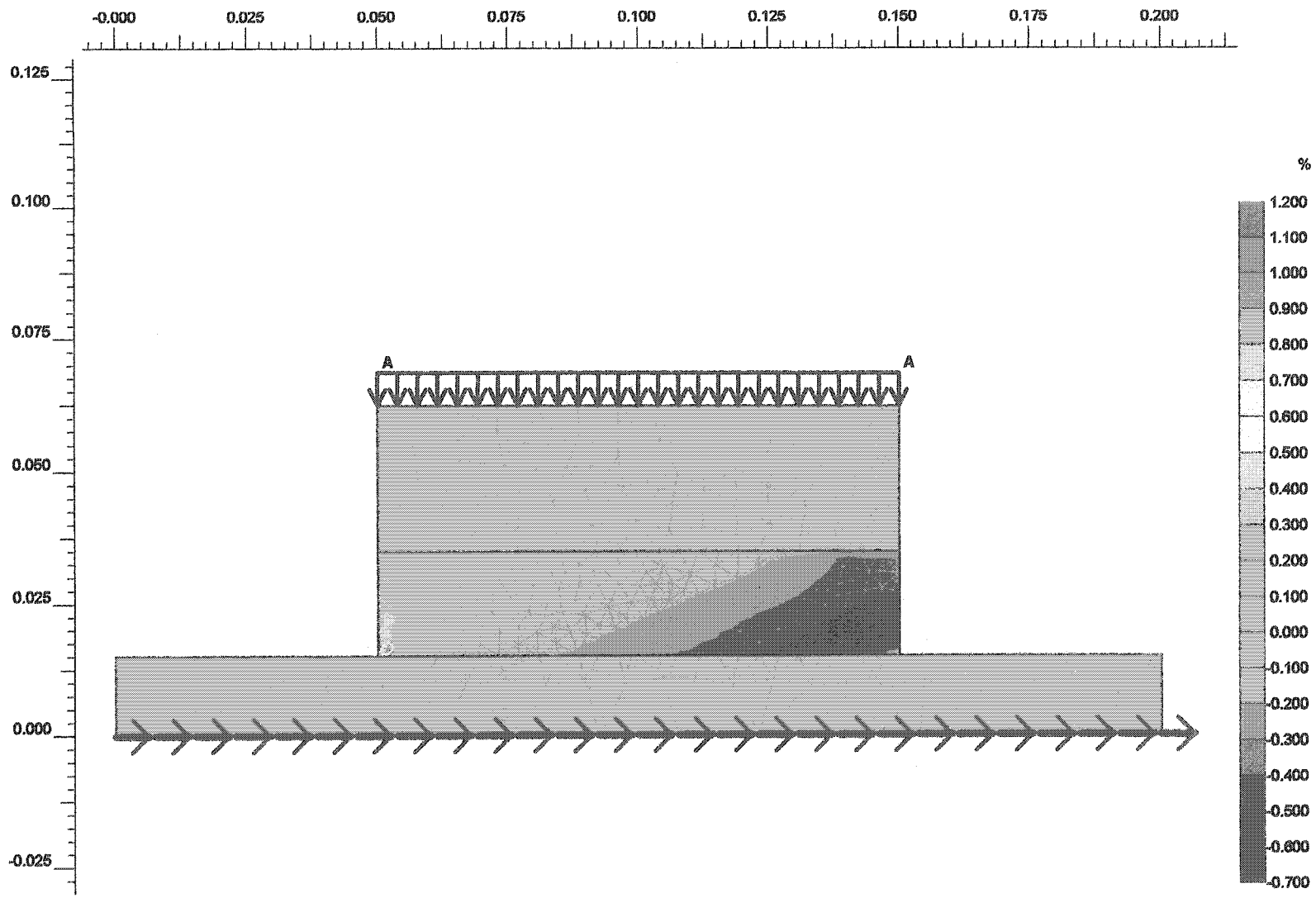

Figure 6.27 Total volumetric strain shading for a constant normal stress = 100 kPa. Compression is negative. Dilation is positive.

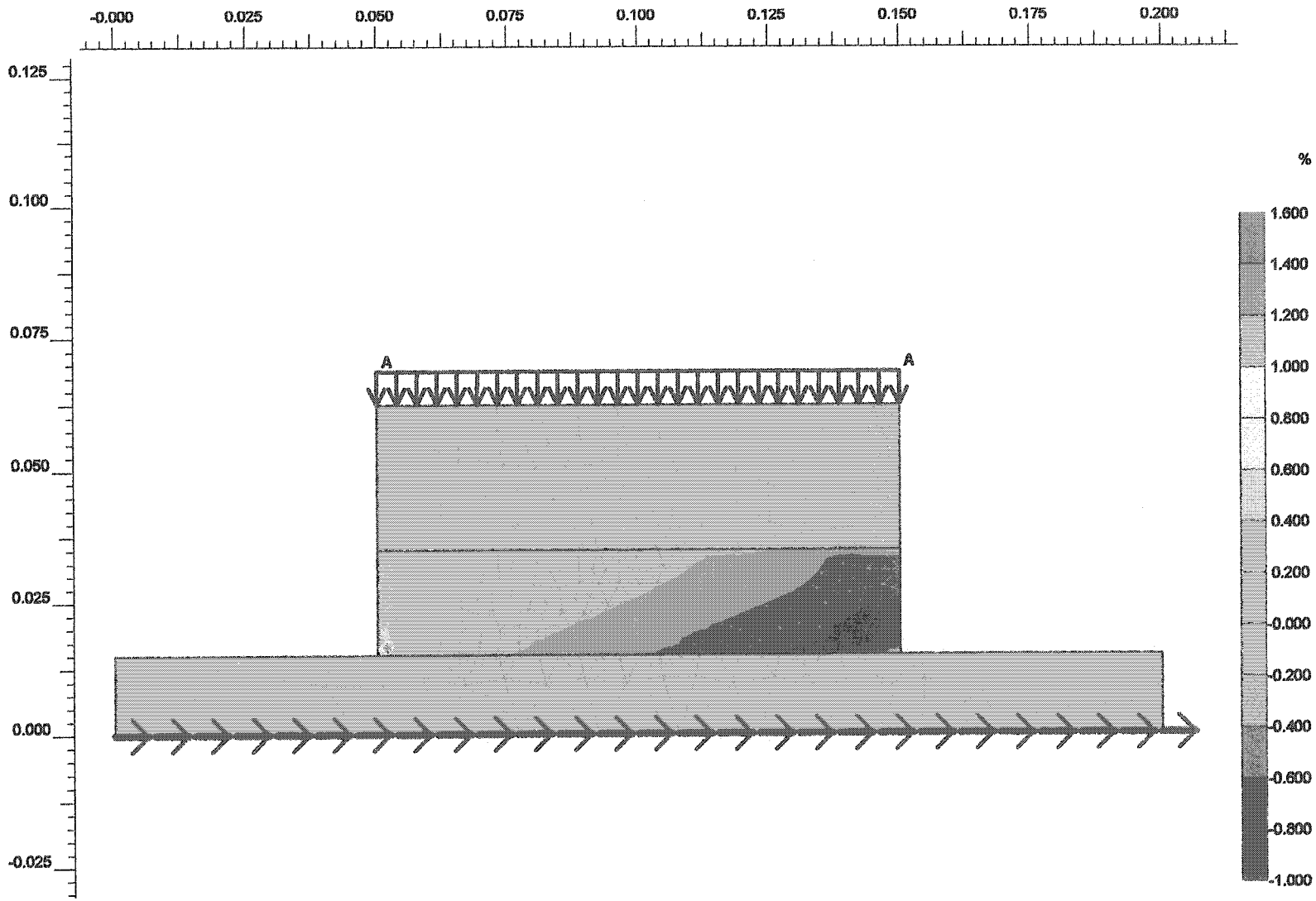

Figure 6.28 Total volumetric strain shading for a constant normal stress = 200 kPa. Compression is negative. Dilation is positive.

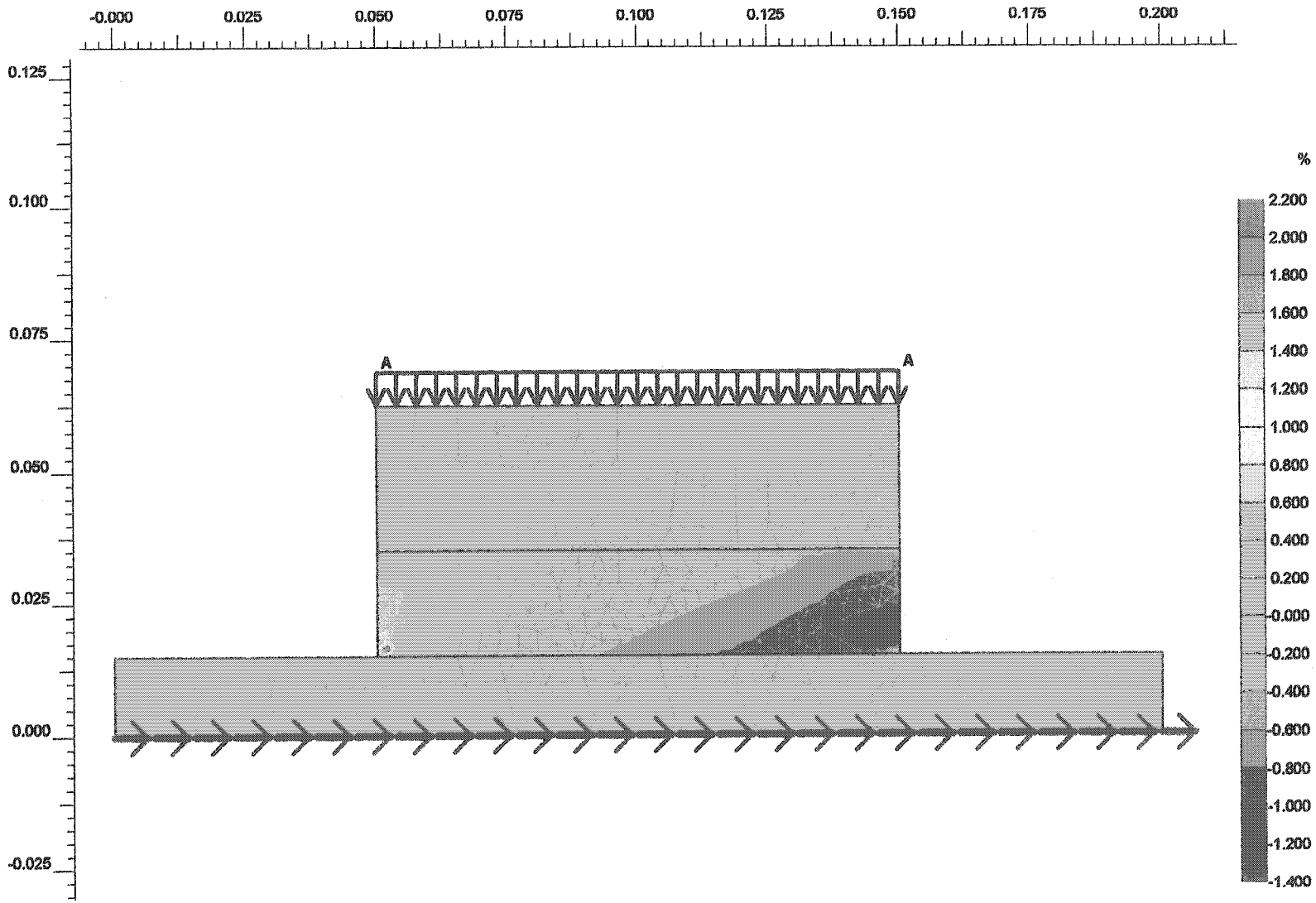

Figure 6.29 Total volumetric strain shading for a constant normal stress = 300 kPa. Compression is negative. Dilation is positive.

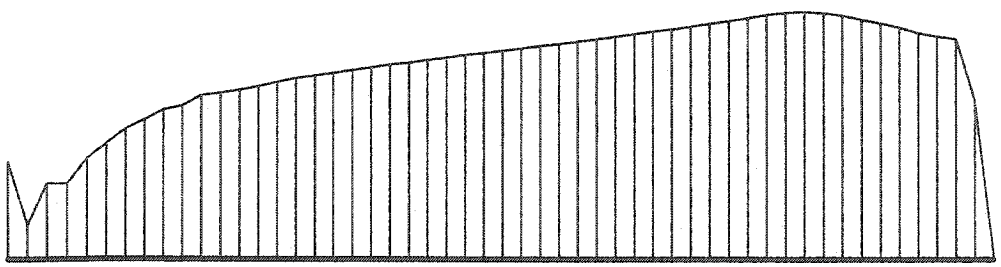

Figure 6.30 Profile of normal stress in the interface for a constant normal stress=100 kPa
Extreme normal stress: 129.90 kPa

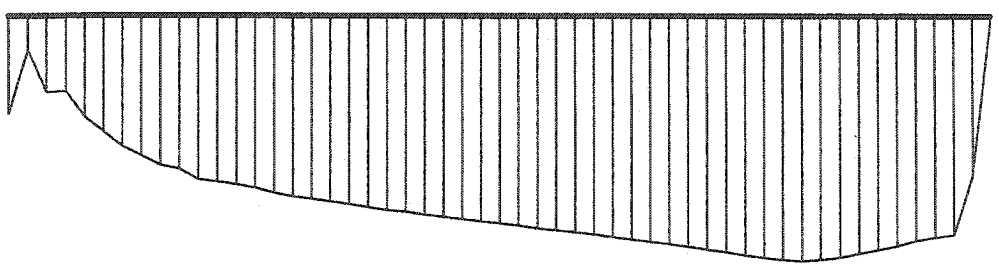

Figure 6.31 Profile of shear stress in the interface for a constant normal stress=100 kPa
Extreme shear stress: 78.01 kPa

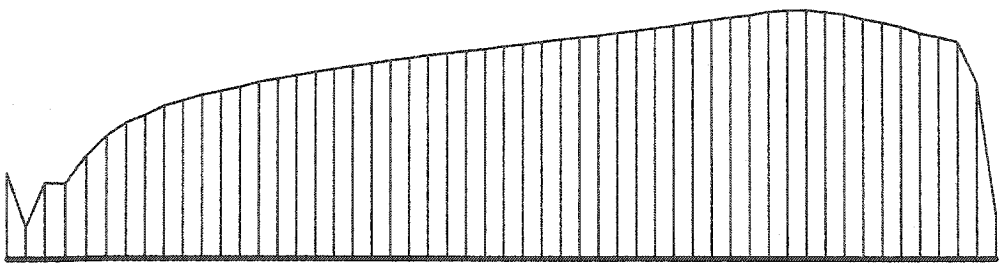

Figure 6.32 Profile of normal stress in the interface for a constant normal stress=200 kPa
Extreme normal stress: 257.21 kPa

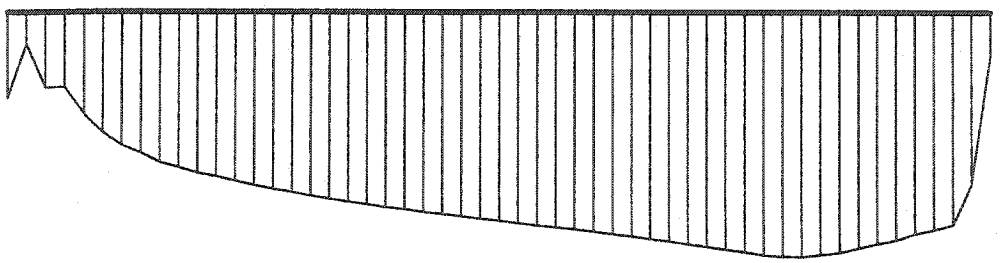

Figure 6.33 Profile of shear stress in the interface for a constant normal stress=200 kPa
Extreme shear stress: 154.30 kPa

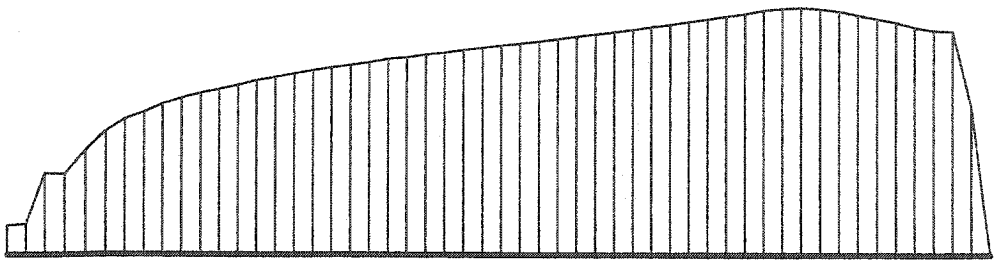

Figure 6.34 Profile of normal stress in the interface for a constant normal stress=300 kPa
Extreme normal stress: 390.20 kPa

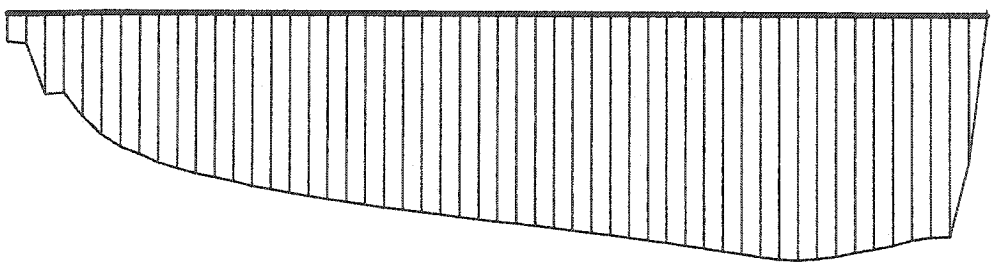

Figure 6.35 Profile of shear stress in the interface for a constant normal stress=300 kPa
Extreme shear stress: 233.99 kPa

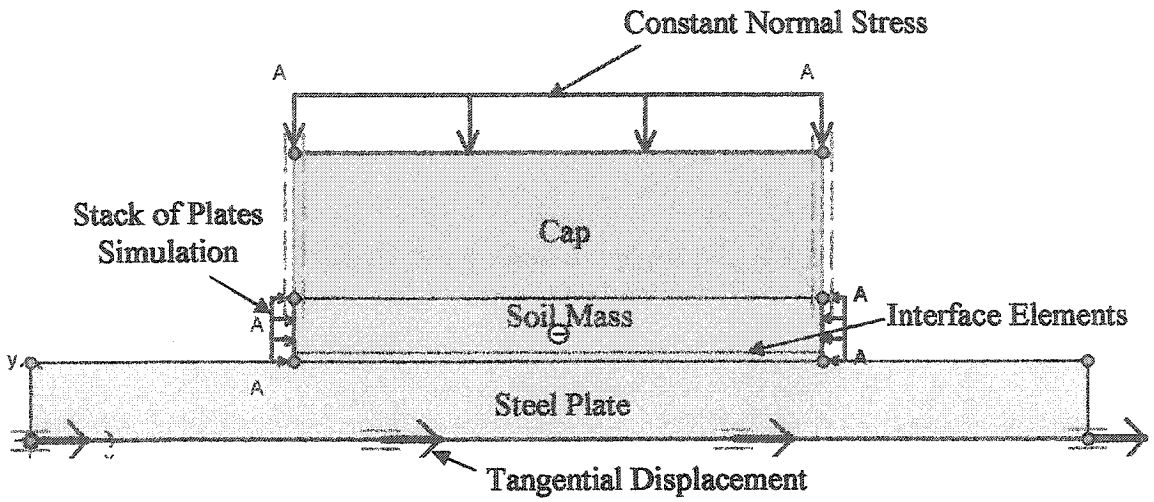

Figure 6.36 Geometry #1: No interface soil layer, interface represented by the Plaxis interface reduction factor, $R_{int} = 0.66$, resulting in an interface friction angle, $\delta = 26.6°$

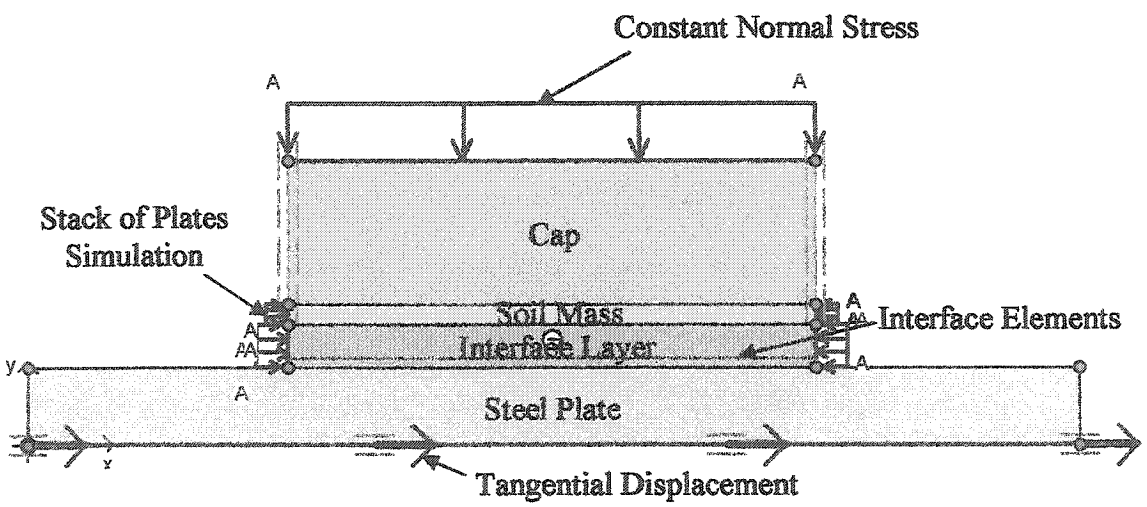

Figure 6.37 Geometry #2: Interface represented by an independent soil layer where $R_{int}=1.0$, $\phi=26.6°$

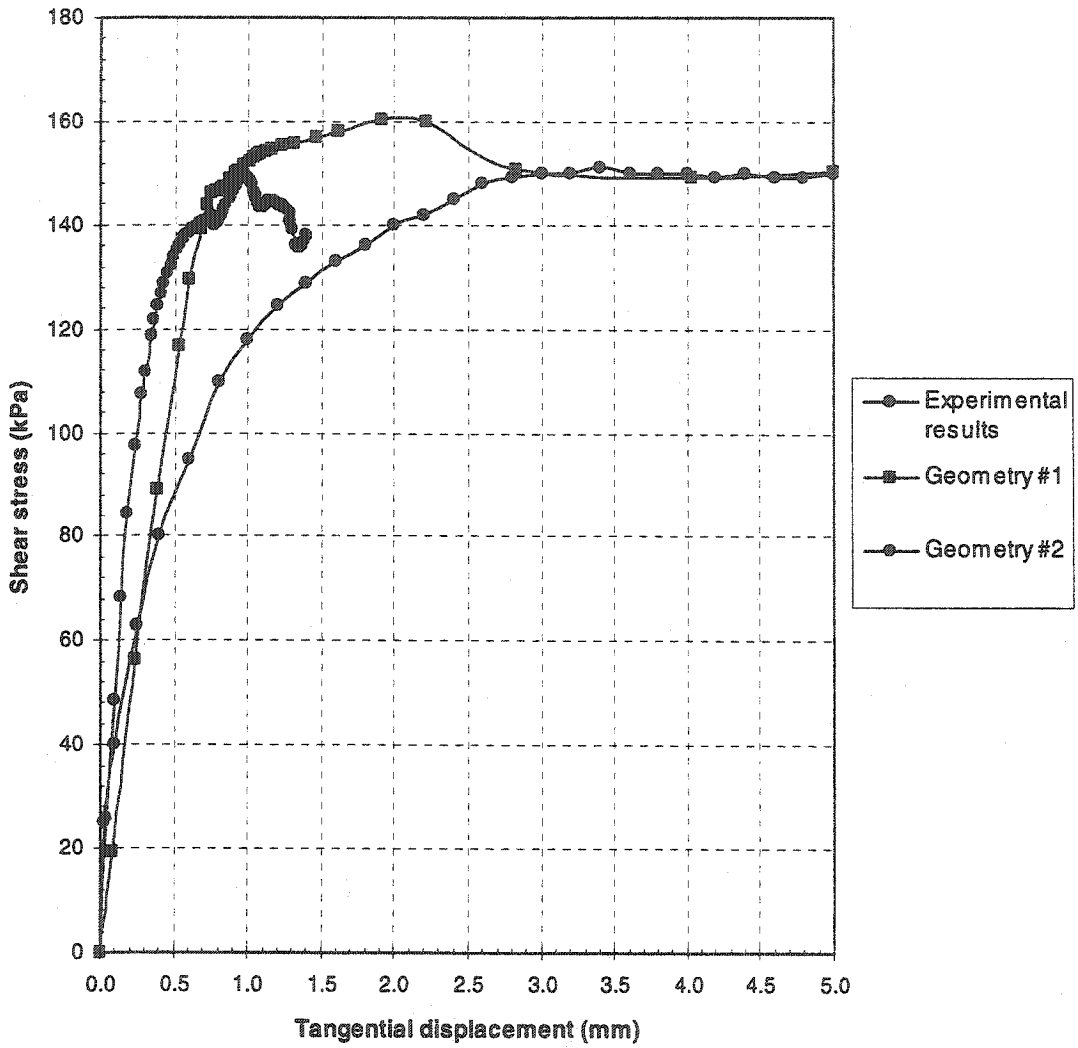

Figure 6.38 Plaxis results for shear stress versus tangential displacement curves for the geometries in Figures 6.36 and 6.37 in comparison to the experimental results, constant normal stress = 300 kPa

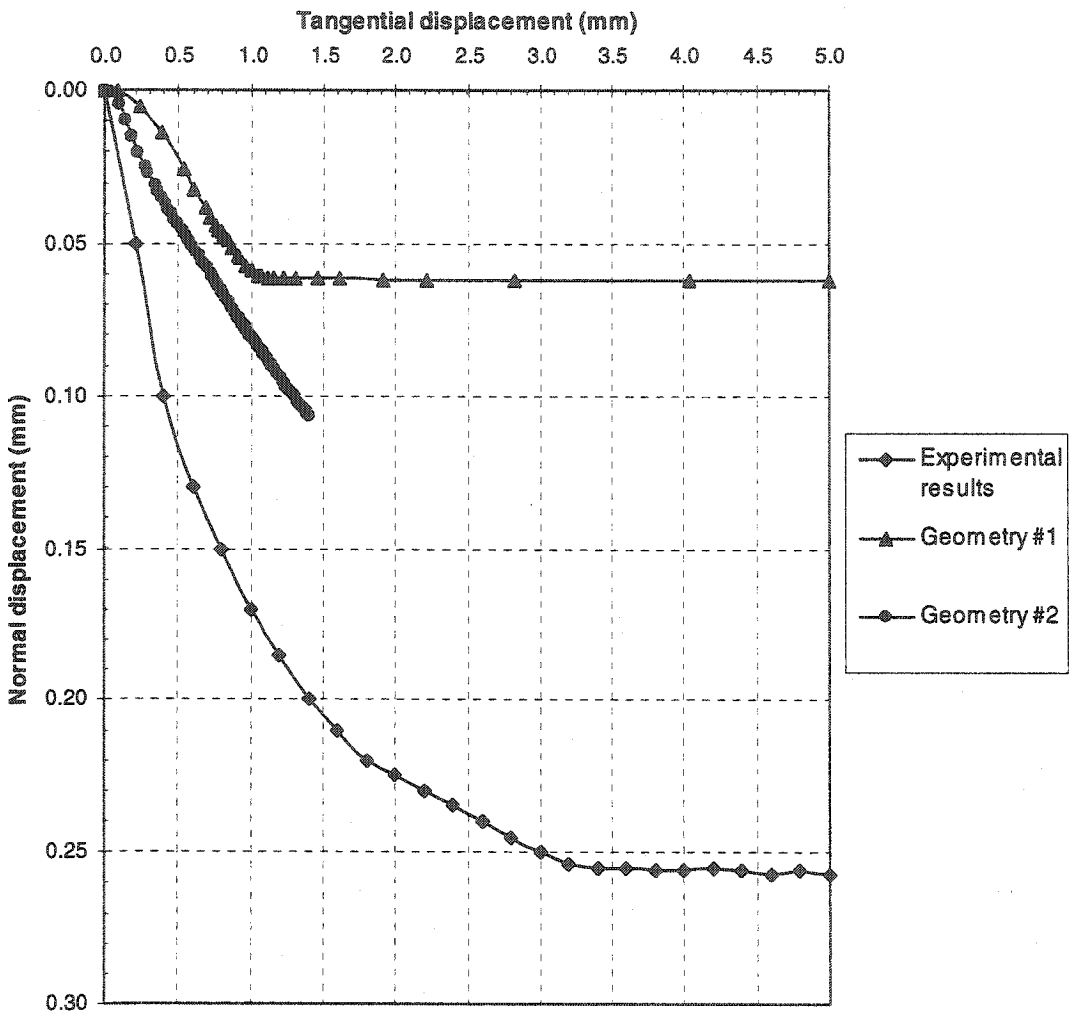

Figure 6.39 Plaxis results for normal displacement versus tangential displacement curves for the geometries in Figures 6.36 and 6.37 in comparison to the experimental results, constant normal stress = 300 kPa

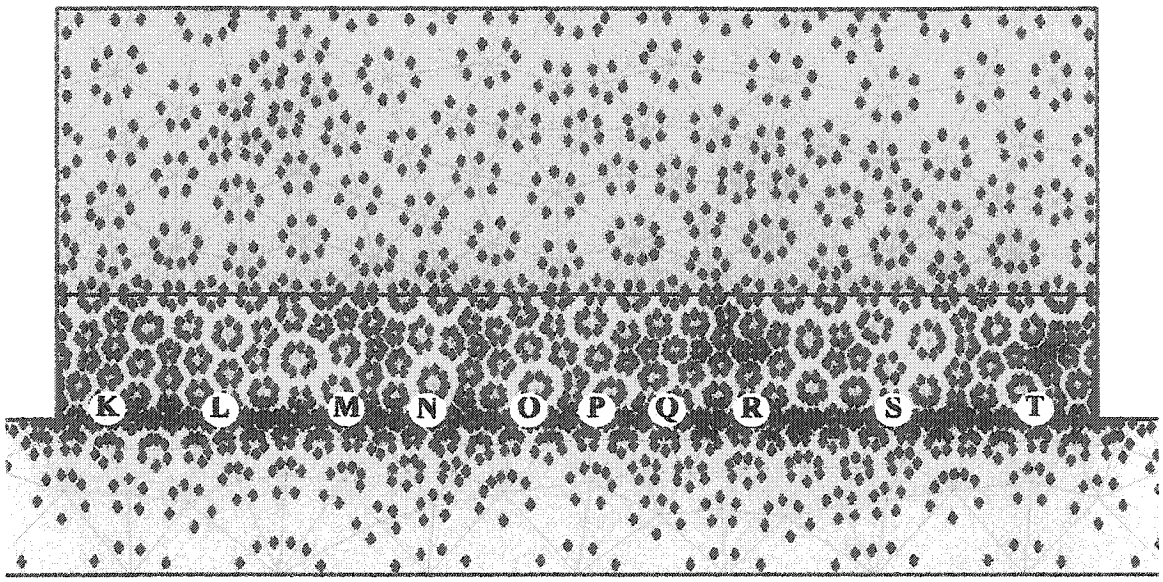

Figure 6.40 Schematic presentation of the locations of stress points for simple shear test

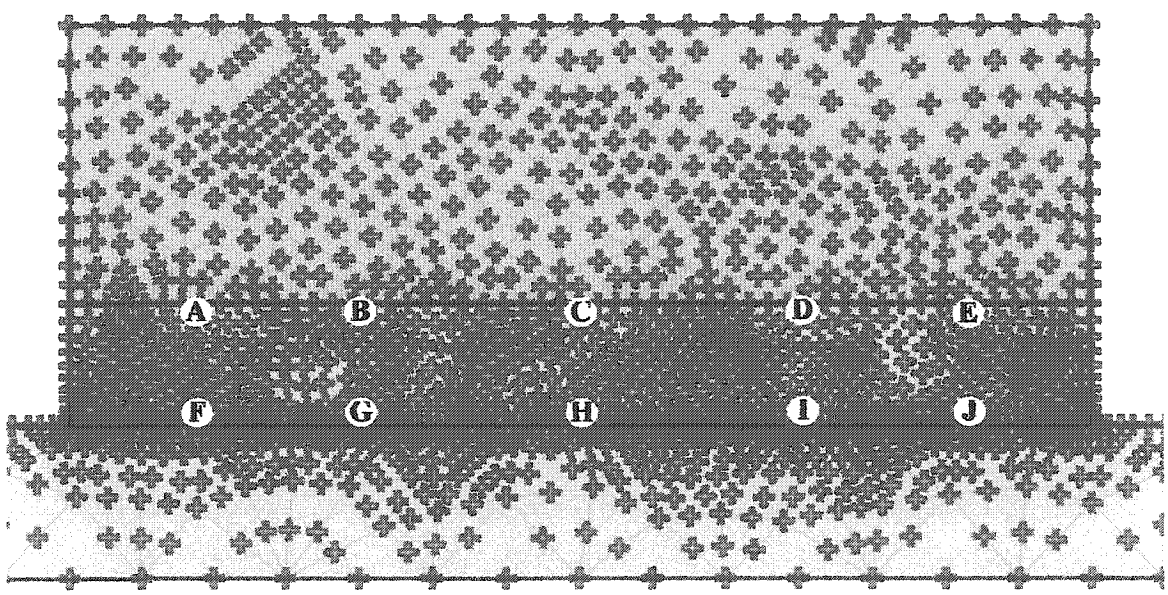

Figure 6.41 Schematic presentation of the locations of nodal points for simple shear test

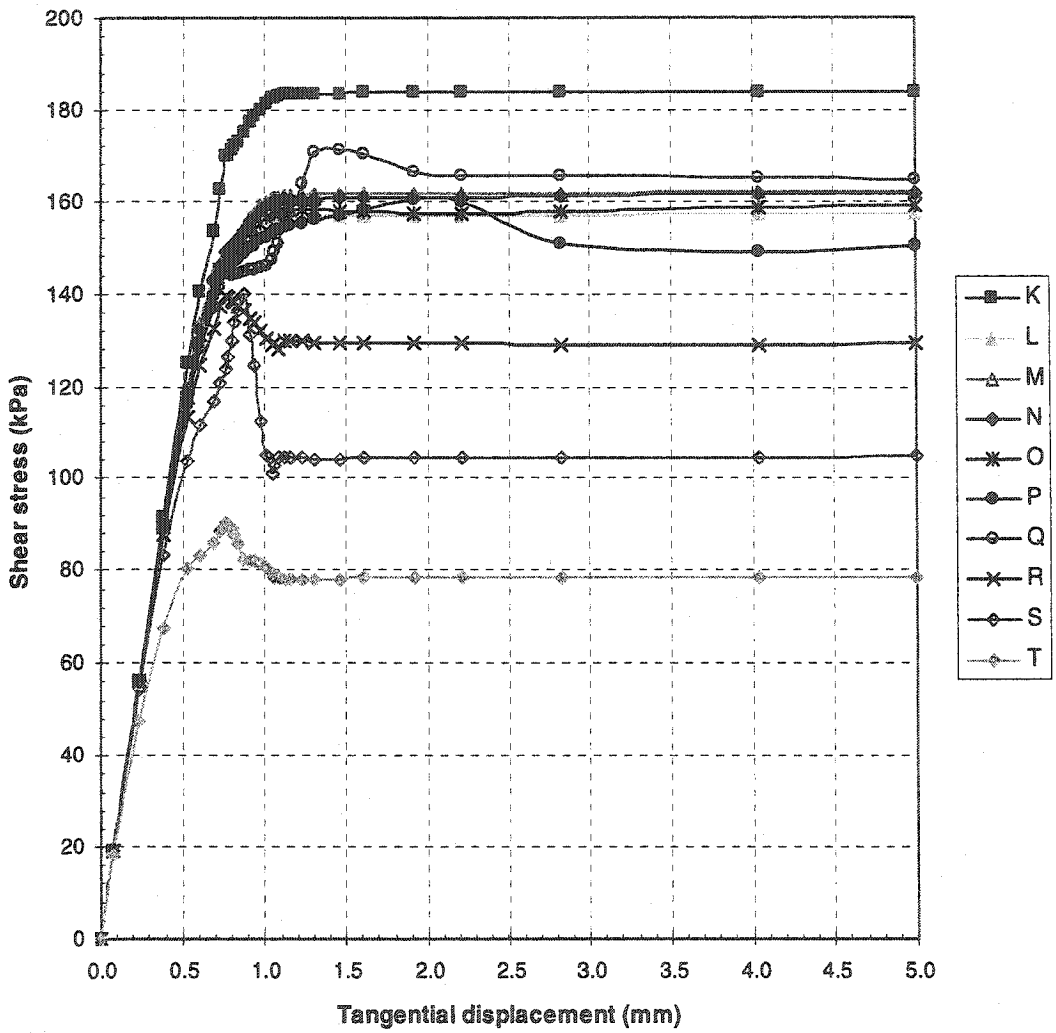

Figure 6.42 Shear stress versus tangential displacement curves for a simple shear test at different locations on the interface, as illustrated in Figure 6.40, constant normal stress = 300 kPa

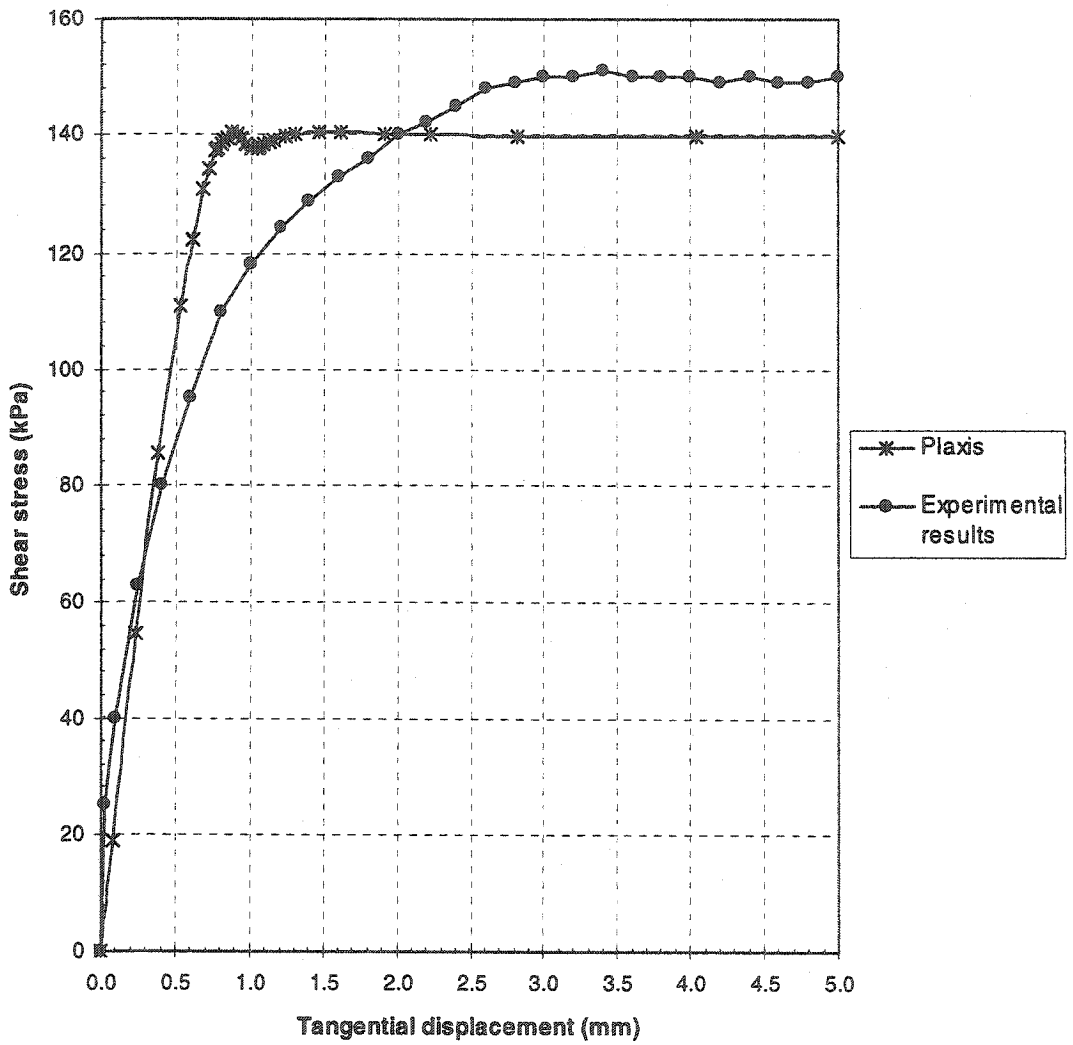

Figure 6.43 Comparison of the results of experiments and Plaxis for shear stress versus tangential displacement curves related to a simple shear test

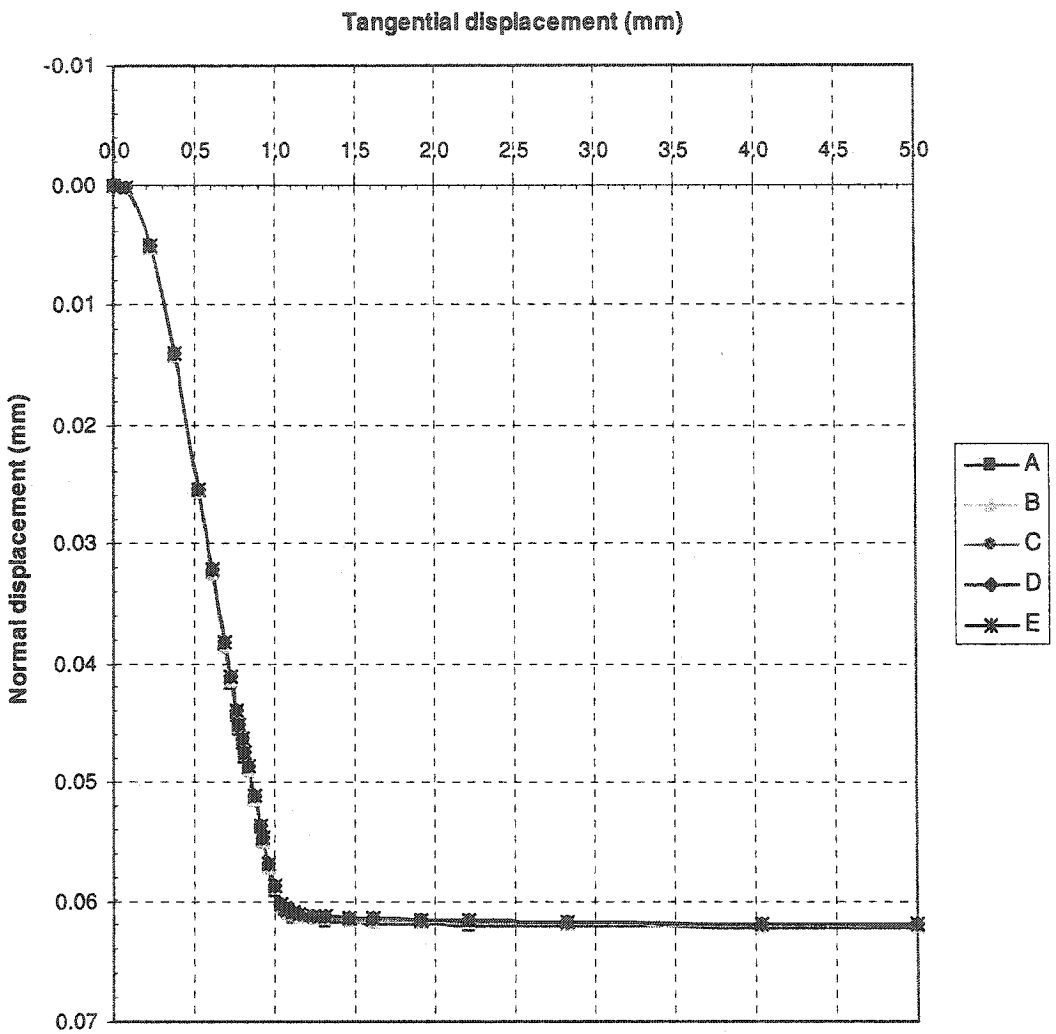

Figure 6.44 Normal versus tangential displacement curves for a simple shear test at different locations on the interface, as illustrated in Figure 6.41, constant normal stress = 300 kPa

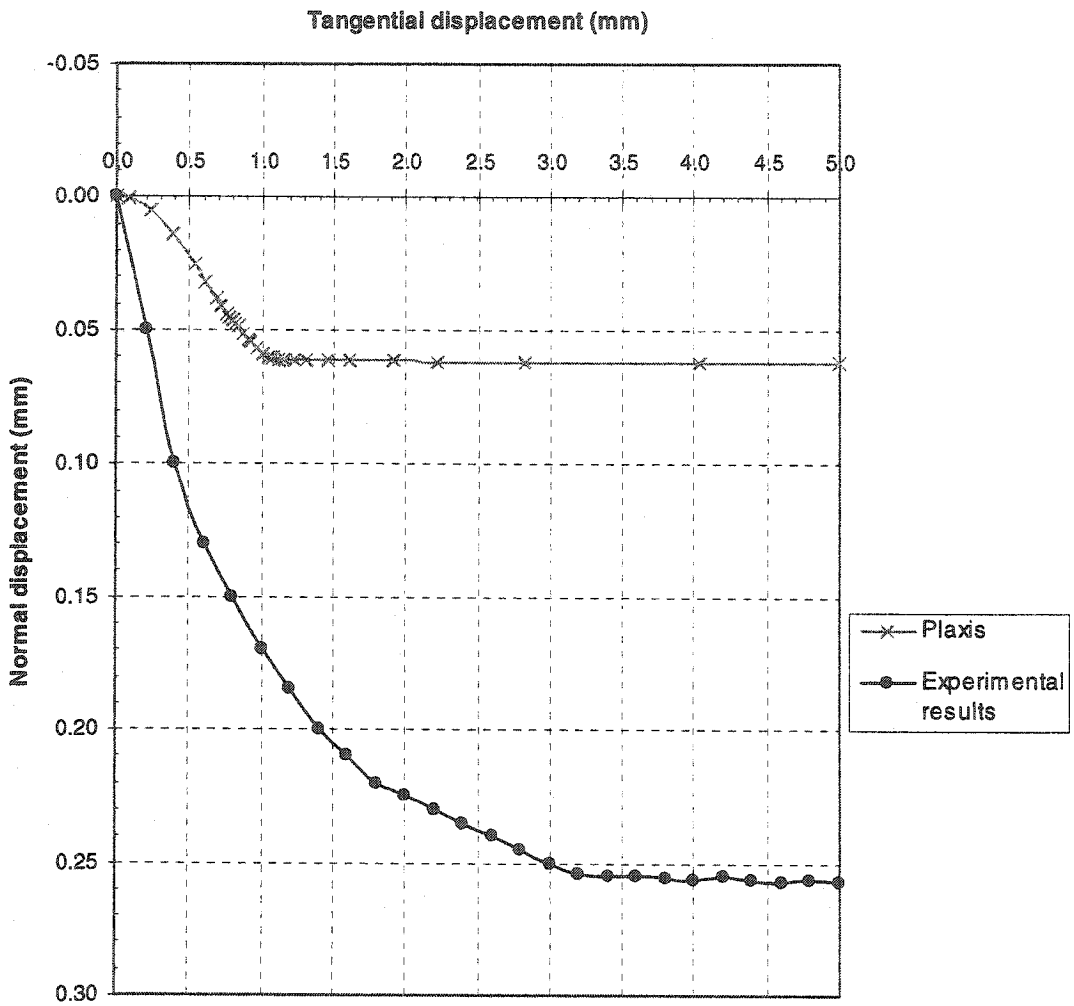

Figure 6.45 Comparison of the results of experiments and Plaxis for normal displacement versus tangential displacement curves related to a simple shear test

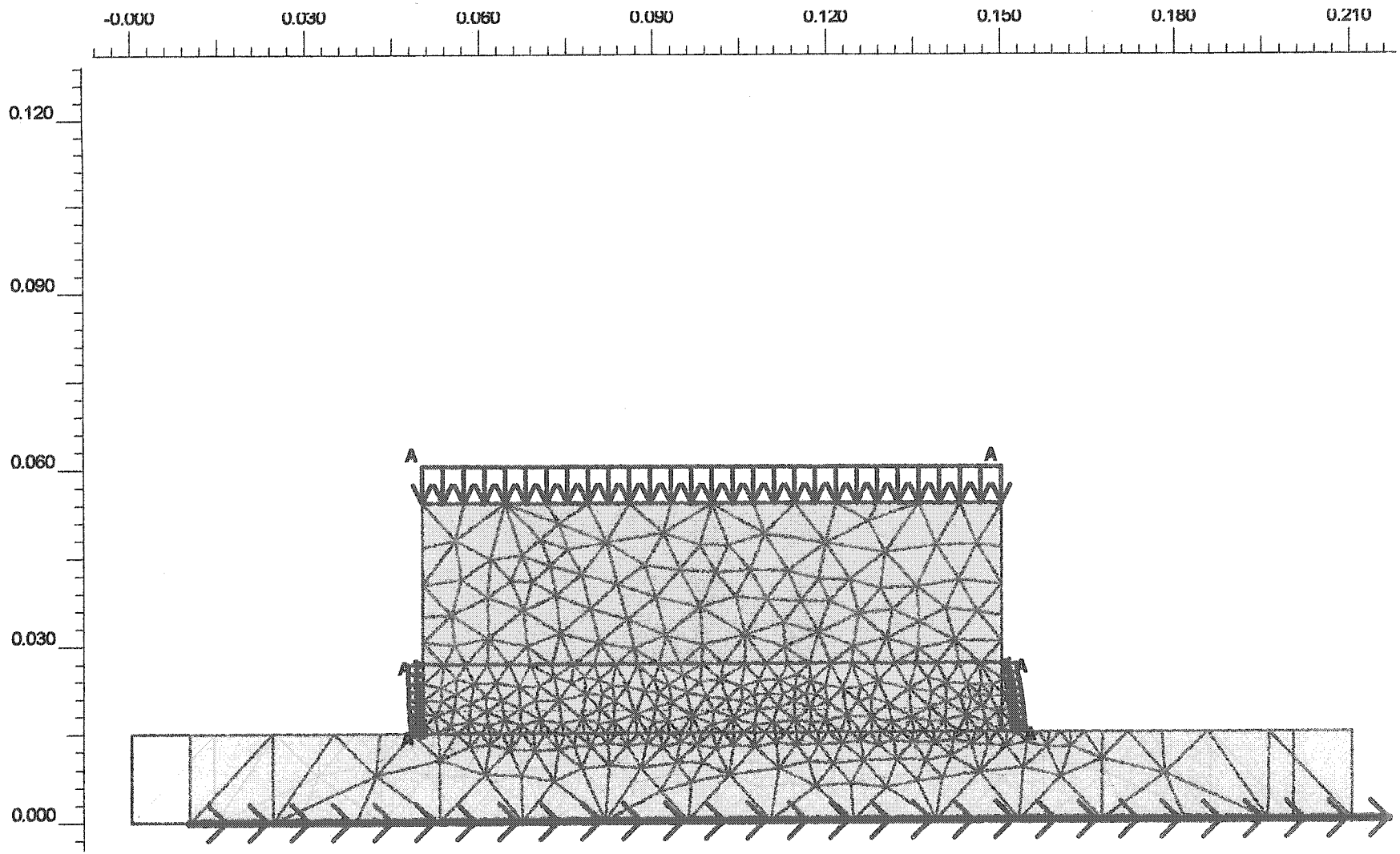

Figure 6.46 Deformed mesh for an applied constant normal stress = 300 kPa

True scale

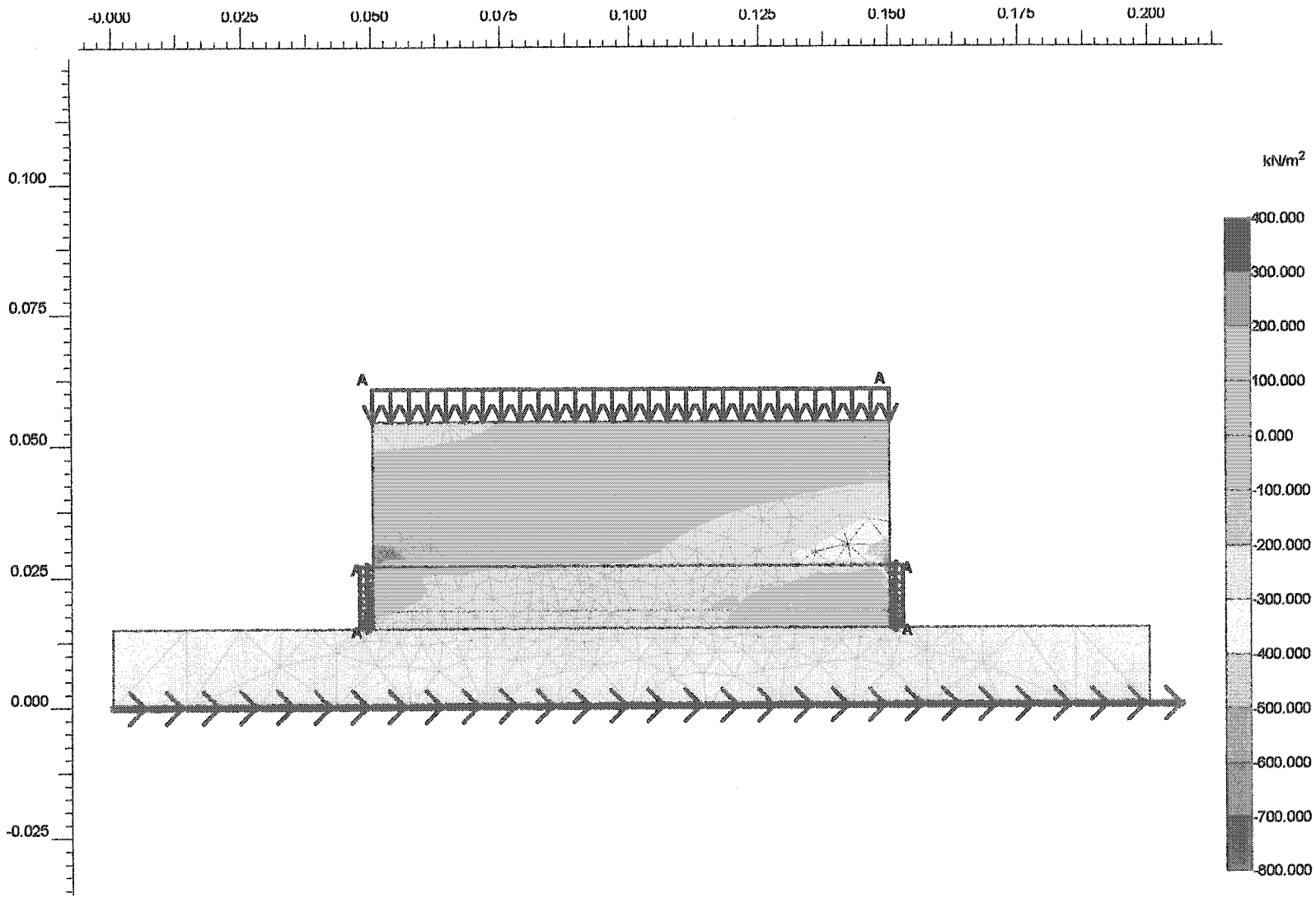

Figure 6.47 Mean stress shading for a simple shear test at an applied constant normal stress = 300 kPa. Compression is negative.

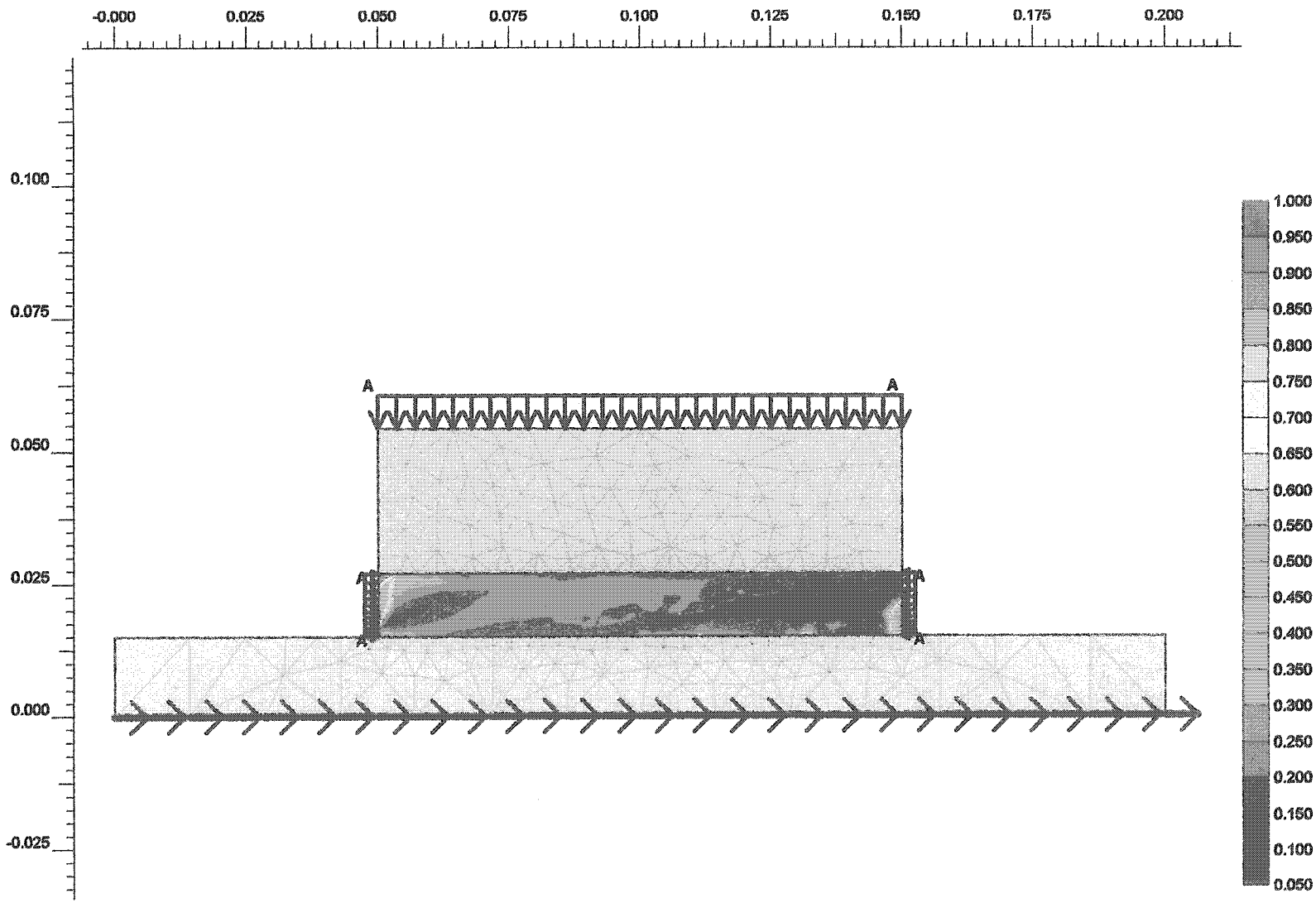

Figure 6.48 Relative shear shading for a simple shear test at an applied constant normal stress = 300 kPa

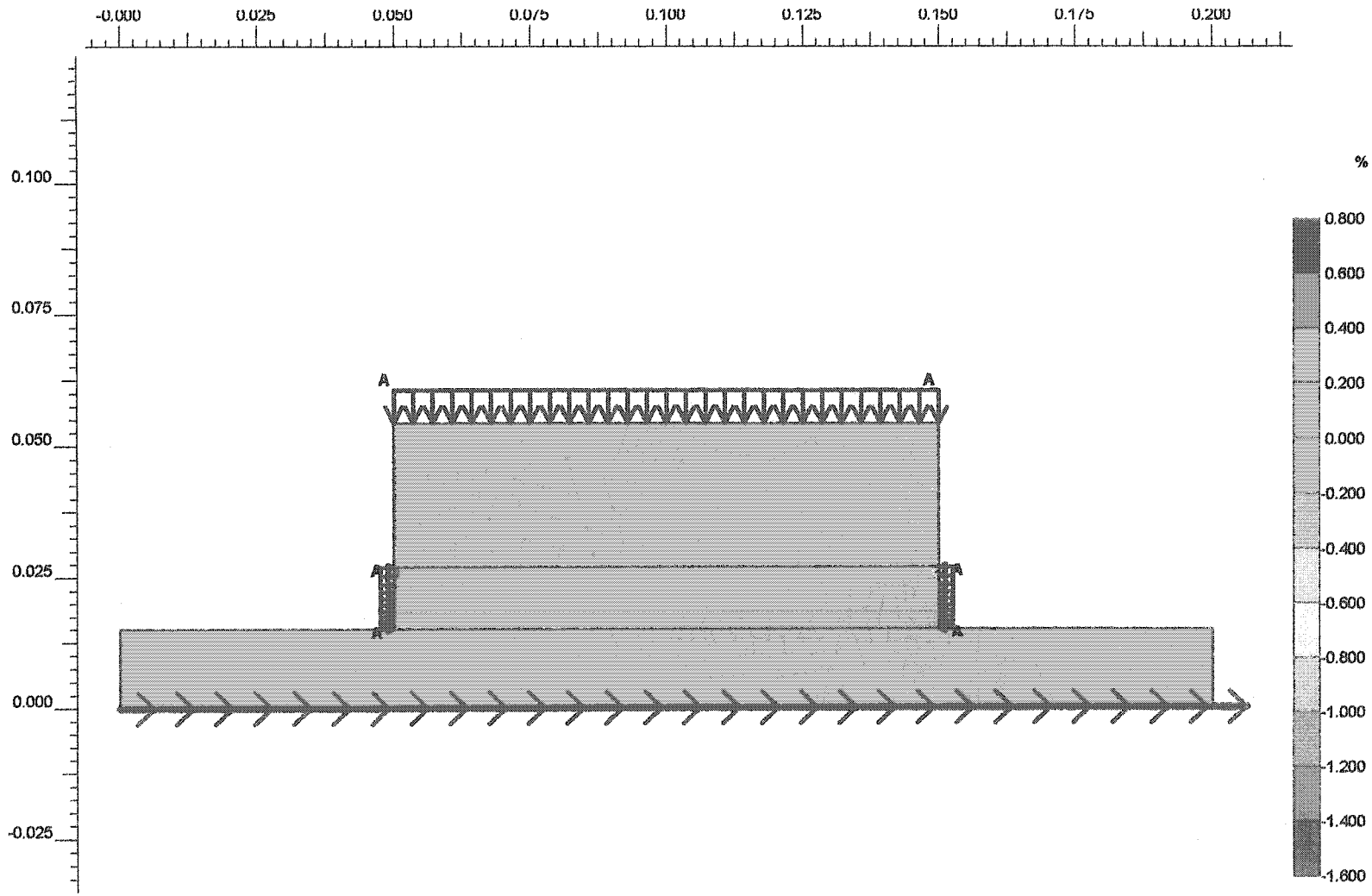

Figure 6.49 Total volumetric strain shading for a simple shear test at an applied constant normal stress = 300 kPa
Compression is negative. Dilation is positive.

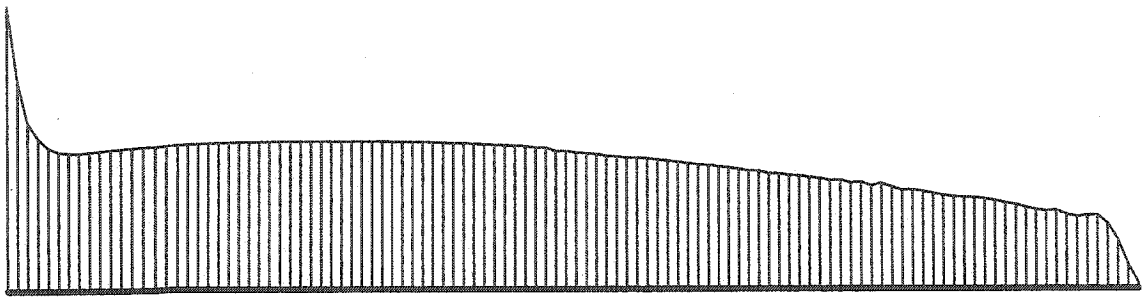

Figure 6.50 Profile of normal stress in the interface for a simple shear test at a constant normal stress=300 kPa. Extreme normal stress: 683.07 kPa

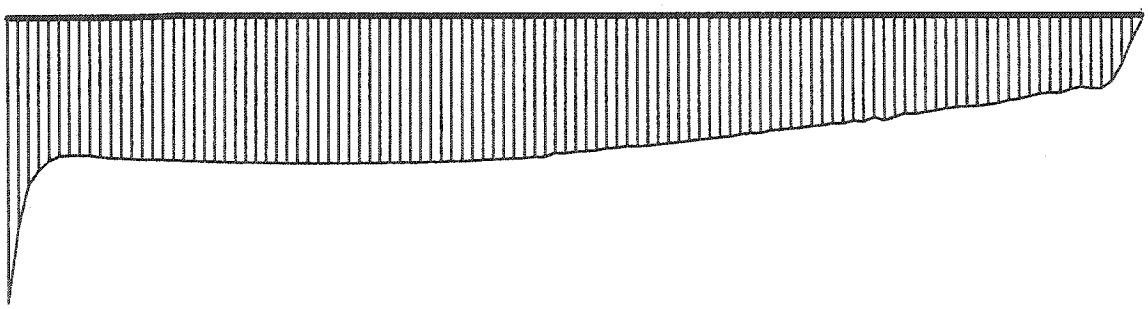

Figure 6.51 Profile of shear stress in the interface for a simple shear test at a constant normal stress=300 kPa Extreme shear stress: 310.27 kPa

CHAPTER 7
STRESS AND STRAIN STATES IN SOIL-STRUCTURE INTERFACE TESTS

To develop a realistic mathematical model for interfaces, which predicts the strain increments for the given stress increments or vice versa, the knowledge of the stress and strain states in a soil sample at all stages of an experiment is required. However, the existing experimental interface testing methods only provide information on the average normal stress and the average shear stress acting on the contact surface. There are no means to-date to determine the magnitude of the normal stress, σ_x, acting on the perpendicular plane to the interface surface. Neither the distribution of normal stresses nor the components of strains are measured. In this chapter, the stress and strain components in the soil sample (interface) are presented.

7.1 Direct shear interface test

In the previous chapter, a finite element analysis of a direct shear interface test, using the finite element code Plaxis, was carried out for a constant normal stress of 300 kPa. The problem was analysed as a plane strain case and the Hardening-soil model was used to simulate the behaviour of the soil. The stress and strain states of the soil, the Mohr circles, the stress paths, and the orientation of the principal stresses at various locations along the interface, as illustrated in Figure 6.11, are presented below. The results of the stress point K, can be overlooked since they are unrealistic due to the modelling limitations of the boundary effects, as explained in the previous chapter.

7.1.1 Stress and strain states

Stress state

Figure 7.1 shows the variation of the horizontal stress, σ_x, as the loading of the interface progressed from the initial condition to the failure state. Initially when the constant normal stress is applied, the horizontal stress is 120 kPa. As the tangential displacement is applied, σ_x increases nonlinearly until a tangential displacement of approximately 0.75 mm. Subsequently, σ_x remains constant except at a few points. The maximum horizontal stress along the interface occurs at the right boundary and decreases towards the left boundary. σ_x is approximately 236 kPa at the left side of the shear box and increases to 723 kPa towards the right side.

The variation of the vertical stress, σ_y, is plotted in Figure 7.2. The initial vertical stress, when only the constant normal stress is applied, is 300 kPa. During the tangential displacement, σ_y slightly changes. Points L and M exhibit a slight decrease from the initial vertical stress value, while the other points show an increase. The vertical stress ranges from 222 kPa to 385 kPa along the interface from the left side to the right side of the interface, respectively.

Strain state

The horizontal normal strains, ε_x, are shown in Figure 7.3 for points along the interface, as the loading of the interface progressed from the initial condition to the failure state. The value of ε_x increased from the left side to the right side of the interface. The maximum horizontal strain at various locations along the interface ranged from 0.03% to 1.28%, where compression is positive.

The vertical normal strains, ε_y, are shown in Figure 7.4. Along the interface, the left side and middle exhibit similar compressive vertical behaviour while at the right boundary,

Points S and T show dilative behaviour. The maximum compressive and dilative vertical strains are 0.16% and 0.47%, respectively.

The shear strains, γ_{xy}, are shown in Figure 7.5. The value of γ_{xy} decreased from the left hand side towards the right hand side of the interface. The maximum shear strain, at various locations along the interface, ranged from 1.90% to 5.40%, where compression is positive.

7.1.2 Mohr circles, stress paths, and orientation of principal stresses

Mohr circles

The experimental set-up of the direct shear interface test is similar to that of the direct shear (DS) test used to investigate the soil behaviour in general. The initial state of stress and the state of stress corresponding to failure in a DS test are shown in Figure 7.6. At failure, the normal stress on the failure plane, σ_{ff}, is the same as the initial normal stress, σ_{yi}. Additionally, the horizontal stress, σ_x, becomes larger in magnitude than the vertical stress, σ_y. The orientation of the failure plane in a direct shear test is horizontal. The position of the pole is shown in the figure.

Figure 7.7 shows the states of stress at Point P in the analysis of direct shear interface test for various tangential displacements. Initially, when the constant normal stress is applied and the tangential displacement is zero, σ_x is less than σ_y. During shearing, the magnitude of σ_x quickly increases and becomes larger than that of σ_y. The sand failure envelope and interface failure envelope are obtained from the experimental results presented in previous chapters.

The states of stress in the direct shear test and in the direct shear interface test are seen to be similar.

Stress paths

The stress paths at various points along the interface are shown in Figure 7.8. Before each point along the interface reaches the interface failure envelope, both the yield surface and the cap yield surface expand. Points R, S, and T do not reach failure.

Orientation of principal stresses

On the planes where the maximum or minimum normal stresses occur, there are no shearing stresses. These planes are called the *principal planes* of stress and the stresses acting on these planes are the maximum principal stress, σ_1, and the minimum principal stress, σ_3.

The orientation of the principal stresses in the soil sample when the constant normal stress is applied and before tangential displacement takes place is shown in Figure 7.9. The vertical red line of the "+" sign represents σ_1 while the horizontal line represents σ_3. The orientation of σ_1 and σ_3 is 90° and 0° to the horizontal, respectively. However, at the end of the test when failure conditions are reached, the orientation of the principal stress changes. The orientation and relative magnitudes of the principal stresses, in the soil sample, are illustrated in Figure 7.10. An enlarged view of the orientations at the bottom right corner of the soil sample are shown in Figure 7.11. It is seen that the principal planes rotate clockwise approximately 60°. The shorter line of the red "+" sign represents σ_3, while σ_1 is represented by the longer line of the "+" sign.

The magnitudes of the principal stress are highest at the right hand side and increase gradually towards the right side.

7.2 Simple shear interface test

In the previous chapter, a finite element analysis of a simple shear interface test was also carried out for a constant normal stress of 300 kPa, using the Plaxis software. The problem was analysed as a plane strain case and the Hardening-soil model was used to simulate the behaviour of the soil. The stress and strain states of the soil, the Mohr circles, the stress paths, and the orientation of the principal stresses at various locations along the interface, as illustrated in Figure 6.40, are presented below.

7.2.1 Stress and strain states

Stress state

Figure 7.12 shows the variation of the horizontal stress, σ_x, as the loading of the interface progressed from the initial condition to the failure state. Initially when the constant normal stress is applied, the horizontal stress is 120 kPa. As the tangential displacement is applied, σ_x increases nonlinearly until a tangential displacement of 0.7 mm, followed by a sudden change in the slope of the curve before it becomes constant. The peak horizontal stress along the interface decreases from the left hand side of the interface to the right hand side. σ_x is approximately 424 kPa at the left side of the simple shear box and decreases to 118 kPa towards the right side.

The variation of the vertical stress, σ_y, is plotted in Figure 7.13. The initial vertical stress is 300 kPa, when only the constant normal stress is applied. During the tangential displacement, σ_y increases from its initial value at the left hand side of the interface while the right hand side shows a decrease in σ_y from the initial vertical stress. σ_y ranges from 367 kPa to 176 kPa along the interface from the left hand side to the right hand side, respectively.

Strain state

The horizontal normal strain, ε_x, at a number of points along the interface is shown in Figure 7.14, as a function of various stages of the test, from the initial condition to the failure state. The highest value of ε_x is at the right boundary and decreases towards the left hand side of the interface. The horizontal normal strain ranged from -1.48% to 0.41% along the interface, where compression is positive.

The vertical normal strains, ε_y, are shown in Figure 7.15. The right hand side of the interface exhibits the largest vertical normal strains and decrease towards the left boundary. It can be noted that no extension is occurring in the vertical direction. The maximum compressive vertical normal strain is 1.26%.

The shear strain, γ_{xy}, at a number of points along the interface is shown in Figure 7.16. The value of γ_{xy} varies significantly along the interface. The maximum shear strain is 6.4%.

7.2.2 Mohr circles, stress paths, and orientation of principal stresses

Mohr circles

The initial state of stress and the state of stress corresponding to failure in a simple shear (SS) test, used to investigate the soil behaviour in general, are shown in Figure 7.17. The inner circle represents the initial state of stress and the outer circle represents the state of stress at failure. Since the horizontal stress, σ_x, and the vertical stress, σ_y, are constant and only the shear stress, τ_{yx}, increases, the Mohr circle enlarges about the same centre as the initial Mohr circle until it becomes tangent to the failure envelope. In addition, the horizontal stress, σ_x, is smaller than the vertical stress, σ_y, contrary to the direct shear test. An important detail to note is the location of the pole. The failure plane is not horizontal as in the direct shear test.

Figure 7.18 shows the numerical results of the states of stress in the simple shear interface test for various tangential displacements at Point P. From the initial condition to the failure state, σ_x is less than σ_y. However, during shearing, the magnitude of σ_x increases at a faster rate than that of σ_y.

The states of stress in the simple shear test and the simple shear interface test are not similar. The Mohr circles of the simple shear interface test, as the test progresses, do not enlarge about the same centre of the initial Mohr circle. The reason being that σ_x increases in the simple shear interface test as opposed to the direct simple shear test where it remains constant.

Stress paths

The stress paths at various points along the interface are shown in Figure 7.19. Before each point along the interface reaches the interface failure envelope, both the yield surface and the cap yield surface expand, except for Point T. For Point T, when the tangential displacement is applied, only the cone yield surface is expanding. After failure conditions have been reached in the interface, the finite element code, Plaxis, predicts randomly changing results that are bounded by the failure envelope of the sand.

Orientation of principal stresses

The orientation of the principal stresses in the soil sample when the constant normal stress is applied and before tangential displacement takes place is shown in Figure 7.20. The vertical red line of the "+" sign represents σ_1 while the horizontal line represents σ_3. Initially, the orientation of σ_1 and σ_3 is 90^o and 0^o to the horizontal, respectively. However, at the end of the test when failure conditions are reached, the orientation of the principal stress changes as in the direct shear interface test. The orientation and relative magnitudes of the principal stresses, in the soil sample, are illustrated in Figure 7.21. An enlarged view of the orientations at the bottom left corner of the soil sample is shown in Figure 7.22. It is seen that the principal planes rotate clockwise approximately 45^o. The magnitudes of the principal stress are highest at the left hand side and decrease gradually towards the right side.

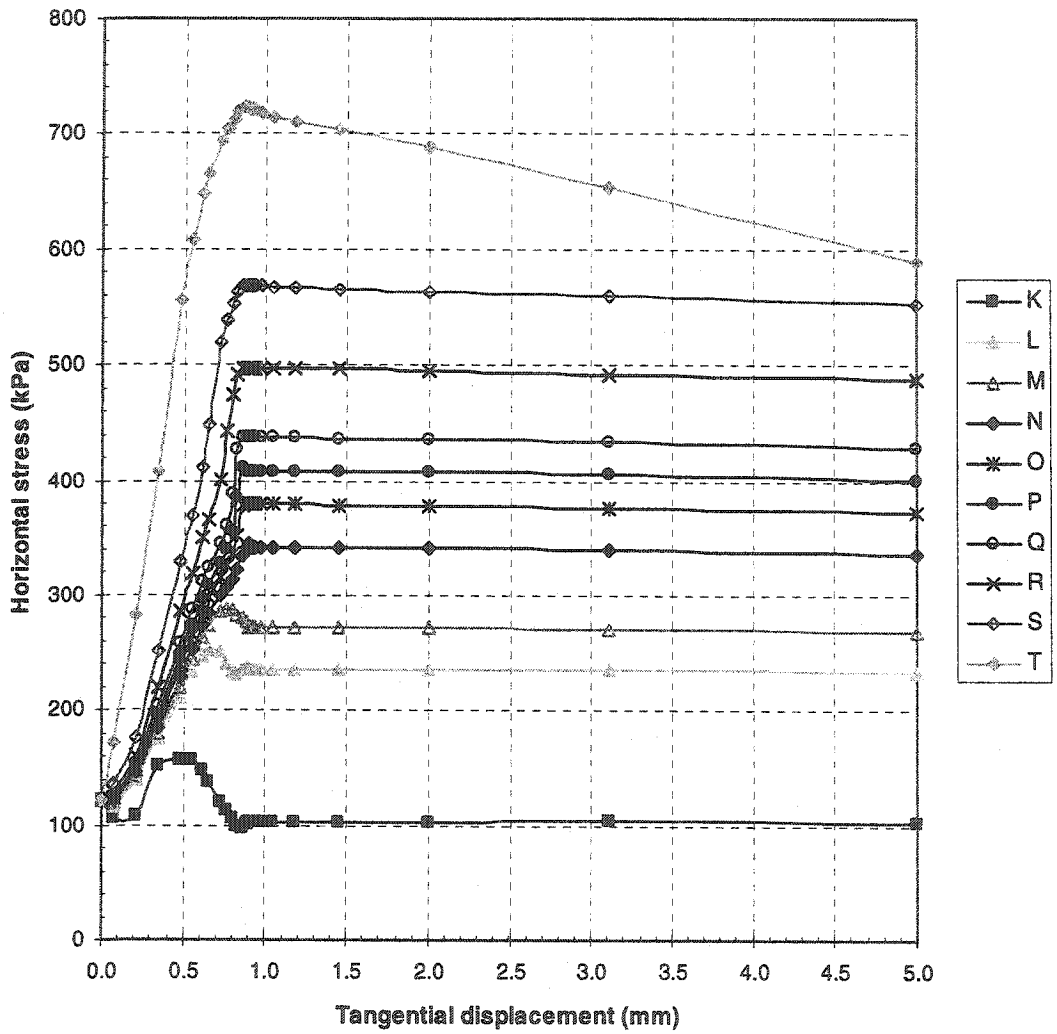

Figure 7.1 Horizontal stress, σ_x, versus tangential displacement curves at different locations on the interface for a direct shear interface test, constant normal stress = 300 kPa

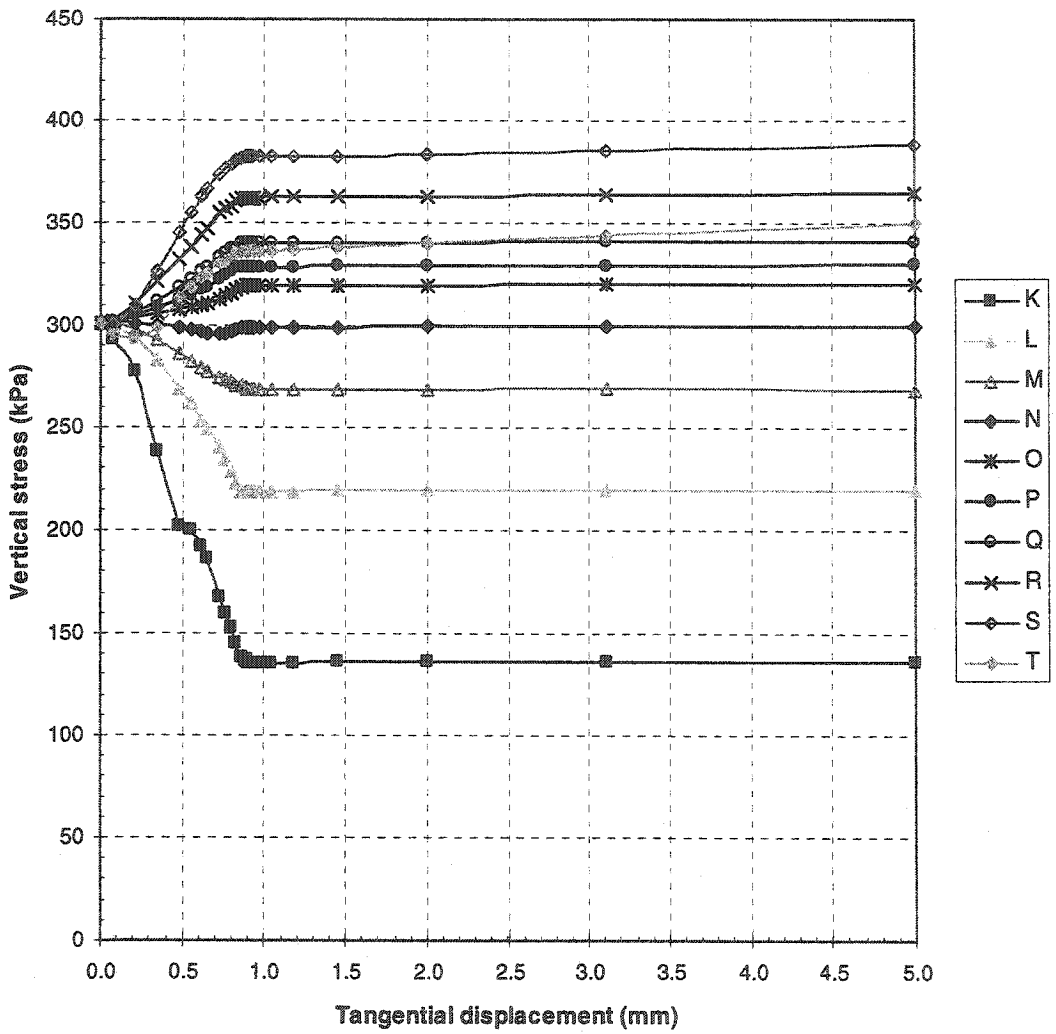

Figure 7.2 Vertical stress, σ_y, versus tangential displacement curves at different locations on the interface for a direct shear interface test, constant normal stress = 300 kPa

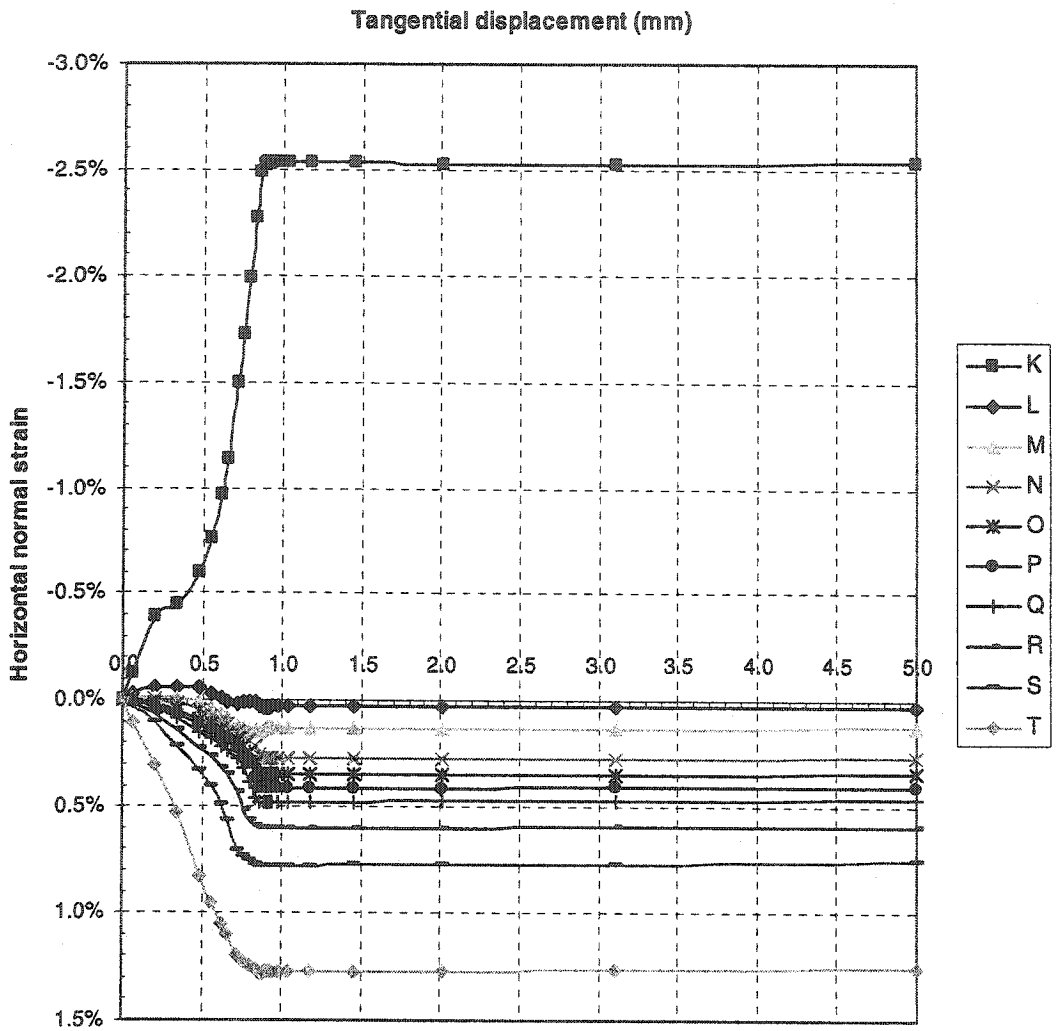

Figure 7.3 Horizontal normal strain, ε_x, versus tangential displacement curves at different locations on the interface for a direct shear interface test, constant normal stress = 300 kPa

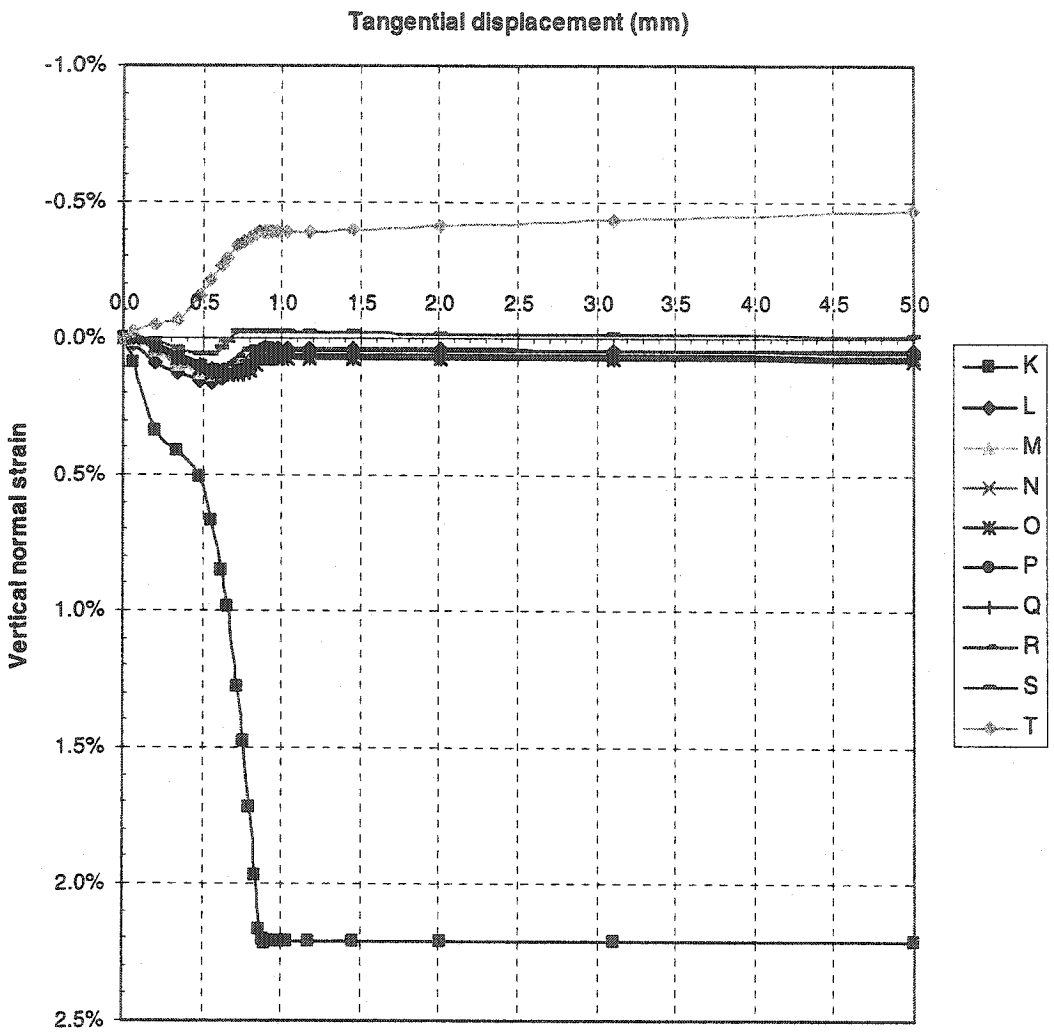

Figure 7.4 Vertical normal strain, ε_y, versus tangential displacement curves at different locations on the interface for a direct shear interface test, constant normal stress = 300 kPa

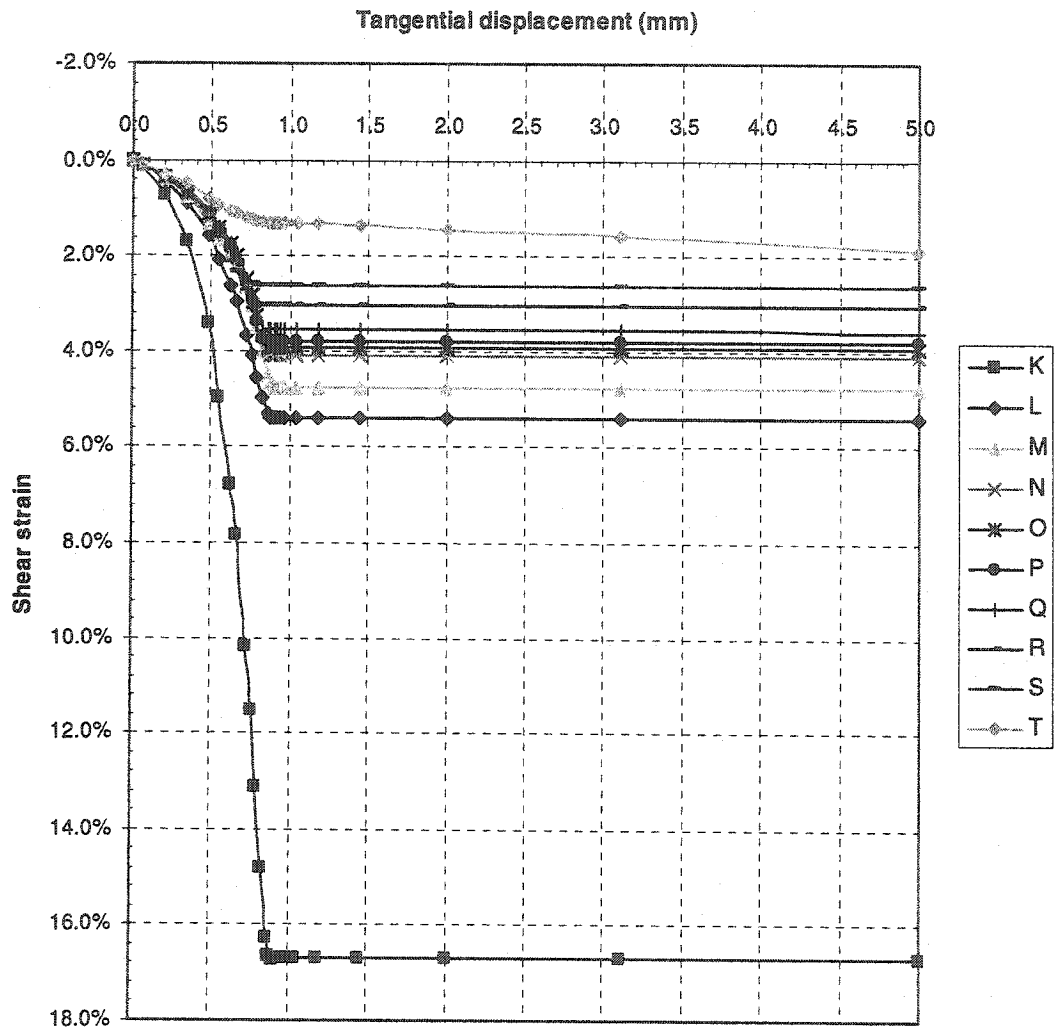

Figure 7.5 Shear strain, γ_{xy}, versus tangential displacement curves at different locations on the interface for a direct shear interface test, constant normal stress = 300 kPa

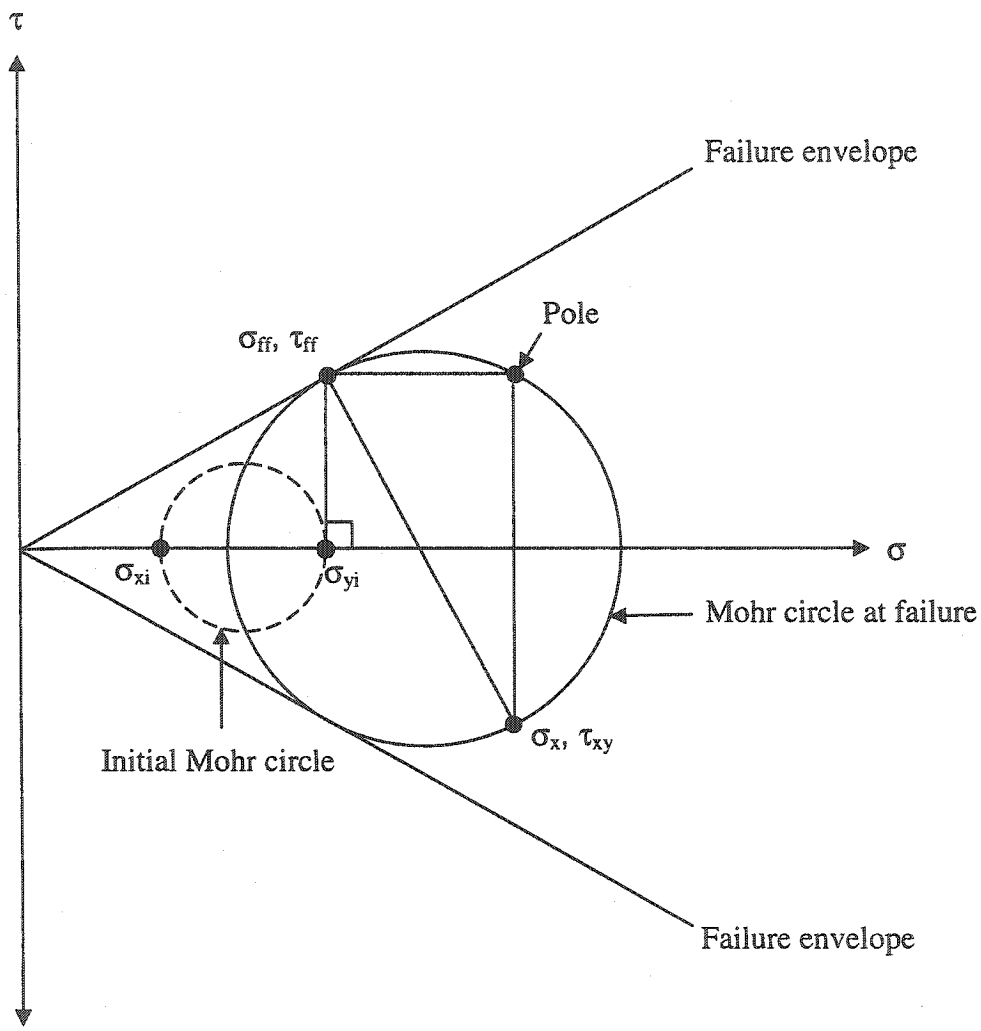

Figure 7.6 Mohr circles corresponding to initial state of stress and failure condition in a direct shear test

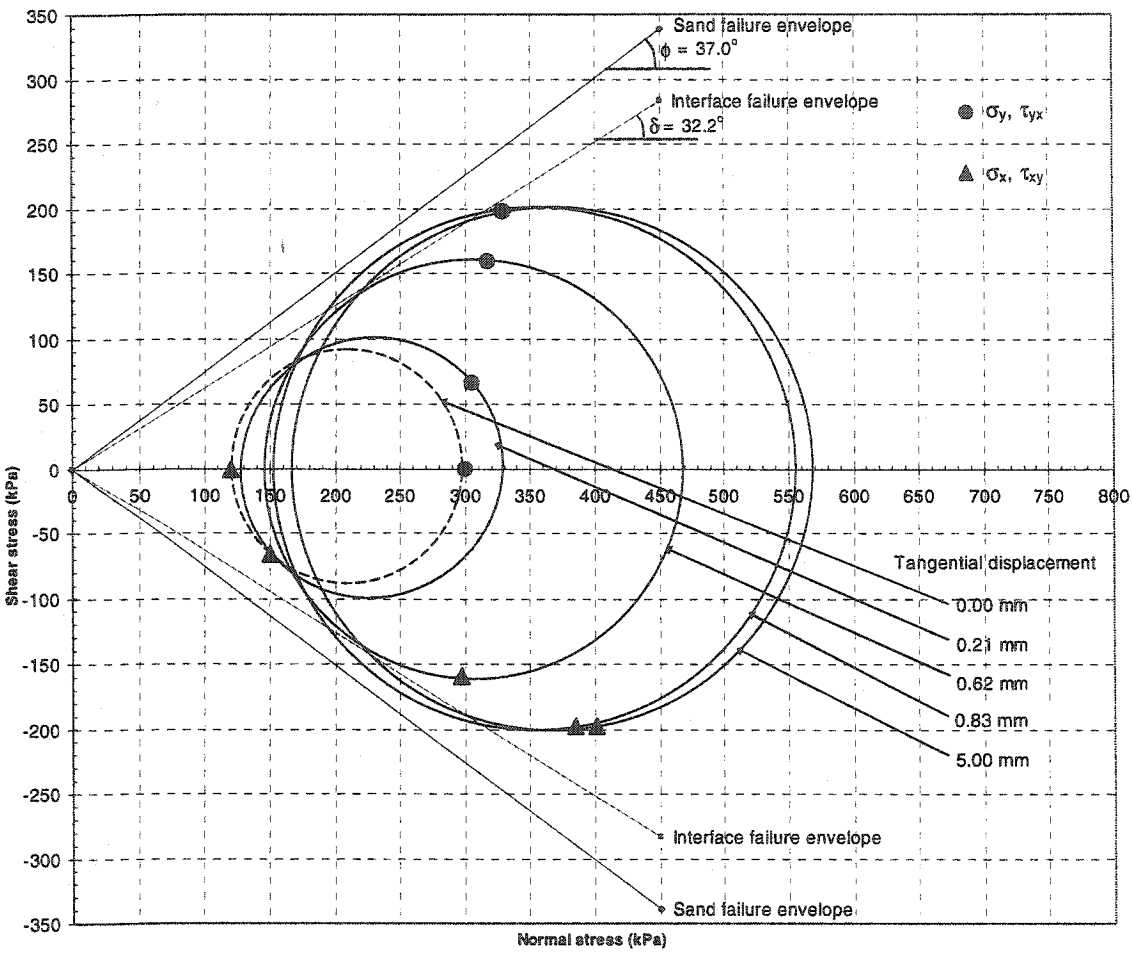

Figure 7.7 Mohr circles for different tangential displacements in a direct shear interface test, at point P, constant normal stress = 300 kPa

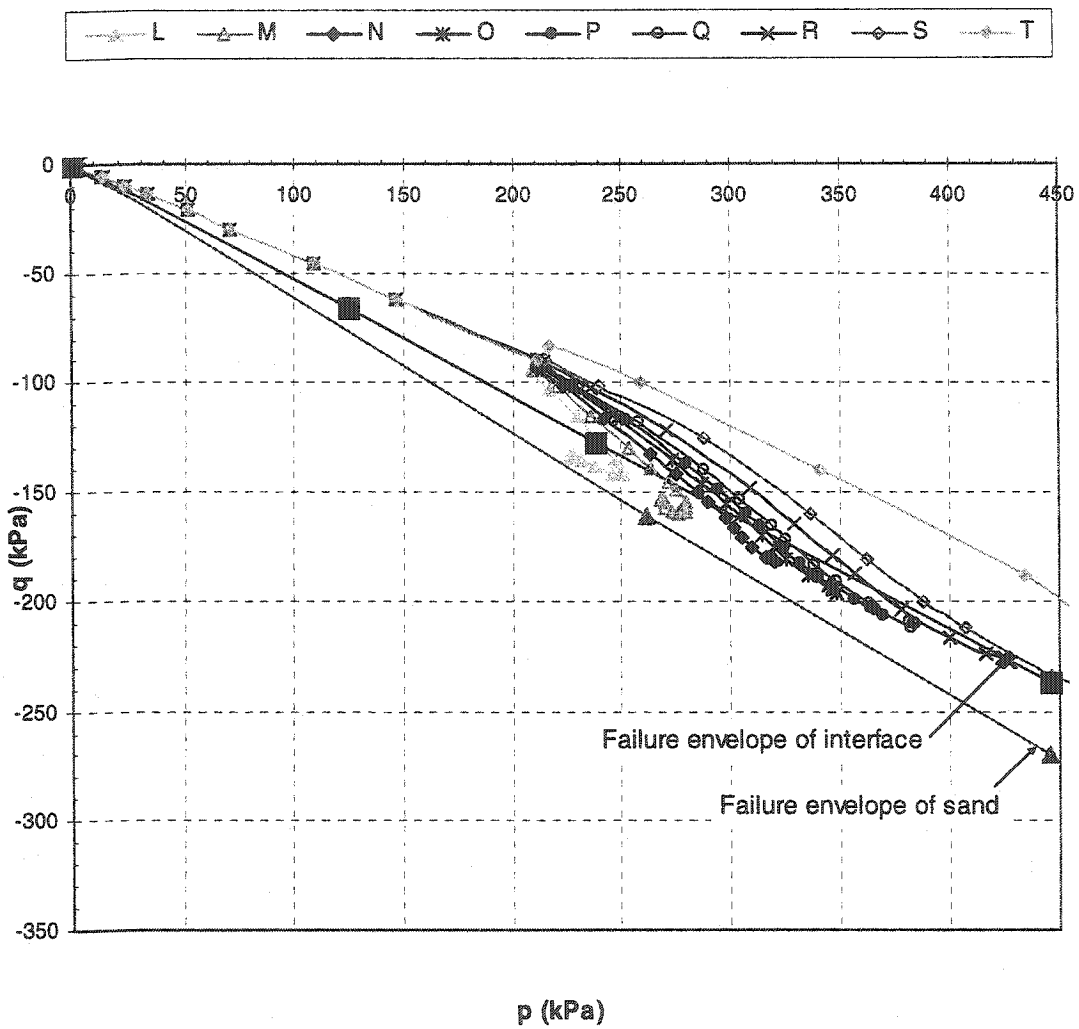

Figure 7.8 Stress paths curves at different locations on the interface for a direct shear interface test, constant normal stress = 300 kPa

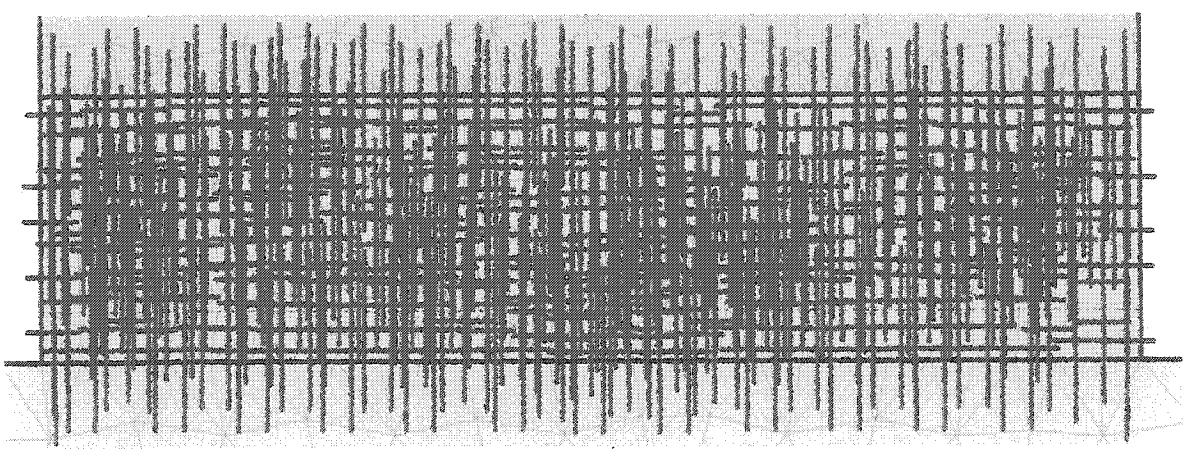

Figure 7.9 Principal stresses and their orientation before a tangential displacement is applied for a direct shear interface test, constant normal stress = 300 kPa

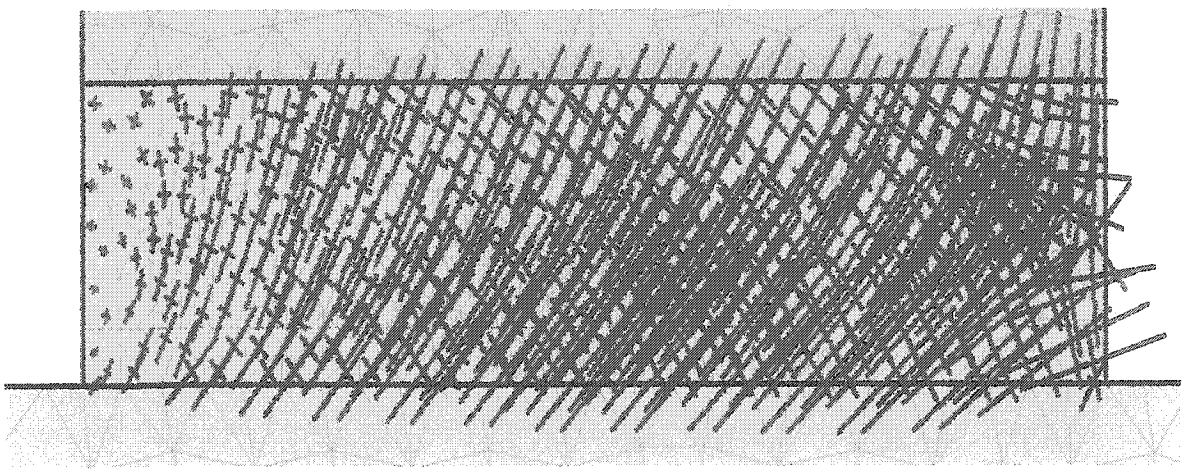

Figure 7.10 Principal stresses and their orientation at failure condition for a direct shear interface test, constant normal stress = 300 kPa

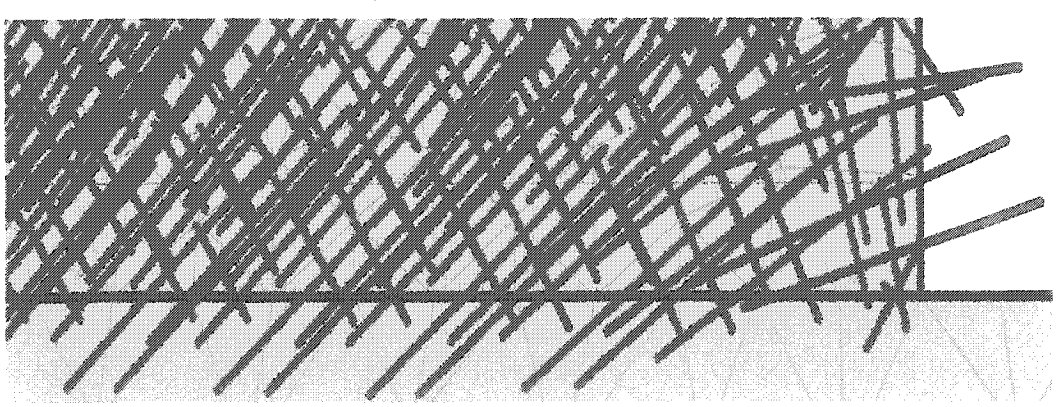

Figure 7.11 Principal stresses and their orientation at failure condition in the bottom right corner of the soil sample for a direct shear interface test, constant normal stress = 300 kPa

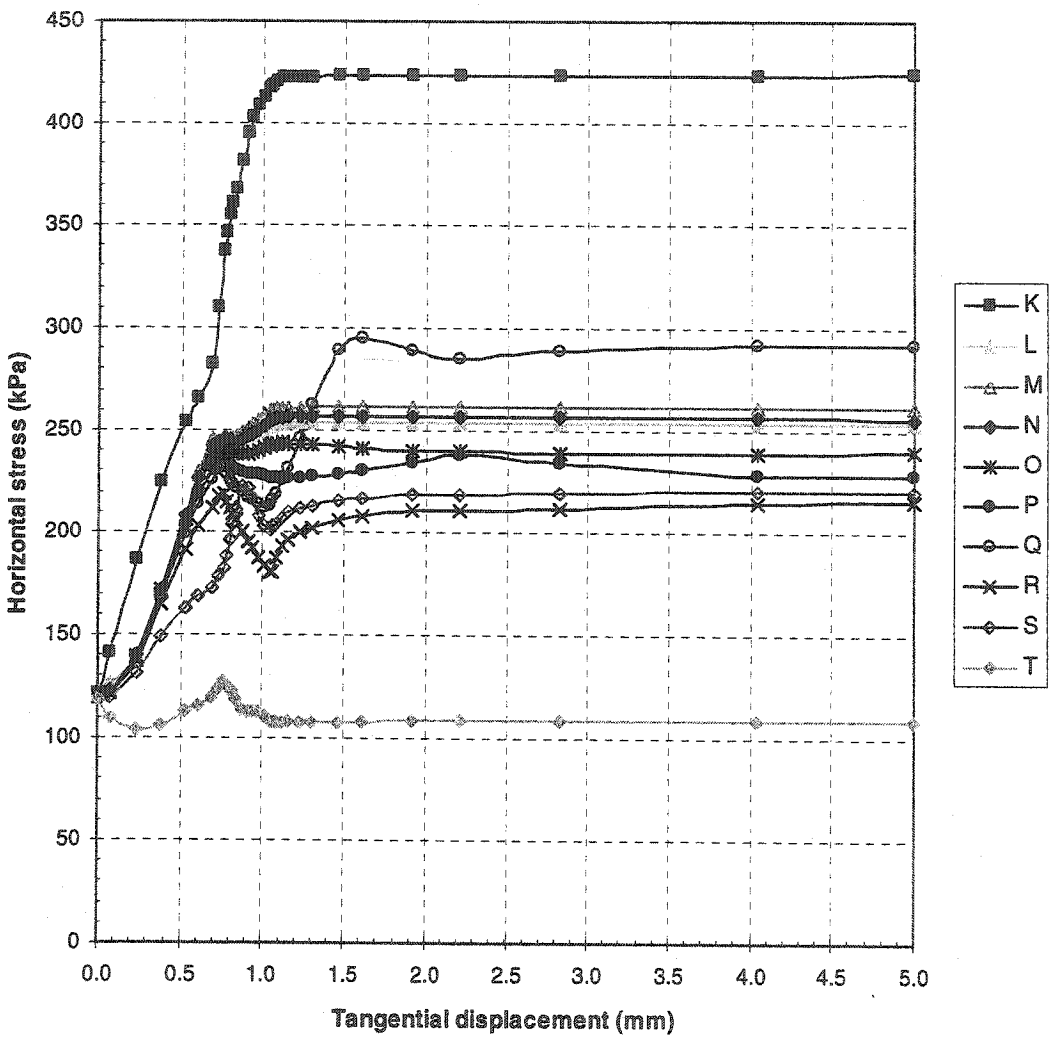

Figure 7.12 Horizontal stress, σ_x, versus tangential displacement curves at different locations on the interface for a simple shear interface test, constant normal stress = 300 kPa

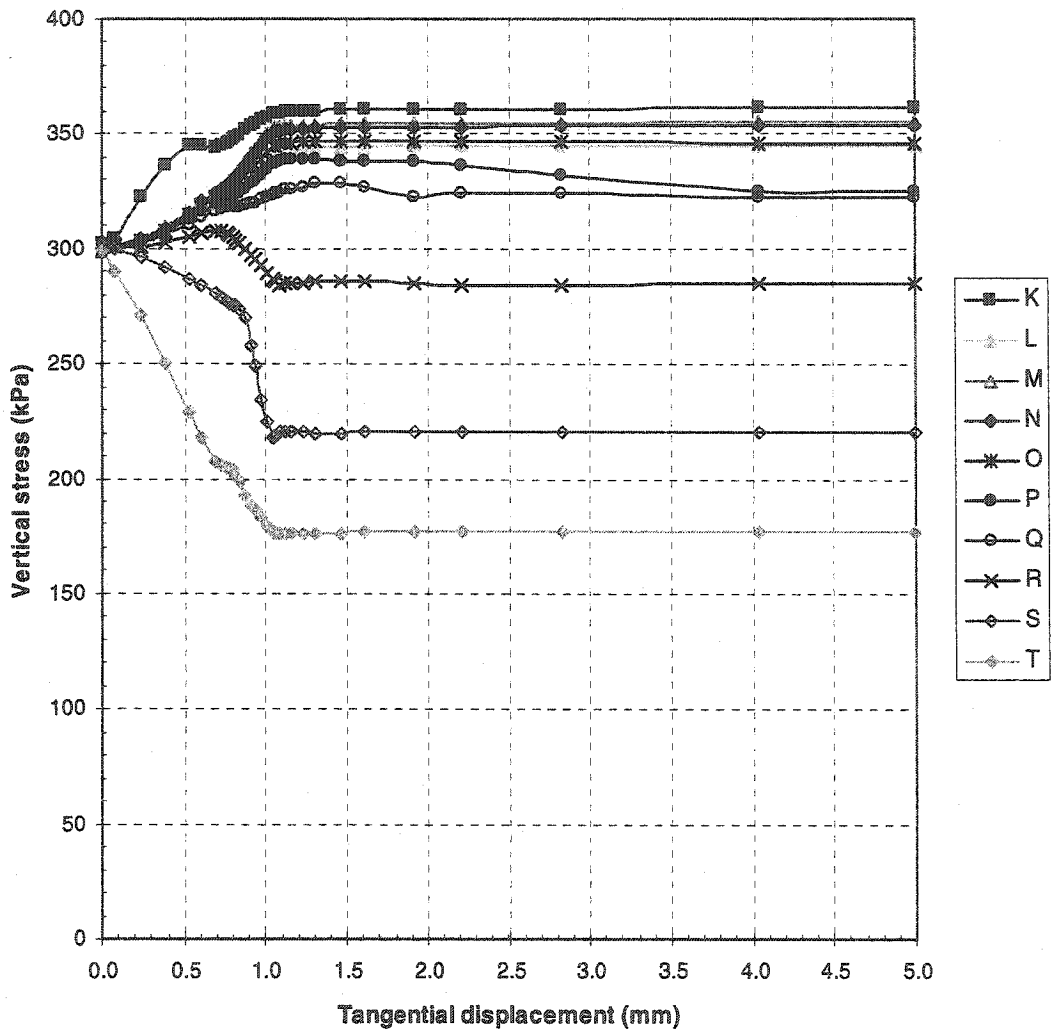

Figure 7.13 Vertical stress, σ_y, versus tangential displacement curves at different locations on the interface for a simple shear interface test, constant normal stress = 300 kPa

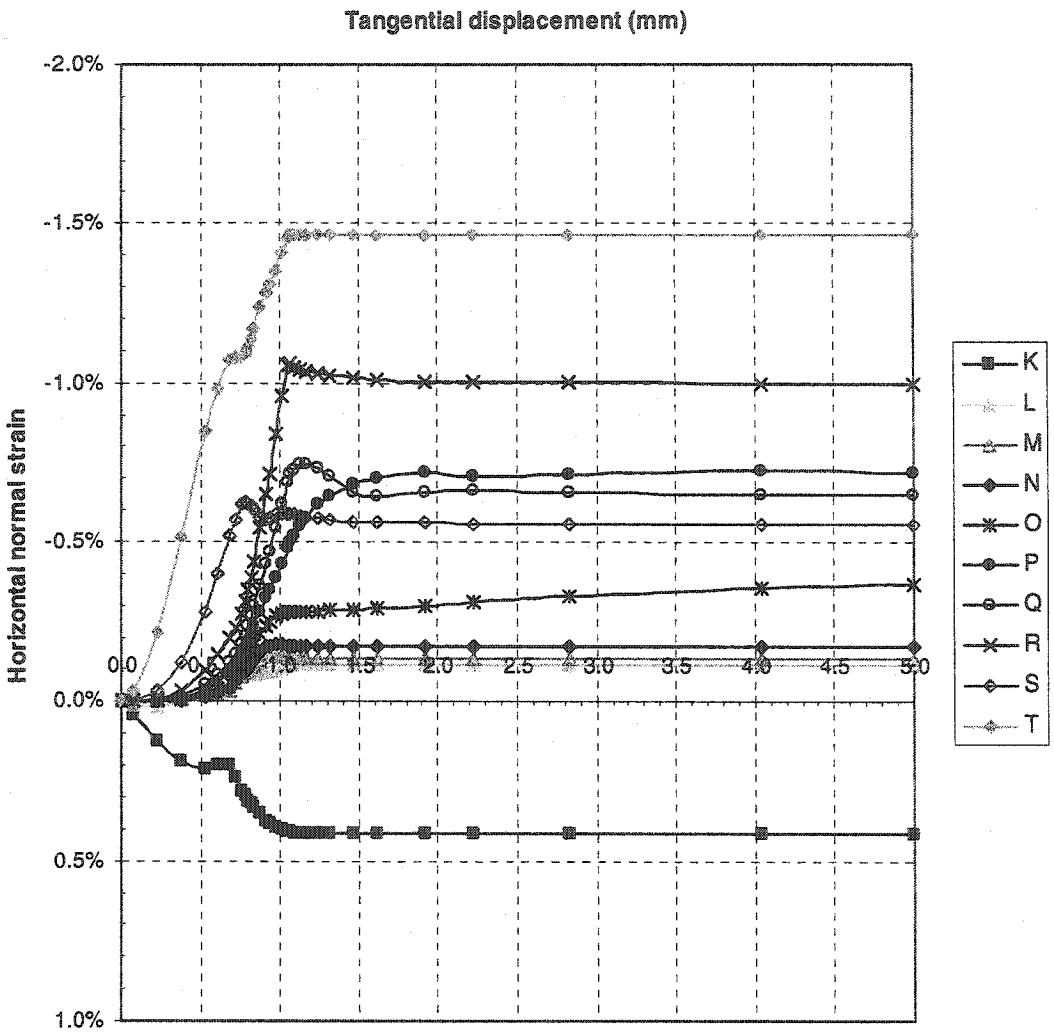

Figure 7.14 Horizontal normal strain, ε_x, versus tangential displacement curves at different locations on the interface for a simple shear interface test, constant normal stress = 300 kPa

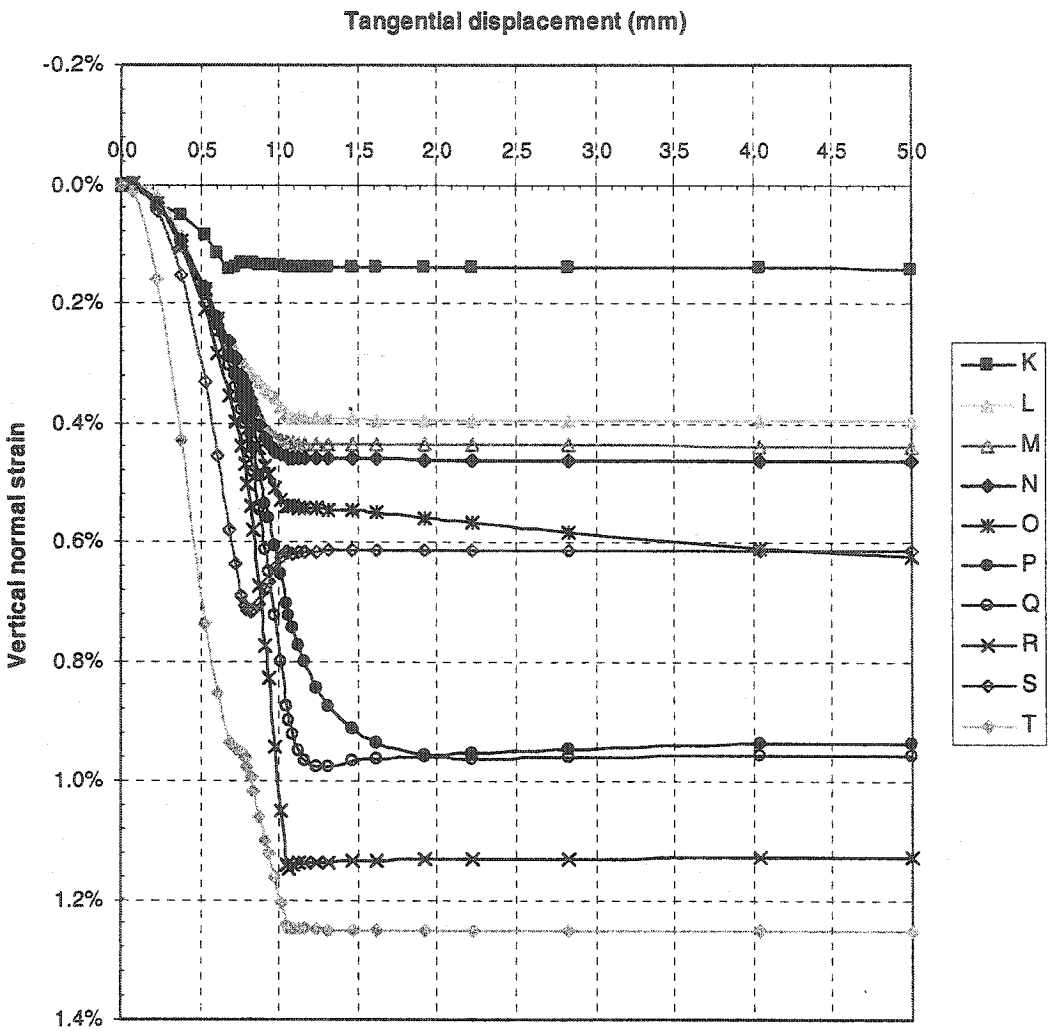

Figure 7.15 Vertical normal strain, ε_y, versus tangential displacement curves at different locations on the interface for a simple shear interface test, constant normal stress = 300 kPa

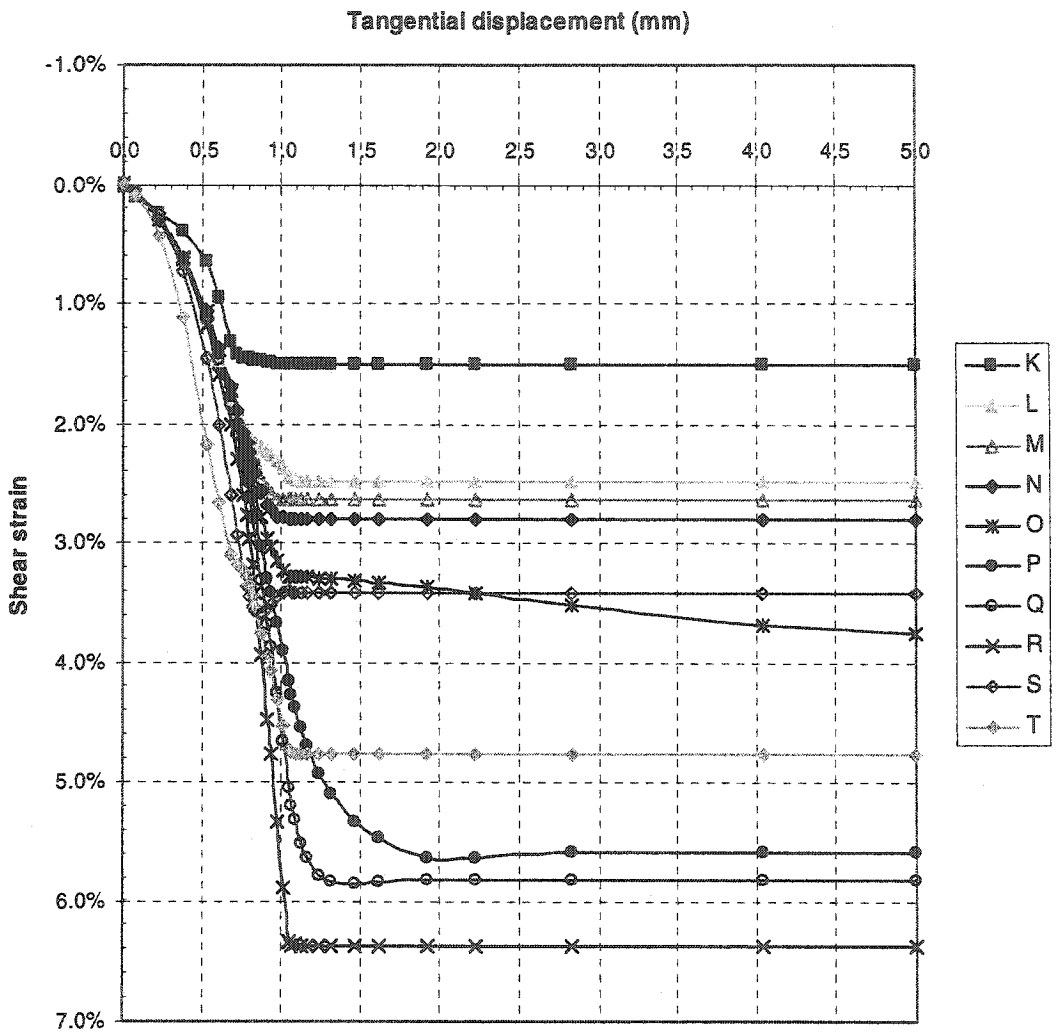

Figure 7.16 Shear strain, γ_{xy}, versus tangential displacement curves at different locations on the interface for a simple shear interface test, constant normal stress = 300 kPa

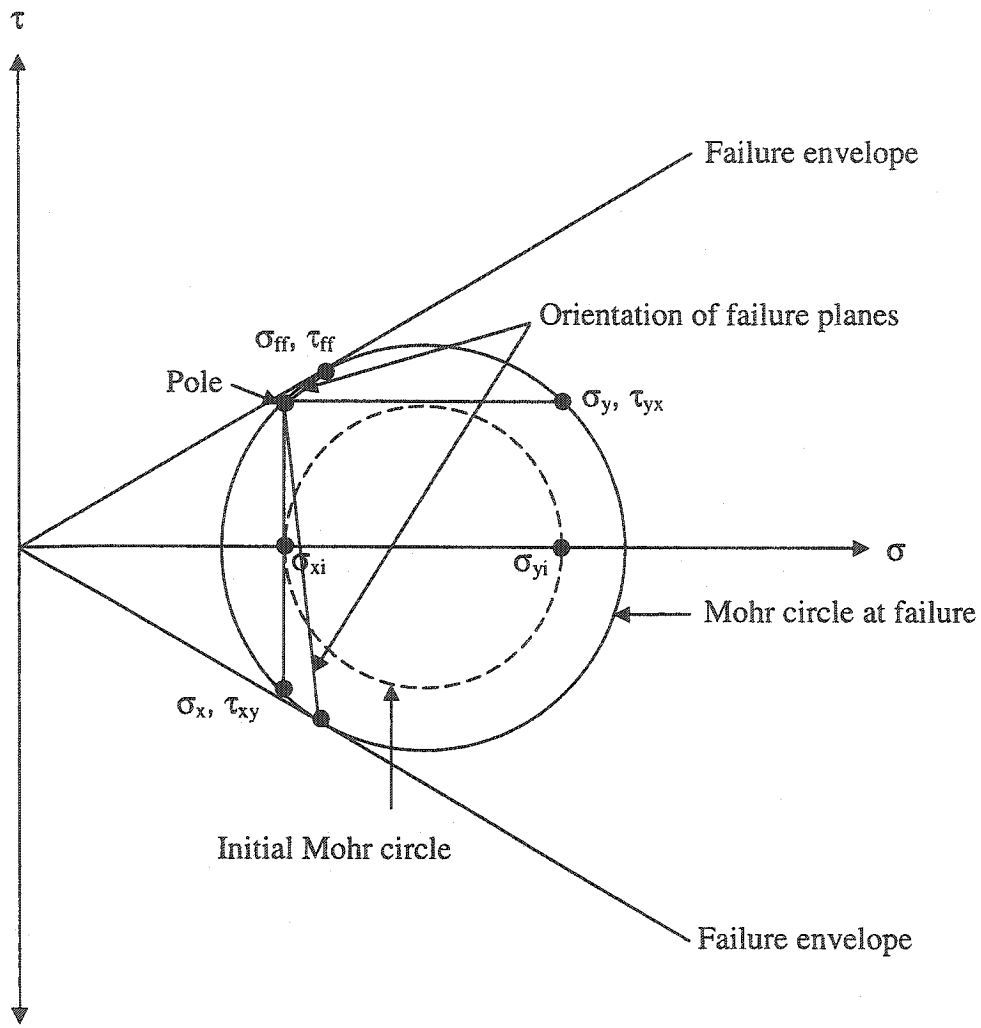

Figure 7.17 Mohr circles corresponding to initial state of stress and failure condition in a simple shear test with σ_x constant

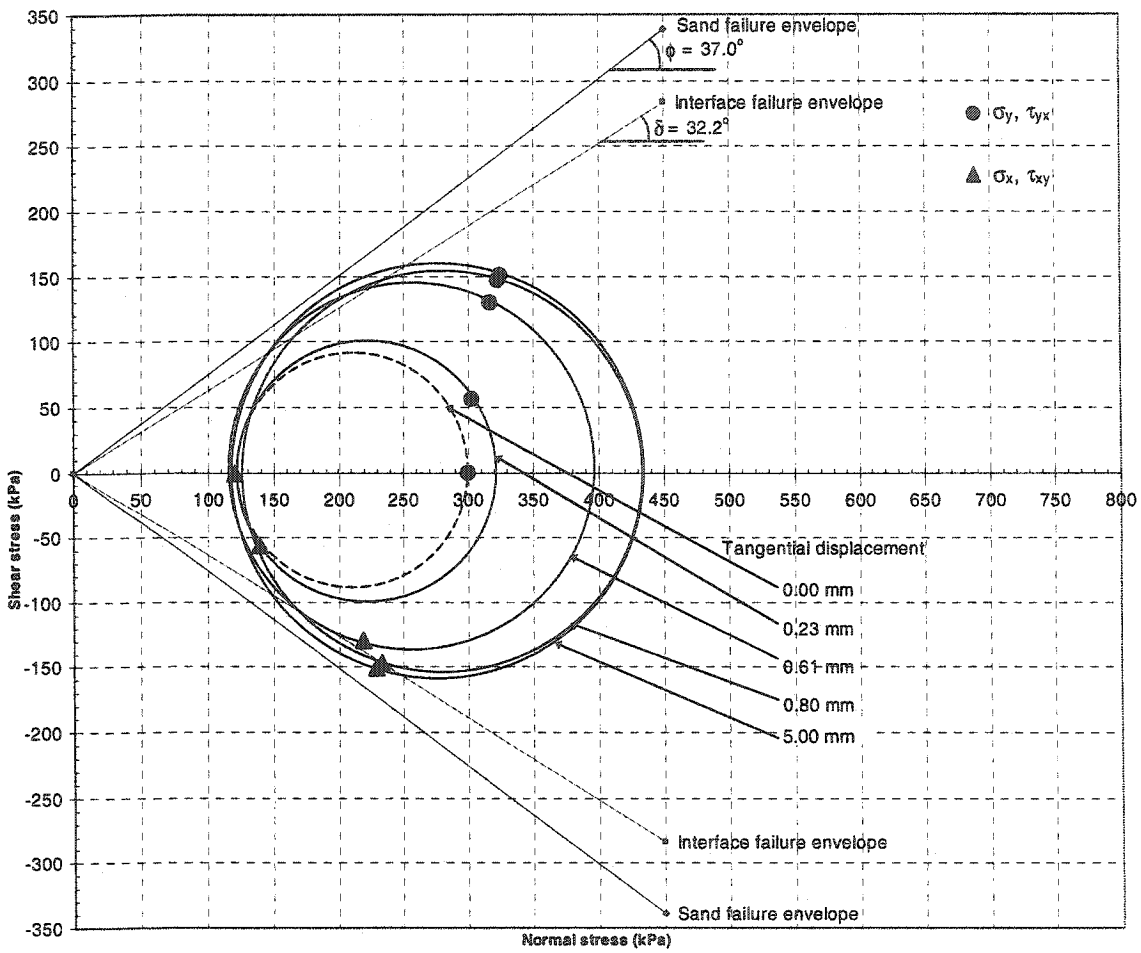

Figure 7.18 Mohr circles for different tangential displacements in simple shear interface test, at point P, constant normal stress = 300 kPa

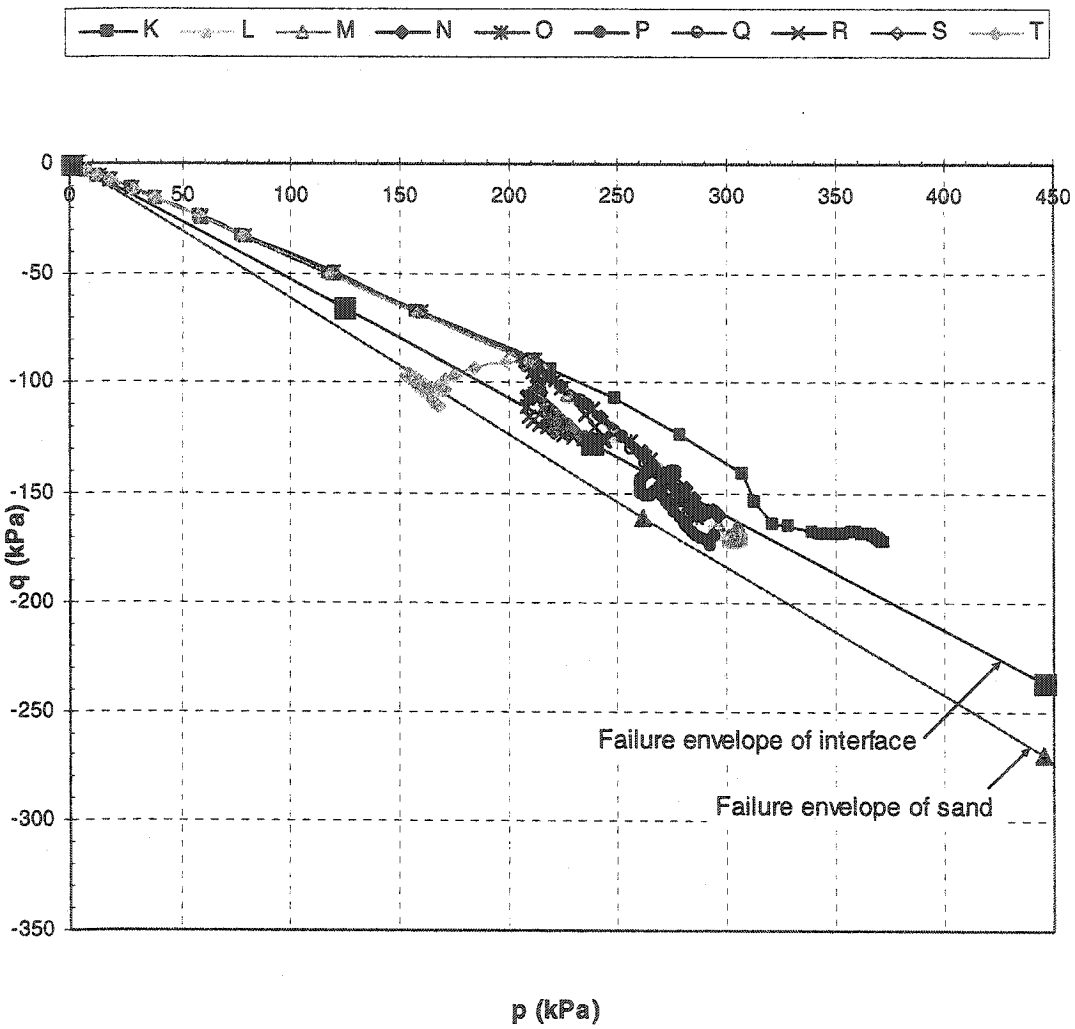

Figure 7.19 Stress paths curves at different locations on the interface for a simple shear interface test, constant normal stress = 300 kPa

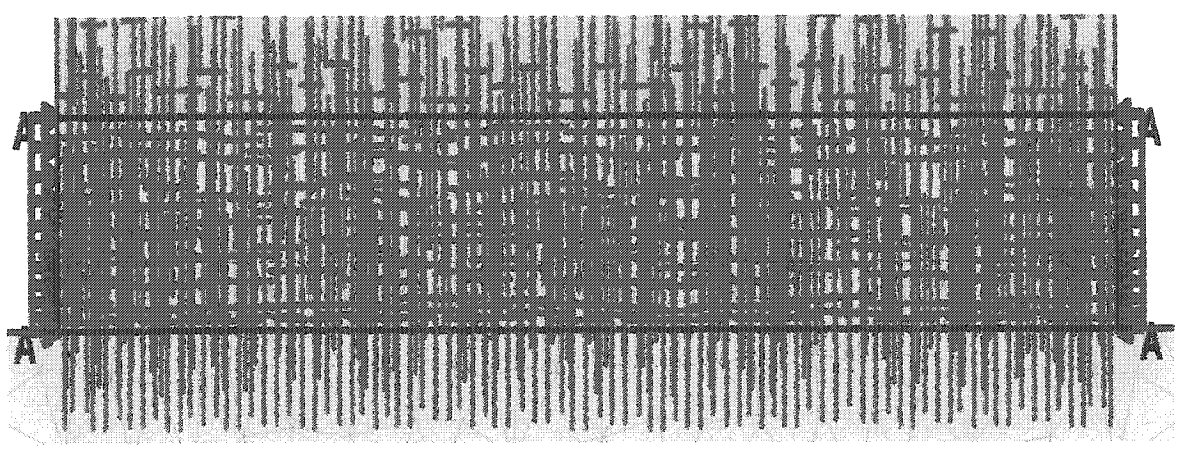

Figure 7.20 Principal stresses and their orientation before a tangential displacement is applied for a simple shear interface test, constant normal stress = 300 kPa

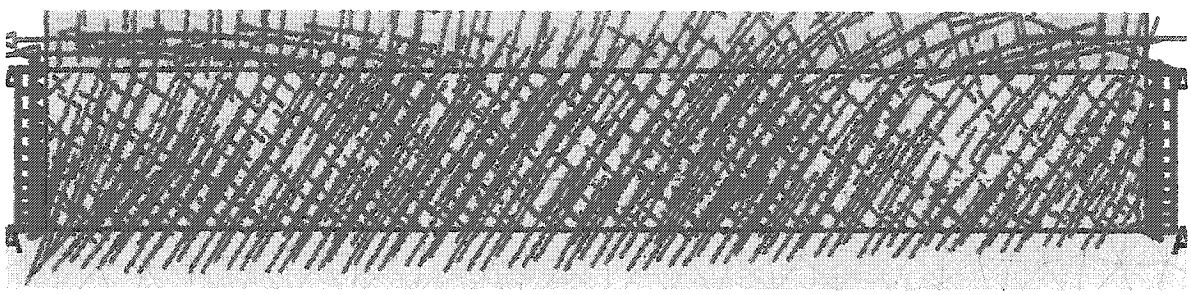

Figure 7.21 Principal stresses and their orientation at failure condition for a simple shear interface test, constant normal stress = 300 kPa

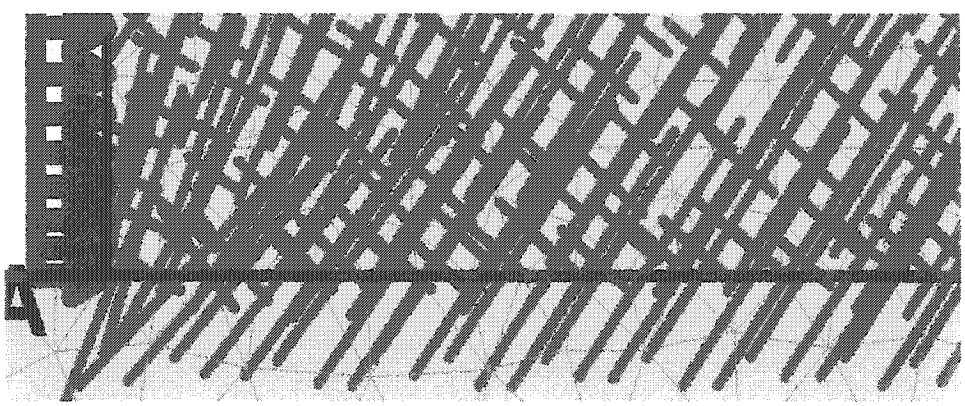

Figure 7.22 Principal stresses and their orientation at failure condition in the bottom left corner of the soil sample for a simple shear interface test, constant normal stress = 300 kPa

CHAPTER 8
SUMMARY AND CONCLUSIONS

8.1 Summary

The development of a mathematical model for the mechanical behaviour of soil-structure interfaces requires a full knowledge of the states of stress and strain within the laboratory soil samples. However, with the existing interface testing devices it is difficult to measure all components of stresses and strains everywhere in a sample. The direct shear type and simple shear type interface tests, provide the average values of normal stress and shear stress acting on the interface, obtained from the measured normal and tangential forces. As for displacements, the tangential displacement of the interface plate and the displacement normal to the top of the soil sample are measured. Additionally, if a simple shear type of apparatus is used in the experiments, it is also possible to measure the amount of slip between the interface plate and soil sample.

The purpose of this study was to characterize the soil-structure interface behaviour in terms of the stress and strain states. This is accomplished by performing a numerical analysis of the direct shear and simple shear interface tests, using the commercial finite element program Plaxis.

An experimental program was carried out for two reasons: (1) to provide input data for the soil model used in the finite element analysis and (2) to assess the reliability of the numerical results given by Plaxis. First, three drained consolidated triaxial tests for medium crushed quartz sand were performed under different confining pressures to determine the soil properties and the Hardening-Soil model parameters for the finite element analyses. Subsequently, a series of direct shear interface tests were conducted between sand and concrete for constant normal stresses of 100 kPa, 200 kPa and 300 kPa.

The measured shear stresses and normal displacements were plotted versus the tangential displacement as basis of comparison for the numerical analyses. The ratio between the interface friction angle and soil friction angle was found to be 0.84.

Finite element analyses were performed simulating the experimental direct shear interface tests (these tests were conducted as part of the present investigation) and a simple shear interface test by Li (2001). The model predictions of the shear stress and normal displacement versus tangential displacement were compared to the experimental observations. The mean stress, relative shear stress, and total volumetric strain within the soil sample and the normal stress and shear stress along the interface were calculated. The states of stress were evaluated at various locations along the interface and the numerical values of the horizontal and vertical stresses were presented. The states of strain were also examined along the interface and the horizontal normal strain, vertical normal strain, and shear strain were presented. The Mohr circles for a point on the interface, at various stages during the tests, are drawn using the numerically determined normal stresses and shear stresses. The Mohr circles of the direct shear type and simple shear type interface tests were compared to the general direct shear test and simple shear test of soils. The stress paths are also presented. Finally, the orientation of the principal stresses at the initial condition and at failure was compared.

8.2 Conclusions

The conclusions of this investigation are as follows.

- For a specified normal stress and shear stress acting on the interface, the calculated and measured tangential displacements do not agree only when the stress state moves closer to the failure state.

- When the compression or dilation of the soil sample in the direction perpendicular to the contact surface is considered, the calculated and measured values become significantly different from each other when failure is approaching.

- The state of stress and the state of strain in the soil samples of interface tests are not uniform. In the direct shear interface tests, stresses and strains near the vertical sides of the sample container are different than those in the middle section of the soil container. However, the stresses calculated in the middle of the interface at the time of failure are very close to the average values of measured normal and shear stresses.

- The stress paths followed in simple shear interface tests are different than the stress paths in simple shear tests used for characterizing the stress-strain behaviour of soils.

- The numerical analysis using Plaxis indicates that the principal stress axes rotate substantially during the application of the tangential displacement in both the direct shear type and simple shear type interface tests.

8.3 Recommendations for future research

The validity of the conclusions provided here is based on the assumption that the results of the numerical analysis are a true representation of interface behaviour. This assumption may be justified when the soil failure is not near. As it is well known, the results of numerical analysis is only as good as the constitutive model used for the material behaviour. In this thesis, various difficulties were encountered using the Hardening-Soil model. In addition, the ability of the Hardening-Soil model used in Plaxis to correctly predict the soil behaviour under the rotation of principal stresses needs to be investigated.

Once the reliability of the calculated states of stress and strain is established, it would then be possible to use this information to develop reliable constitutive models for interfaces. It appears that by making corrections to a presently used model, one can eventually reach a more reliable constitutive relation.

REFERENCES

Acar Y.B., Durgunoglu T., and Tumay M.T. (1982). Interface properties of sand, Proceedings of the American Society of Civil Engineers, Vol. 108, No. GT4, pp. 648-654.

Altaee, A., Fellenius, B.H., and Evgin, E. (1992). Axial load transfer for piles in sand. I. Tests on an instrumented precast pile, Can. Geotech. J., 29, pp. 11-20.

Altaee, A., Evgin, E., and Fellenius, B.H. (1992). Axial load transfer for piles in sand. II. Numerical analysis, Can. Geotech. J., 29, pp. 21-30.

American Society of Testing Material (ASTM) (1995). Standard test method for minimum index density and unit weight of soils and calculation of relative density, ASTM D 4254-91, Vol. 04.08, 1995.

Atkinson, J.H. and Bransby, P.L. (1978). The mechanics of soils, An introduction to critical state soil mechanics, McGraw Hill.

Been, K., Jefferies, M.G., and Hachey, J. (1991). The critical state of sands, Geotechnique, Vol.41, No. 3, pp. 365-381.

Boulon, M., Garnica, P., and Vermeer, P.A. (1995). Soil-structure interaction: FEM Computations, Mechanics of Geomaterial Interfaces, Elsevier Science B.V.

Boulon, M. and Plytas, C. (1986). Soil structure directionally dependent interface constitutive equations - Application to the prediction of shaft friction along piles, Proceedings, 2nd International Symposium on Numerical Models in Geomechanics, pp. 43-54.

Brummund, W.F. and Leonards, G.A. (1973). Experimental study of static and dynamic friction between sand and typical construction materials, Journal of Testing and Evaluation, JTEVA, Vol. 1, No. 2, pp. 162-175.

Chen W.F. (1984). Constitutive modelling in soil mechanics, Mechanics of Engineering Materials, John Wiley & Sons, pp. 91-120.

Chen, Y. and Krauthammer, T. (1987). Soil-structure interface effects on dynamic interaction analysis of reinforced concrete lifelines, Soil-Structure Interaction, Computational Mechanics Publications, pp. 89-101.

Desai, C.S. (1980). A general basis for yield, failure and potential functions in plasticity, Int. J. Numer. And Analyt. Methods in Geomech., Vol. 4, 361-375.

Desai, C.S. (1981). Behaviour of interfaces between structural and geologic media, Proceedings, International conference on recent advances in geotechnical earthquake engineering and soil dynamics, Vol. 2, pp. 619-638.

Desai, C.S., Drumm, E.C., and Zaman, M.M. (1985). Cyclic testing and modeling of interfaces, Journal of Geotechnical Engineering, Vol. 11, No. 6, pp. 793-815.

Desai, C.S. and Nagaraj, B.K. (1988). Modeling for cyclic normal and shear behavior of interfaces, Journal of Engineering Mechanics, Vol. 114, No. 7, pp. 1198-1217.

Desai, C.S. and Rigby, D.B. (1995). Modelling and testing of interfaces, Mechanics of Geomaterial Interfaces, Elsevier Science B.V.

Desai, C.S. and Siriwardance, J.J. (1984). Constitutive laws for engineering materials with emphasis on geologic materials, Prentice-Hall, Inc., Engewood Cliffs, NJ 07632.

Drucker, D.C., Gibson, R.E., and Hentel, D.J. (1975). Soil mechanics and work-hardening theories of plasticity, J. Soil Mech. Fdn. Eng. Div. Am. Soc. Civ. Engrs 122, pp. 338-346.

Duncan, J.M. and Chang, C.Y. (1970). Nonlinear analysis of strain and stress in soils, Journal of the Soil Mechanics and Foundations Division, Proceedings of the ASCE, September, pp. 1629-1653.

Evgin, E., Boulon, M., and Armand, G. (1996). Effect of oil contamination on the behaviour of an interface, 49th Canadian Geotechnical Conference of the Canadian Geotechnical Society, pp. 377-384.

Evgin, E. and Fakharian, K. (1993). A three-dimensional apparatus for cyclic testing of interfaces, Proceedings, 46th Annual Canadian Geotechnical Conference, Saskatoon, Canada, pp. 485-493.

Evgin, E., Fakharian, K., and Mohareb M. (2003). Numerical analysis of stress states in Soil-Structure Interface Tests, The 13th International Offshore and Polar Engineering Conference, Honolulu, Hawaii, USA.

Evgin, E., Liang, Z., and Konuk, I. (1998). Distinct element analysis of interfaces in particulate media, Proceeding of the Eighth International Offshore and Polar Engineering Conference, pp. 643-648.

Fakharian, K. and Evgin, E. (1996). An automated apparatus for three-dimensional monotonic and cyclic testing of interfaces, Geotechnical Testing Journal, GTJODJ, Vol. 19, No. 1, pp. 22-31.

Fakharian, K. (1996). Three-Dimensional monotonic and cyclic behaviour of sand-steel interface behaviour, Master's Thesis, University of Ottawa, ON.

Fishman, K.L. and Desai, C.S. (1987). A constitutive model for hardening behaviour of rock joints, Desai et al., Editors, Constitutive Laws for Engineering materials: Theory and Applications, pp. 1043-1050.

Fu, T. (1998). Experimental study and discrete element simulation of sand-steel interface behaviour, Master's Thesis, University of Ottawa, ON.

Ghaboussi, J., Wilson, E.L., and Isenberg, J. (1973). Finite elements for rock joints and interfaces, Journal Soil Mechanics and Found. Div. ASCE, 99, SM10, pp. 833-848.

Huck, P.J., Liber, T., Chiapetta, R.L., Thomopoulos, N.T., and Singh, N.M. (1973). Dynamic response of soil-concrete interfaces at high pressure, Report AFWL-TR-73-264, Air Force Weapons Laboratory, New Mexico.

Huck, P.J. and Saxena, S.K. (1981). Response of soil-concrete interface at high pressure, In Proceedings of 10th ICSMFE, Stockholm, Sweden.

Kondner, K.L. (1963). A hyperbolic stress-strain formulation for sands, Sec. Pan. Am. ICOSFE Brazil, Vol. 1, pp. 289-324.

Kishida, H. and Uesugi, M. (1987). Tests of the interface between sand and steel in the simple shear apparatus, Geotechnique, Vol. 37, No. 1, pp. 45-52.

Kolar, V. and Nemec, I. (1989). Modeling of soil-structure interaction, Developments in Geotechnical Engineering, Vol. 58.

Lade, P.V. and Duncan, J.M. (1975). Elastoplastic stress-strain theory for cohesionless soil, Journal of the Geotechnical Engineering Division, pp. 1037-1053.

Li, B. (2001). An experimental study and numerical simulation of sand-steel interface behaviour, Master's Thesis, University of Ottawa, ON.

Massicotte, D. (2000). Finite element calculations of stresses and deformations in buried flexible pipes, Master's Thesis, University of Ottawa, ON.

Navayogarajah, N., Desai C.S., and Kiousis P.D. (1992). Hierarchical single-surface model for static and cyclic behavior of interfaces, Journal of Engineering Mechanics, Vol. 118, No. 5, pp. 990-1011.

Plaxis User Guide (1998). PLAXIS Finite Element Code for Soil and Rocks Analyses, Edited by Brinkgreve, R.B.J. and Vermeer, P.A., Published by A.A. Balkema, Rotterdam.

Potyondy, J.C. (1961). Skin friction between various soils and construction materials, Geotechnique, Vol. 11, No. 4, pp. 339-353.

Ramberg, W. and Osgood, W.R. (1943). Description of stress-strain curves by three parameters, Technical Note 902, National Advisory Committee for Aeronautics, Washington, D.C.

Roscoe, K.H., Schofield, A.N., and Wroth C.P. (1958). On the yielding of soils, Geotechnique, Vol. 8, No. 1, pp. 22-53.

Schofield, A.D. and Wroth, C.P. (1968). Critical state soil mechanics, McGraw Hill Book Co., London.

Shen, J. and Kushwaha, R.L. (1998). Soil-Machine Interactions, Marcel Dekker Inc., NY.

Somasundaram, S. and Desai C.S. (1988). Modeling and testing for aniso tropic behavior of soils, Journal of Engineering Mechanics, Vol. 114, No. 9, pp. 1473-1496.

Tejchman, J. and Wu, W. (1995). Experimental and numerical study of sand-steel interfaces, Int. J. for Num. and Anal. Mech. In Geotech., Vol. 19, pp. 513-536.

Uesugi, M. and Kishida, H. (1986). Influential factors of friction between steel and dry sands, Soils and Foundations, Vol. 26, No. 2, pp. 33-46.

Wroth, C.P. and Bassett, R.H. (1965). A stress-strain relationship for the shearing behaviour of a sand, Geotechnique, Vol. 15, No. 1, pp. 32-56.

Yoshimi, Y. and Kishida, T. (1981). Friction between sand and metal surface, Proceedings of 10^{th} International Conference on Soils Mechanics and Foundation Engineering, Vol. 1, pp. 831-834.

Zaman M., Desai C.S., and Drumm E.C. (1984). Interface model for dynamic soil-structure interaction. Journal of Geotechnical Engineering, Vol. 110, No. 9, pp. 1257-1273.

Zhang, H. (1997). Steady state behaviour of sands and limitations of the triaxial test, Ph.D Thesis, University of Ottawa, ON.